DESIGN OF AN EXPERIMENTAL FACILITY FOR HYBRID GROUND SOURCE HEAT PUMP SYSTEMS

By

SHAWN ALEX HERN

Bachelor of Science

Oklahoma State University

Stillwater, Oklahoma

2002

Submitted to the Faculty of the
Graduate College of the
Oklahoma State University
in partial fulfillment of
the requirements for
the Degree of
MASTER OF SCIENCE
December, 2004

DESIGN OF AN EXPERIMENTAL FACILITY

FOR HYBRID GROUND SOURCE HEAT

PUMP SYSTEMS

Thesis Approved:

Dr. Daniel Fisher

Thesis Advisor

Dr. Jeffrey Spitler

Dr. Afshin Ghajar

Dr. A. Gordon Emslie

Dean of the Graduate College

ACKNOWLEDGEMENTS

I would first like to thank my advisor Dr. Fisher for his continuous guidance and support. His energy always made any problem seem trivial and with his optimistic attitude, you would believe that any problem could be solved. I will always be grateful for the experiences learned under his tutelage.

I would also like to extend my gratitude to the other committee members, Dr. Jeffrey Spitler and Dr. Afshin Ghajar, for their guidance on improving my work.

Numerous individuals provided their support and talents in completing my research. Dr. Marvin Smith, Randy Perry and Fred Schroeder all assisted with questions or problems that would arise during construction. Their knowledge and help was indispensable during the initial construction phase. Ben Alexander used his many abilities to assist installing the electrical system, placing the buffer tanks and numerous other jobs. I would also like to thank Brian Kastl for his diligent work ethic installing instrumentation, creating a data acquisition interface and performing experiments in my absence. Bill Holloway provided his expertise and practical knowledge during controls hardware development as well as supplying custom control and instrumentation boards. If not for the friendship and help of these people, completion of the project would have been a very difficult task.

Finally, I would like to thank my family and friends for their love and support. Their constant encouragement always let me know that it can only get better, no matter

how bad it seems. Without their understanding and help, completion would have been a significantly more difficult and lonely road.

TABLE OF CONTENTS

LIST OF TABLES

LIST OF FIGURES

NOMENCLATURE

ΔT	Temperature Difference
A	Ampere
BTU	British Thermal Unit
ft	Foot
gpm	Gallons Per Minute
hr	Hour
HVAC	Heating Ventilation and Air Conditioning
in	Inch
lbs	Pounds
lpm	Liters Per Minute
m	Meter
mA	Milliampere
mm	Millimeter
PVC	Polyvinyl Chloride
Q	Heat Transfer Rate
V	Volumetric Flow Rate
Vac	Voltage Alternating Current
Vdc	Voltage Direct Current
W	Watt

1. Introduction

The global energy crisis has led to the development of a number of new low energy systems for building heating and cooling. These systems provide viable alternatives to conventional energy systems and have the capability to significantly reduce electrical energy usage. To effectively design these systems, computer programs that simulate the building and its mechanical equipment as an integral system are needed.

The Department of Energy's (DOE), EnergyPlus and the National Institute of Science and Technology's (NIST) HVACSim+ are two such programs. They use integrated solution techniques to solve the source sides of zone, system and plant sub-systems. This solution technique makes EnergyPlus and HVACSim+ prime candidates for analyzing and designing low energy building systems. Each aspect of these programs is based on mathematical computer models developed by researchers to accurately simulate complex environmental systems. These computer models must be verified by experimental data gathered from real systems.

1.1 Overview

This thesis reports on the development of an experimental facility to test and validate the hybrid ground-source heat pump (HGSHP) models in EnergyPlus and HVACSim+. A HGSHP system consists of a ground-loop heat exchanger (GLHE) with a supplemental heat rejecter (e.g., cooling tower, fluid cooler, pond coil, etc.). This system is advantageous for buildings where the annual cooling loads are larger than the

annual heating loads. For a HGSHP system, the borefield can be sized based on the heating loads. The borefield in conjunction with a supplemental heat rejecter would allow the system to meet the cooling loads. The main advantage of this system is that it more closely balances the heat rejected and extracted for the GLHE over the course of a year. Another added benefit is the possible decrease in first cost and operating cost compared to conventional ground source heat pump systems.

Although HGSHP systems show considerable promise, they have not been widely adopted. This is largely due to the fact that until recently, tools capable of HGSHP system design were not available. Recently HGSHP modeling capabilities have been developed for HVACSim+ and EnergyPlus, but both programs are based on quasi-steady state solution techniques and steady state models. Over a ten or twenty year simulation using relatively short (ten minute to one hour) timesteps, the accumulation of error due to transient aspects of the system can be significant.

The main objective of the research is to develop an experimental facility capable of accurately measuring system performance for a wide range of HGSHP system configurations. Instrumentation and datalogging capabilities were specified to allow calculation of heat transfer rates, flow rates and power inputs required for the calculation of system performance metrics.

A secondary objective of the research is to design and implement the control hardware and software required to develop optimal control strategies for HGSHP systems. A related objective is to provide long term performance data for ground loop heat exchangers (GLHE)-a critical component in any HGSHP system. In order to validate proposed GLHE models, the data set must include continuous flow and

temperature data. Currently, such data sets do not exist in the literature. The experimental facility was designed to provide this data.

To achieve these objectives a HGSHP system consisting of two heat pumps, two storage tanks, 5 boreholes, a pond loop and a cooling tower was constructed. The following sections will discuss design, construction, instrumentation and validation of the experimental facility.

2. Background and Literature Review

This literature review focuses on both the design and simulation of HGSHP systems. This focus will facilitate the design and instrumentation of a facility for the validation of simulation models.

2.1 Hybrid Ground Source Heat Pump System Design

A literature review for hybrid ground source systems yielded a small number of papers covering system experimentation and design. Much of the literature consisted of system design with very little experimental data.

2.1.1 Design

The ASHRAE Ground Source Heat Pump Engineering Manual (ASHRAE, 1995b) discusses the design and sizing of ground loop heat exchangers and supplemental heat rejecters. The design procedure suggests that the ground loop be sized based on the average monthly heating and cooling loads. The minimum and maximum temperatures entering the heat pump are set as limits for sizing the ground loop length. In a cooling dominated application, the ground loop is sized for the heating load, and the supplemental heat exchanger is sized to meet the remainder of the cooling load. For this system, a series of guidelines are given discussing the installation of the supplemental heat exchanger and internal piping, the use of an isolation plate heat exchanger when an open cooling tower is used, options on set point controls, and year round operation in warm, southern climates. It is also suggested that the supplemental heat rejecter be used at night to facilitate cold storage in the ground.

Kavanaugh and Rafferty (1997) present a few hybrid ground source heat pump alternatives for the design and sizing of ground loop heat exchangers. The sizing of the ground loop and supplemental heat rejecter is based on the peak block load at the design conditions. The supplemental heat rejecter is sized to meet the difference between the required ground loop heat exchanger lengths for heating and cooling. Recommendations are made to integrate the supplemental heat rejecter in parallel with the ground loop heat exchanger system to lower the pumping losses and to decrease operating costs by using variable speed pumps.

Kavanaugh (1998) introduces a revised design method for sizing fluid coolers and cooling towers for hybrid ground loop heat exchanger systems. The revised design procedure considers system controls, piping requirements, equipment efficiency, maintenance, freeze protection, and ground heat exchange and heat buildup. To limit heat pump performance degradation due to heat buildup, the revised procedure proposes a method for balancing the heat extracted from the ground with heat rejected to the ground on an annual basis. A set point control of the ground loop temperature (typically 27 to 32°C; 80 to 90°F) is used to calculate the required operating hours of the supplemental heat rejecter to balance the heat extraction and rejection in the ground loop. The revised method is then utilized for the design of a hybrid ground source system for a four-story office building located in three different climate conditions. The installation and operating costs are discussed. The author concludes that the hybrid system is economically valuable in warm or hot climates where the differences between the heating and cooling loads are greatest. The economic value of the hybrid system is somewhat

attractive in moderate climates but difficult to justify in cold climates except for buildings with high internal loads.

Phetteplace and Sullivan (1998) present performance data for a 22-month period on a hybrid ground source system at a 24,000 ft^2 military base administration building in Fort Polk, La. The hybrid system consists of 70 vertical closed loop boreholes, 200 ft deep with 10 ft spacing. This loop was designed to meet the heating requirements of the building and a 78-ton closed circuit cooling tower is used as a supplemental heat rejecter to meet the cooling requirements. The data showed that the heat rejected to the ground was 43 times higher than the amount extracted. The control system activates the cooling tower fan and circulation pump when the exiting water temperature from the heat pumps exceeds 97°F and deactivates when the temperature falls below 95°F. The authors note some heat buildup in the ground loop due to the imbalance in the loop field heat transfer. Lowering the control set point or operating the cooling tower in the winter months could possibly offset the heat buildup. Relative energy consumption for the major system components are 77% for the heat pumps, 19% for the circulating pumps, 3% for the cooling tower fan, and 1% for the tower circulating pump. An estimate was performed on the possible conversion of the constant volume circulating pumps to variable speed pumps. This estimate found that the pumping energy could possible be reduced by as much as 45%.

2.1.2 Experimental Procedures

A review of the literature for the experimental testing of a ground loop heat exchanger yields several test procedures. One important procedure involves numerical

models and methods for estimating the thermal conductivity of the ground surrounding a ground loop. Many of these methods are transient, varying the temperature with time.

The development of a GLHE thermal response testing device and a two-dimensional parameter estimation model are presented by Austin (1998). Water is heated and circulated through the borehole. The water flow rate, inlet and outlet temperatures, and the power input to the water are recorded. This data can then be analyzed to estimate the thermal conductivity of the borehole which can be used for system design. A two-dimensional parameter estimation model was then developed and tested against the more common line source and cylinder source methods. The results from this model and the parameter estimation showed that a testing time of fifty hours would give an accurate number for determining the borehole thermal conductivity.

Shonder and Beck (1999) present a new method for determining the soil conductivity and borehole resistance of a ground loop heat exchanger. The method presented determines the transient conduction equation for a one-dimensional cylindrical model using parameter estimation. By using a numerical method, the estimated solution to the heat conduction equation is calculated more accurately for tests where unstable voltage causes the power input into the water to vary over time. The method is solved using a finite difference grid and a Crank-Nicolson scheme. The method also provides confidence intervals for the parameter estimates, which can be used to assess the accuracy of the results.

Shonder and Beck (2000) compare their one-dimensional model to the line source and cylinder source methods for three in-situ tests. The time period for each model to converge varied for each test. The line source and cylinder source methods were greatly

affected by power fluctuations and overestimated the thermal conductivity. After a 50 hour time period, the values of thermal conductivity predicted by these two methods, had not yet converged. The authors concluded that the one-dimensional model was more accurate for tests that included variations in power input and for shorter test periods. The model was implemented into a computer program that is available for download from Oakridge National Laboratory.

There are a few papers that describe experimental procedures and testing experience. Martin and Kavanaugh (2002) performed tests on four ground loop heat exchangers to observe the effects of power quality, test duration, and delay time for retesting. The paper also presents results for thermal conductivity from several variations of the line source method, the cylinder source method, and the one-dimensional model presented by Shonder and Beck (1999). The power quality was observed by creating a one hour power interruption in the test. The results from each of the thermal conductivity models showed that this power interruption led to a significantly lower estimated value of thermal conductivity. This shows that uninterrupted power is critical for obtaining good data sets for testing ground loop heat exchangers. After a period of about 48 hours, each of the models converged to the same thermal conductivity. The authors recommend a minimum of 11 days between tests on the same borehole to allow the heat from the previous test to fully dissipate. Some of the thermal conductivity models showed errors of up to 24% if a retest was performed too quickly. To determine the undisturbed ground temperature, the authors recommend recording the minimum loop temperature obtained from the test loop on start-up.

Witte et al. (2002) compared different methods and models for obtaining the thermal conductivity of a borehole. The first method used to determine the soil thermal conductivity was a traditional approach of obtaining a detailed soil profile during drilling. This method can prove to be difficult and can give a wide range of values for the soil conductivity. The second method was to analyze each of the soils in a laboratory. The results obtained from this method were similar to the first method. The final method was to perform an in-situ test on the borehole. The results obtained from the test were then analyzed using the line source model and a two-dimensional finite volume model. It was shown that atmospheric temperatures can affect the results. If the test apparatus and the piping attached to the borehole were not insulated properly, unmeasured heat can be added or subtracted from the system. Different time periods were analyzed for each model and the models exhibited no change after 72 hours of test data.

Gehlin and Hellstrom (2003) evaluated four different models for determining the thermal conductivity of a ground loop heat exchanger. Three of the models were analytical and based on line and cylinder source methods. The fourth model was an explicit one-dimensional finite difference numerical model. Three experimental data sets were then analyzed to determine their thermal conductivity. The analysis showed that the two line source models closely matched each other while the cylinder source model tended to overestimate the thermal conductivity of the ground loop heat exchanger. The numerical model closely matched the results of the line source model. The average deviation between the models was 1-5%. The cylinder source model tended to be about 10-15% higher than the other models but the deviation between all of the models decreases with longer measurement times. The paper concluded that the line source

model works best with a minimum of 50 hours of data. A note was made that the numerical model would work better if the test included variable heat injection.

Gehlin and Nordell (2003) studied three methods for determining the undisturbed ground temperature for a ground loop heat exchanger. Each method requires water to be placed in the borehole and remain undisturbed so that equilibrium with the surrounding ground is reached. The first method involves lowering a temperature sensing device down a water filled borehole and logging temperatures at set distances. The second approach requires the borehole be attached to a thermal response testing device. Water is then circulated through the borehole and measurements of the inlet and outlet temperatures were taken at ten second intervals. These measurements were then analyzed assuming plug flow, which states that measurements taken at specific times correspond to certain borehole depths. The third method involves the circulation of the water for a period of time. The temperature difference between the outlet and inlet temperatures will converge to the mean borehole temperature but steadily increase afterwards due to heat input from the circulation pump.

Gehlin and Spitler (2003) reviewed the testing apparatus used throughout the world and how they differ. They discuss the effect of test duration, uncontrolled heat loss or gain due to inadequate insulation of exposed pipes, instability fluctuation of the power supply and ground water flow around the ground loop. Different analytical and numerical models for calculating the ground thermal conductivity are then discussed.

2.2 Hybrid Ground Source Heat Pump System Simulation

Yavuzturk and Spitler (2000) study a hybrid ground source heat pump system by applying a short time step simulation model to a small office building. The hybrid

system consists of an open cooling tower coupled by an isolation plate heat exchanger to the ground loop. The life cycle cost of set point control, differential control, and scheduled control are compared for two different climates over twenty years. The set point control activates the cooling tower when the entering or exiting heat pump temperatures exceed 96.5°F. The differential control scheme operates the cooling tower based on the temperature difference between the entering or exiting heat pump temperatures and the ambient wet bulb temperature. The schedule control scheme activates the cooling tower during the evening for a set period of time at specific times of the year. Set point control is also integrated into this scheme to prevent temperature spikes in the ground loop. The results from the system simulation show a significant savings in the first cost over a conventional ground source system. Additional savings are obtained from reduced operational costs due to the smaller circulating pumps used for the ground loop and cooling tower. These reduced operational costs were more prevalent in cases where the building cooling loads were much greater than the heating loads.

3. Design Criteria

3.1 Range and Types of Experiments

The main design objective is to develop an experimental facility capable of accurately measuring system performance for a wide range of HGSHP system configurations. To accomplish this goal, a configurable source system was installed to allow GLHE and component testing.

The source side of the system conditions the water entering the heat pumps. Three independent source components are installed in the system: a ground loop heat exchanger, a pond loop heat exchanger, and an evaporative cooling tower. Conventional water source heat pump systems use only one of these components. A cooling tower is often installed along with a boiler in larger systems. Other large commercial designs use a ground loop year round for heat extraction/rejection on the source side.

In order to develop and validate hybrid system design procedures the facility must cover a range of source side configurations. Experiments can be performed with a valve board that allows the source side components to be configured in any combination of parallel/series flows. Even with these combinations, the experiments must cover a range of capacity splits between components. To achieve this objective, a configurable borefield was installed that permits the selection of 1 to 5 boreholes. A full sized cooling tower is installed so that it can be cycled to simulate part load operation. Two heat pumps and a variable speed pump are included in the system to allow a wide range of loads and temperatures to be tested.

3.2 Simulation Validation Considerations

3.2.1 Component Level Validation

New component models can also be developed and validated using the test facility. Instrumentation is installed on each component so that water side heat transfer rates and electric power use can both be determined. Input parameters such as water temperature and flow rate can also be varied to validate mathematical component models over a range of operating conditions.

Thermocouples measure water temperature at the inlet and outlet of each component. Flowmeters are installed in each branch of the system to measure water flow rates. Watt transducers measure power input to the circulating pumps, heat pumps, and the evaporative cooling tower. A relative humidity sensor and thermocouple measure outdoor air conditions near the evaporative cooling tower. These measurements provide sufficient information to validate component models over a range of steady-state and transient conditions.

3.2.2 System Level Validation

Component interaction such as loop capacitance and transient effects also needs to be measured in the system. In commercial systems, the loop capacity is often large and can affect the operational control strategy. The system capacity for the experimental facility is known from the size and lengths of piping and other components. Instrumentation is placed at the inlet and outlet of each component to measure these system effects.

A secondary objective is the development of operational control strategies for HGSHP systems. The EnergyPlus and HVACSim+ simulation environments allow the

development and testing of new strategies. The experimental facility can support this effort with operating data. To accommodate this requirement, control hardware and software was developed and implemented in the facility. The program is modular allowing the user to create new control algorithms to operate the system. Additional instrumentation, such as the thermocouple probes installed into the chilled and hot water storage tanks support investigation of control strategies.

A robust data acquisition system was installed to ensure that complete and accurate data sets could be collected. The data sets can be analyzed and used for both short and long term trend prediction. This is particularly important for HGSHP system simulation, since the simulation period is typically ten to twenty years.

4. Experimental Facility Design and Construction

The experimental facility is located in a research park on the campus of Oklahoma State University. The facility consists of two buildings: the test cell and the plant building. One of the two test cells as shown in Figure 4.1, provides a cooling or heating load on the plant. Both the tests cells were constructed under a previous research project, ASHRAE 1117-RP (Eldridge et. al, 2003). The plant building houses the water conditioning equipment along with the associated data acquisition system. Environmental heat exchangers are located near the plant building as shown in Figure 4.1.

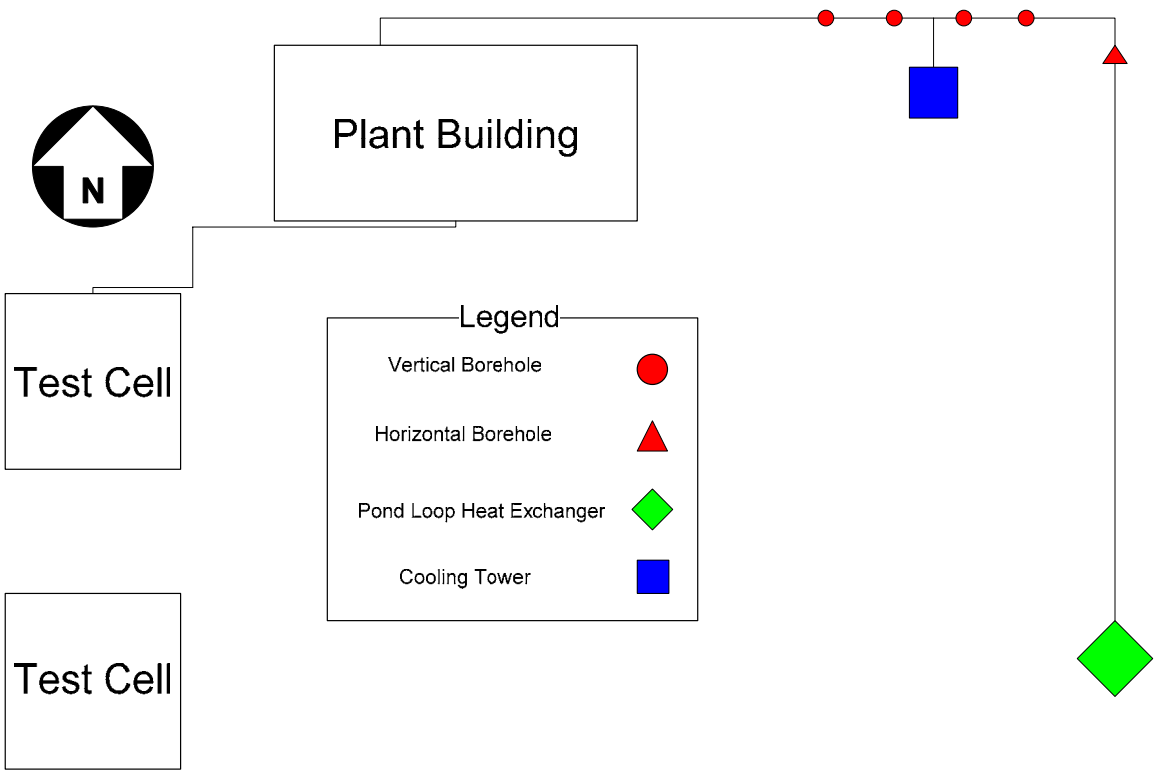

Figure 4.1 – Plant Building

For purpose of discussion, the system may be divided into three subsystems: the load side, the source side, and the primary equipment. The load side consists of all piping and equipment connected to the test cell-side of the heat pump. The source side

consists of the three environmental heat exchangers and the primary equipment encompasses the heat conditioning equipment, storage tanks, and circulation pumps. In the following sections, an overview of the design procedure is followed by a detailed discussion of each subsystem.

4.1 Design Procedure

The design procedure included: determining the system requirements, sizing and selecting system components and determining component placement and connection. Each part of the procedure was critical to achieving the objective of a start-of-the-art experimental HGSHP facility.

The most difficult task in the system design was configuring the hydronic loops. Circulation pumps were sized to specific design flow rates as required by environmental and load side heat exchangers and the system heat pumps. The piping for each subsystem has an associated pressure loss based on a particular flow rate. A spreadsheet program described below was used to calculate the pressure drop for each section of piping. The input data used in pressure drop calculations is found in Appendix B. This spreadsheet uses a modified and reduced version of the Bernoulli equation to calculate the head loss in a length of pipe as shown below.

$$P_1 - P_2 = l_f \tag{4.1}$$

The value for l_f, the friction loss, can be found from the Darcy-Weisbach equation for head loss in a pipe (McQuiston et al., 2000).

$$l_f = f \frac{L}{D} \frac{\bar{V}^2}{2g} \tag{4.2}$$

Where:
f = Moody friction factor

L = length of the pipe, *ft* or *m*
D = diameter of the pipe, *ft* or *m*
V = average pipe velocity, *ft/sec* or *m/s*
g = acceleration due to gravity, *ft/sec*^{2} or *m/s*^{2}

The value for f can be obtained from a Moody diagram or by solving the Colebrook equation. The problem is that both of these methods require iteration to obtain the correct value of f. Churchill (1977) derived a single expression that represents the friction factor for all flow regimes as given below.

$$f = 8\left[\left(\frac{8}{\mathrm{Re}_D}\right)^{12} + \frac{1}{(A+B)^{1.5}}\right]^{1/12}$$

$$A = \left\{2.457 \ln\left[\frac{1}{(7/\mathrm{Re}_D)^{0.9} + (0.27\varepsilon/D)}\right]\right\}^{16} \qquad (4.3)$$

$$B = \left(\frac{37530}{\mathrm{Re}_D}\right)^{16}$$

Where:
Re_D = Reynolds number
ε/D = relative pipe roughness

The pressure drop for the heat pumps, pipe-fittings, flowmeters, strainers, and plate frame heat exchanger were added to the appropriate piping section. The component pressure loss was calculated by the equation given below.

$$l_f = K\frac{\bar{V}^2}{2g} \qquad (4.4)$$

Where:
K = loss coefficient
V = average pipe velocity, *ft/sec* or *m/s*
g = acceleration due to gravity, *ft/sec*^{2} or *m/s*^{2}

The values for K where obtained from Crane (1957) for each pipe fitting. K-values for the remaining equipment were based on manufactures' catalog data.

4.2 Load Side Design

The load side of the heat pump system meets the heating or cooling demands of the test cell. The following sections describe the configuration and design of the load side system.

4.2.1 Load Side Layout

The load side consists of two subsystems: the test cell, and the plant fan coil. The test cell is connected to the plant building by piping running through a 2 ft deep trench. The piping consists of hot and chilled water supply lines, and a common return line, as shown in Figure 4.3. The piping terminates at T-fittings and ball valves located in a 3 ft diameter manhole as shown in Figure 4.2.

Figure 4.2 – Load Side Manhole

The piping downstream of one set of valves leads to the test cell. The piping downstream of the other set of valves is capped after it exits the manhole to allow for future expansion to the remaining test cell. Pumps that circulate water to the test cell are located in the plant building on the return pipe as shown in Figure 4.3. Placing the pumps on the return line allows the system to operate independently of the test cell flow rate requirements.

The fan coil provides conditioning air to the plant building. A manual three way valve determines whether hot or chilled water is circulated through the fan coil. The return from the fan coil joins the common return from the test cell.

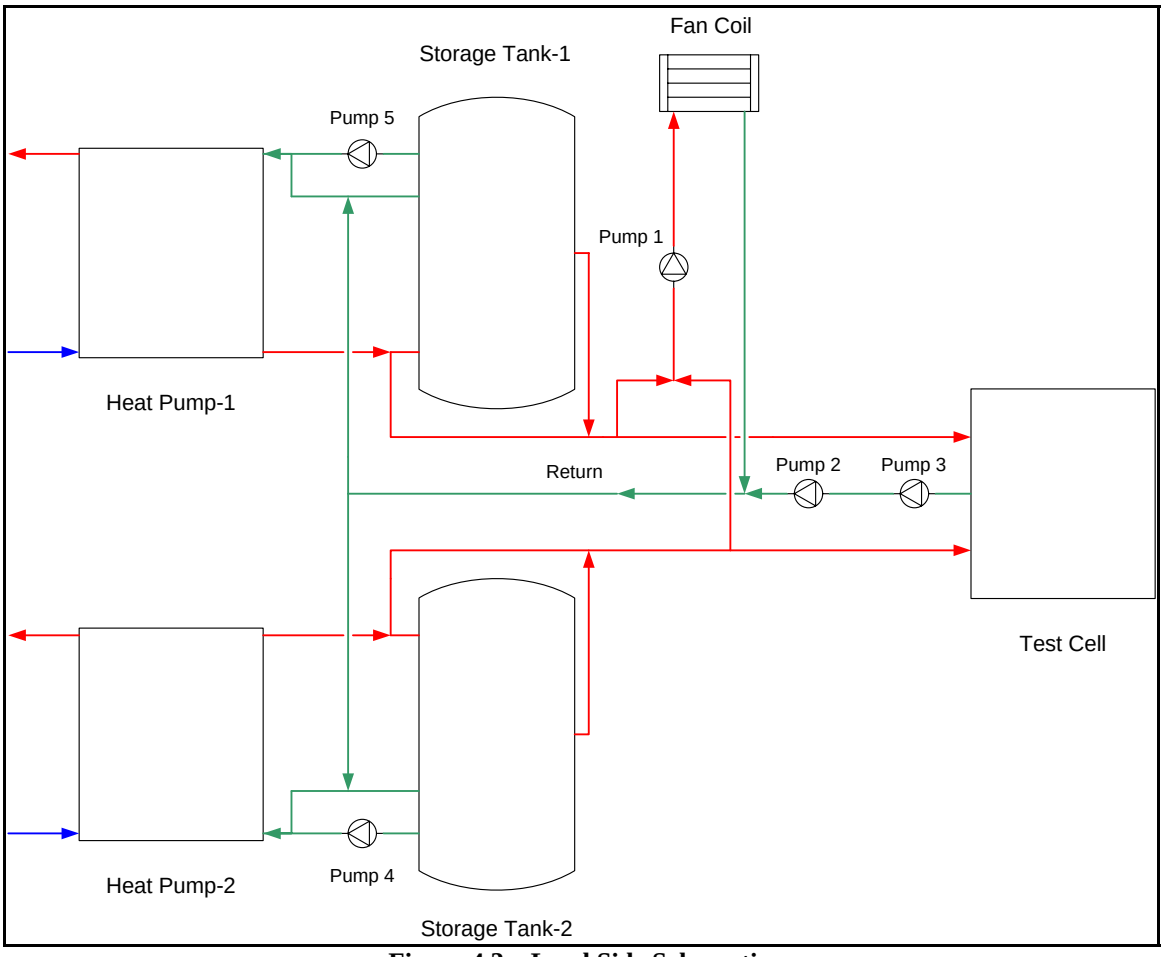

Figure 4.3 – Load Side Schematic

4.2.2 ASHRAE 1117-RP Test Cell

The test cell was previously constructed and instrumented to validate cooling load procedures (Eldridge et. al, 2003). The buildings were constructed in a two-story fashion such that the test cell of each building is on the second story above a conditioned equipment and control room as shown in Figure 4.4.

Figure 4.4 – Twin Test Cells

A calibrated model of the test cell for use with system simulations was previously developed. Measured diurnal and seasonal load profiles which can be used for HGSHP studies are also available. The test cells were designed so that the cooling loads are greater than the heating loads. This simulates a commercial building application where a HGSHP could be installed.

The cooling loads for the test cell were previously experimentally measured and are shown in Figure 4.5.

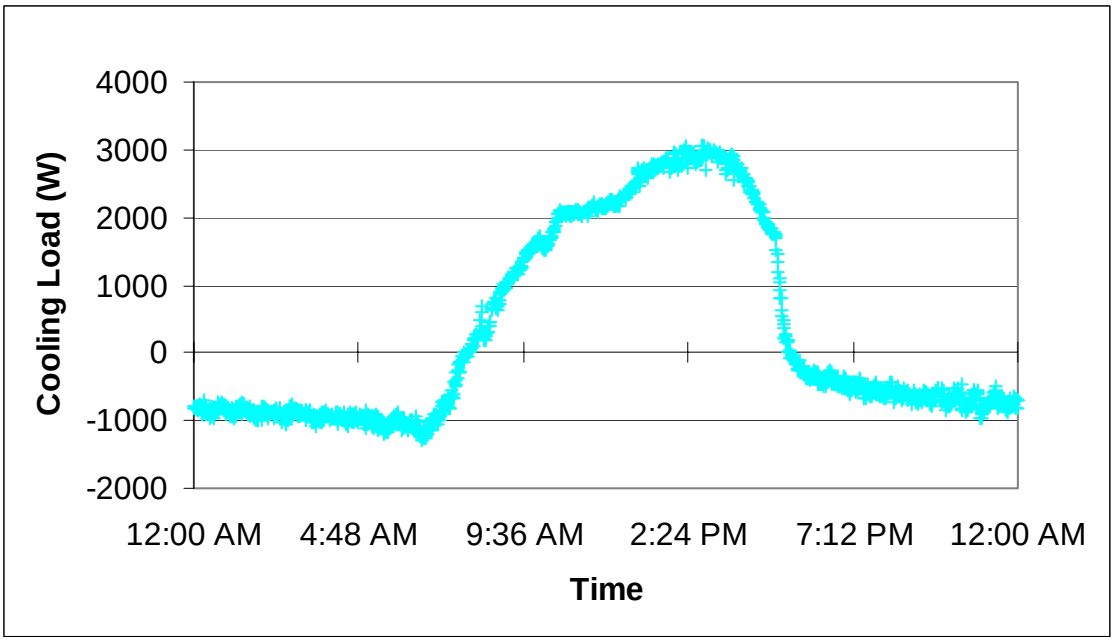

Figure 4.5 – Measured Test Cell Cooling Load

As shown, the cooling load for the test cell is approximately 1-ton (12,000 Btu/hr or 3-kW). A 3-ton system capable of meeting the combined load of the two test cells, and the load required for conditioning the equipment building was specified.

Each test cell was originally designed with a water-to-air heat pump followed by a water-to-air reheat coil supplied from the ground loop. Water is now supplied to the reheat coil from the HGSHP plant. A radiant floor and radiant ceiling panels were also installed in the test cell to expand the hydronic system configurations supported by the test cell. The system uses a combination of three-way and two-way electronic valves to control the temperature and flow of water in each of the sub-systems.

4.2.3 Plant Fan Coil

A McQuay fan coil (model number FTHC1H04AA70A00X17AZA1) was selected to provide conditioning to the plant building. This fan coil is capable of 1.2-tons (14400 Btu/hr or 4.2 kW) of cooling and 2.2-tons (26400 Btu/hr or 7.7 kW) of heating at

the manufacturer's design conditions. The 2-pipe fan coil shown in Figure 4.6 is a self contained unit with a three speed fan.

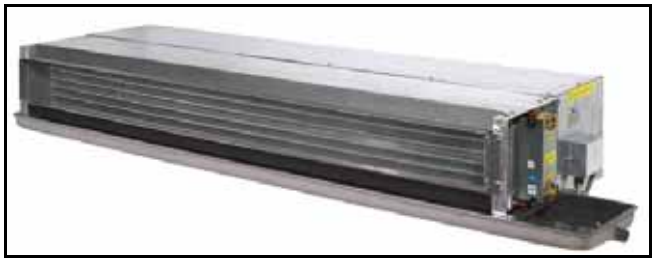

Figure 4.6 – Fan Coil Unit (McQuay, 2003)

A thermostat controller was attached to the fan coil to control the room temperature, and the fan speed. A circulating pump is wired to the thermostat controller so that it is engaged along with the fan coil. The fan coil draws water from either the hot or chilled side of the system by changing a manual three-way valve.

4.3 System Source Design

4.3.1 Source Side Layout

The source side consists of three separate heat exchangers: a ground loop heat exchanger, an evaporative cooling tower, and a pond loop heat exchanger. Each heat exchanger is connected to the plant building with its own supply and return pipes running through a 5 ft deep trench. The three supply pipes and three return pipes are routed separately through penetrations in the north wall of the plant building as shown in Figure 4.7.

Figure 4.7 – Source Installation Into Plant Building

The pipes terminate in a loop selection board, which consists of twelve ball valves and associated piping as shown in Figure 4.8. The valves can be set to configure the environmental heat exchangers for any combination of series or parallel flow. The figure also shows the Armaflex insulation used to insulate pipes and the water storage tanks. Armaflex is a flexible elastomeric thermal insulation that comes in varying thicknesses and has a nominal thermal conductivity of 0.27 BTU-in/hr-ft^2-°F (0.0389 W/m-K). Each water tank was insulated with 1 in Armaflex sheets while all of the piping in the plant side was insulated with 1/2 in Armaflex.

Figure 4.8 – Mounted Loop Board

Figure 4.9, shows the valve layout required to set up the desired combinations of source side components. There are 19 possible heat exchanger configurations that can be set by selecting different valve combinations. These combinations represent the full range of HGSHP source side configurations.

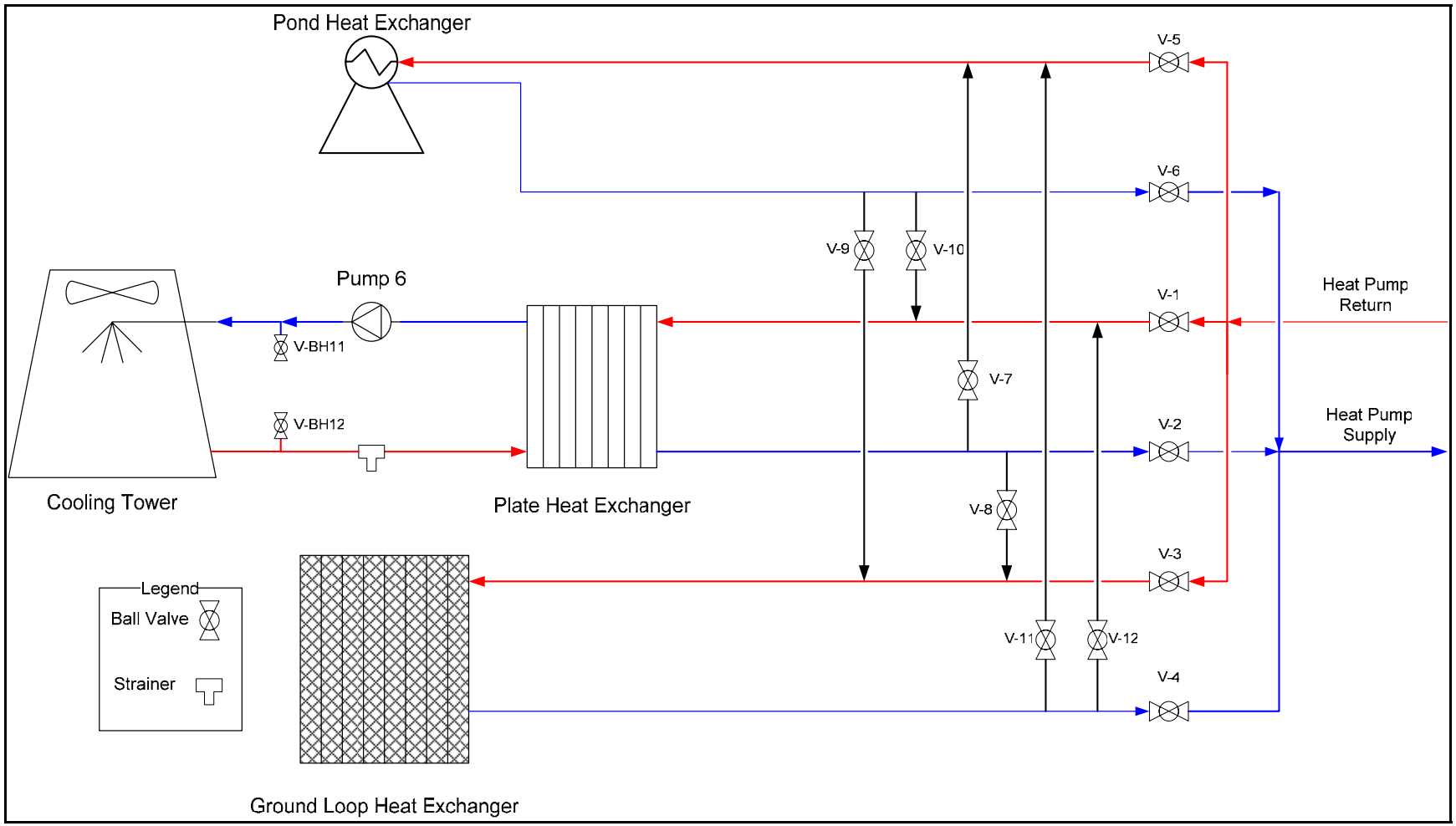

Figure 4.9 – Source Side Schematic

4.3.2 Ground Loop Heat Exchanger

The ground loop heat exchanger consists of 4 vertical boreholes with a diameter of 4.5 in, and 1 horizontal loop placed with a horizontal drilling machine. The boreholes were installed as part of the 2003 International Ground Source Heat Pump Association (IGSHPA) Technical Conference and Expo. A description of each borehole is shown in Table 4.1.

Table 4.1 – Borehole Configuration

Borehole #	Orientation	Length	Pipe Size	Grout	Geo-Clip
1	Vertical	250'	¾ "	ThermoGrout Light 0.88	No
2	Vertical	236'	¾ "	ThermoGrout Light 0.88	No
3	Vertical	249'	¾ "	Barotherm 88	No
4	Vertical	248'	¾ "	E-Z Seal	Yes
5	Horizontal	245'	¾ "	None	No

The pipe used in each borehole is ¾" IPS DR 11 DriscoPlex 5300, a high-density polyethylene designed for use in ground source systems, with a thermal conductivity of 0.225 BTH-h/ft-°F (0.389 W/m-K). To facilitate data collection, the boreholes were brought into a single 4.0 ft (1.22 m) diameter manhole and connected to a supply and return header shown in Figure 4.10.

Figure 4.10 – Ground Loop Manhole

Valves placed in this header allow for individual or combinations of loops to be selected for purging and testing. A schematic showing the relative location of the boreholes and the manhole are shown in Figure 4.11.

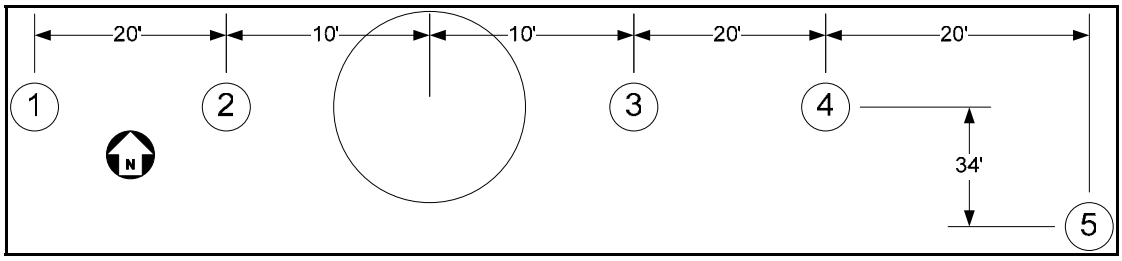

Figure 4.11 – Ground Loop and Borehole Spacing

4.3.3 Evaporative Cooling Tower

A 3-ton, direct contact, evaporative cooling tower was installed on one of the three source side loops. One drawback to an open-loop cooling tower is that contaminants can enter the rest of the piping system through the tower.

A solution to the open loop design is to use a cooling tower – plate heat exchanger (PHE) combination as shown in Figure 4.9. This design allows the main system, including the heat pumps, to operate in a closed loop configuration.

The cooling tower, shown in Figure 4.12, is a model ST-5 fiberglass unit manufactured by Amcot. Four adjustable rotating sprinklers distribute water over the towers honeycomb PVC fill material. A float system attached to an outdoor hydrant maintains a constant water level in the cooling tower basin. A series of drain valves placed in the manhole allow the system to be drained during the winter months.

Figure 4.12 – Evaporative Cooling Tower

The counterflow PHE, shown in Figure 4.13, consists of a series of grooved plates that are individually gasketed and pressed tightly together by compression bolts within a frame. Fluid enters and exits the PHE through portholes in one end of the frame. The counter flow design allows for maximum heat transfer efficiency. A Paul Mueller PHE AT4C-20 that would transfer approximately 3-tons (36,000 BTU/hr or 10.55 kW) at a

flow rate of 9-10 gpm (34.07-37.85 lpm) was selected. The PHE is available with a number of different plate materials and plate configurations. For the plate material 316 stainless steel was selected due to its excellent corrosion resistance and low cost. The plate configuration was selected to give a pressure loss through the closed side of the PHE that was near the pressure loss through the ground loop. Equal pressure drops through the two loops facilitates flow rate balancing when they are operated in a parallel configuration.

Figure 4.13 – Plate Heat Exchanger

4.3.4 Pond Loop Heat Exchanger

The pond loop was constructed of two parallel 1 in. nominal (K) copper pipes, 90 ft (27.43 m) long, arranged in a compact slinky configuration as shown in Figure 4.14. The installed loop is supported 18 in. (0.46 m) off the bottom of the pond. Supply and return lines run along the bottom of the pond to the heat exchanger.

The heat transfer rate of the pond heat exchanger was estimated by using the method described in section 3.4.1.7 of Chiasson (1999). Nusselt numbers were calculated for the inside and outside of the copper tube. The desired system heat transfer

rate of 3-tons (36,000 BTU/hr or 10.55 kW) was used with the temperature difference between the pond and the circulating fluid to calculate an overall heat transfer coefficient. A pond temperature of 17°C was used with an average fluid circulating temperature of 28°C. The overall heat transfer coefficient was then used with the Nussult numbers and copper tubing conductivity to estimate the heat exchanger pipe length of 38 ft (11.5 m) per circuit. This length was increased to 90 ft (27.43 m) to allow for extra capacity and to provide a safety factor in the heat transfer estimate.

Figure 4.14 – Pond Loop Coil.

4.4 Primary Equipment Selection

The primary plant equipment which is located in the plant building consists of two heat pumps, six circulation pumps and two water storage tanks as shown in Figure 4.15. The figure also shows strainers installed at six locations in the system. The strainers are glass-reinforced polypropylene units with an operating range of 30 to 140°F and removable screens rated at 149 microns

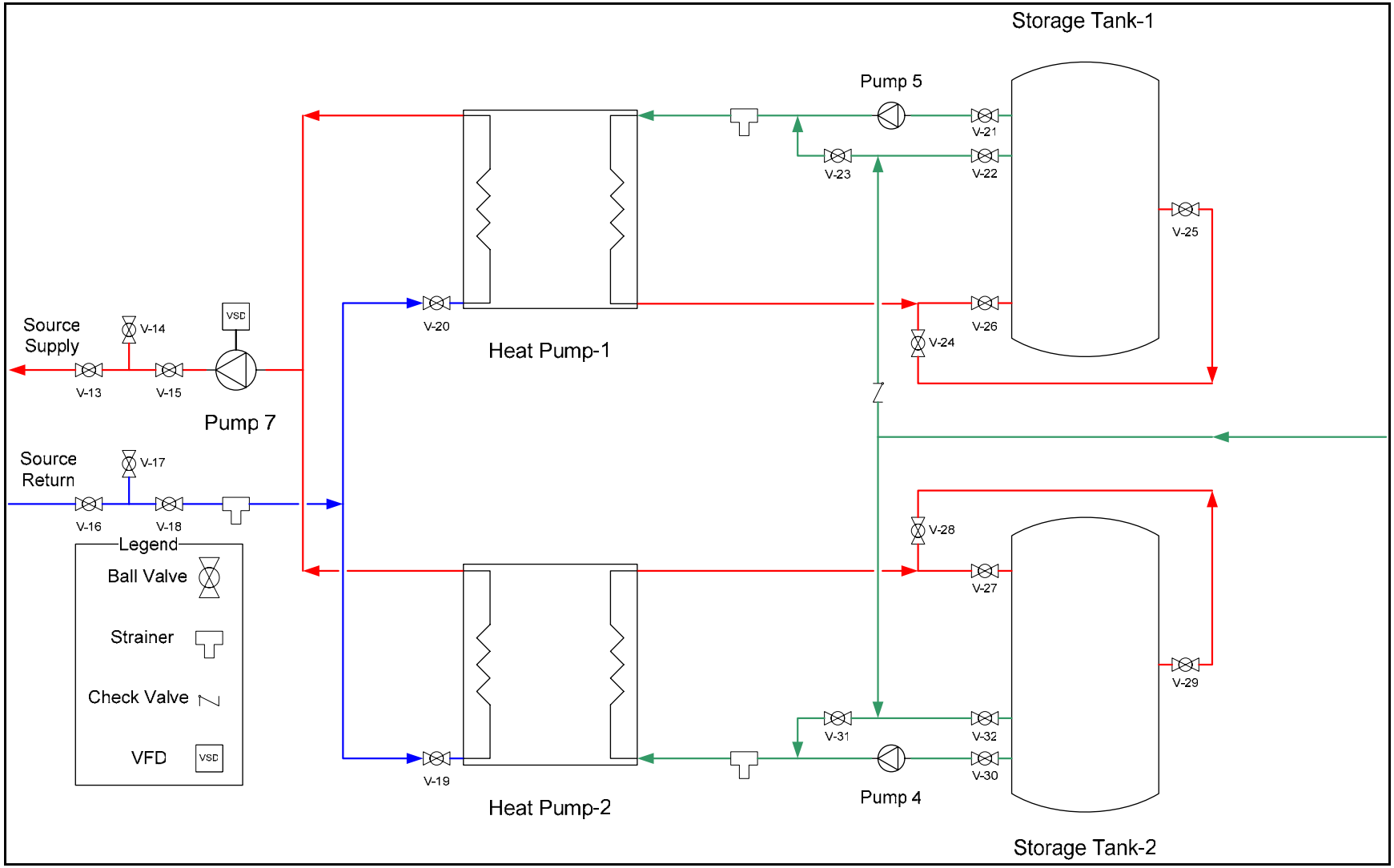

Figure 4.15 – Primary Equipment Schematic

4.4.1 Heat Pump

Two packaged, residential water to water heat pumps (WP036 – 1CSC – FXX Florida Heat Pump) as shown in Figure 4.16, condition the water in the system. Each heat pump is rated at a nominal capacity of 3-tons (36,000 BTU/hr or 10.55 kW).

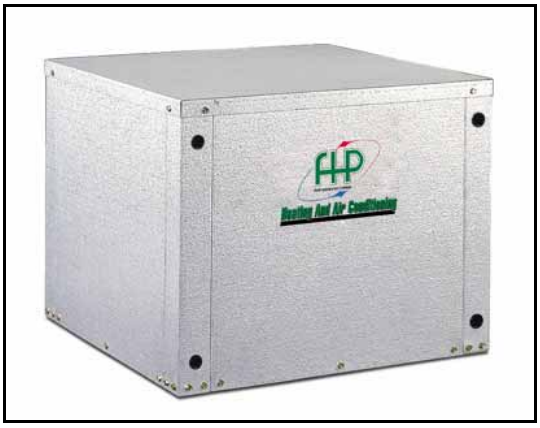

Figure 4.16 – Residential Heat Pump Unit

The major components in the heat pump include a Copeland ZR34K3-PFV-230 scroll compressor, coaxial water to refrigerant heat exchangers, a thermostatically controlled expansion valve, and a refrigerant reversing valve. The reversing valve allows the unit to heat or cool the load side water.

4.4.2 Circulation Pumps

The pumps located between the storage tanks and heat pumps as shown in Figure 4.14 circulate water at a flow rate of 9-10 gpm (34.07-37.85 lpm). Grundfos UP 43-75 F pumps were selected for this application based on pressure drop calculations. The cooling tower requires a dedicated circulating pump to maintain a flow rate between 9-10 gpm (34.07-37.85 lpm). Based on the loop pressure drop calculations, a Grundfos UP 26-64 F pump was selected. A three speed Grundfos UPS 15-42 F/FR was chosen to

circulate water to the fan coil. This pump was chosen based on a flow rate of 2.5-3.5 gpm (9.46-13.25 lpm) and a pressure drop across the longest pipe length.

A variable speed pump was selected to serve as the main circulation pump between the heat pumps and the three source side components. The pump selected for this application was an ITT – Bell & Gossett 80 1-1/2X1-1/2X7B with a 6.5 in impeller. This pump was sized for a source side flow rate of 10 gpm (37.85 lpm) and the maximum system pressure drop that could occur with the three source side loops connected in series. A Siemens SED2-1.5/22X model number 6SE6436-2UC21-5B80 variable frequency drive (VFD) shown in Figure 4.17, controls the speed of the pump and provides flow rate control for source side system configurations.

Figure 4.17 – Siemens Variable Frequency Drive

This VFD is designed specifically for HVAC applications and comes with options such as digital and analog inputs and outputs to allow for sensing and control.

The load side requires a wide range of flows depending on the configuration of the test cell hydronic systems. The pumps for this part of the system were sized based on a design flow rate of 14-16 gpm (53.00-60.57 lpm) through one of the supply lines. Two ITT-Bell & Gossett PL-55B pumps were specified and installed prior to installation of the test cell hydronic ceiling and floor. Pressure drop calculations based on the ceiling and floor design determine that a third PL-55B would be needed for experiments that bypassed the water storage tanks and used all test cell hydronic systems at maximum flow rate. This extra pump was placed in the test cell due to limited room in the plant building.

4.4.3 Water Storage Tanks

Two, three hundred gallon water storage tanks were installed to provide a continuous supply of chilled and hot water for test cell experiments. The 0.25 in. (6.35 mm) sheet steel tanks add capacitance to the system and prevent short cycling of the heat pumps. Tanks penetrations including inlet and outlet ports and thermocouple ports are shown in Figure 4.18.

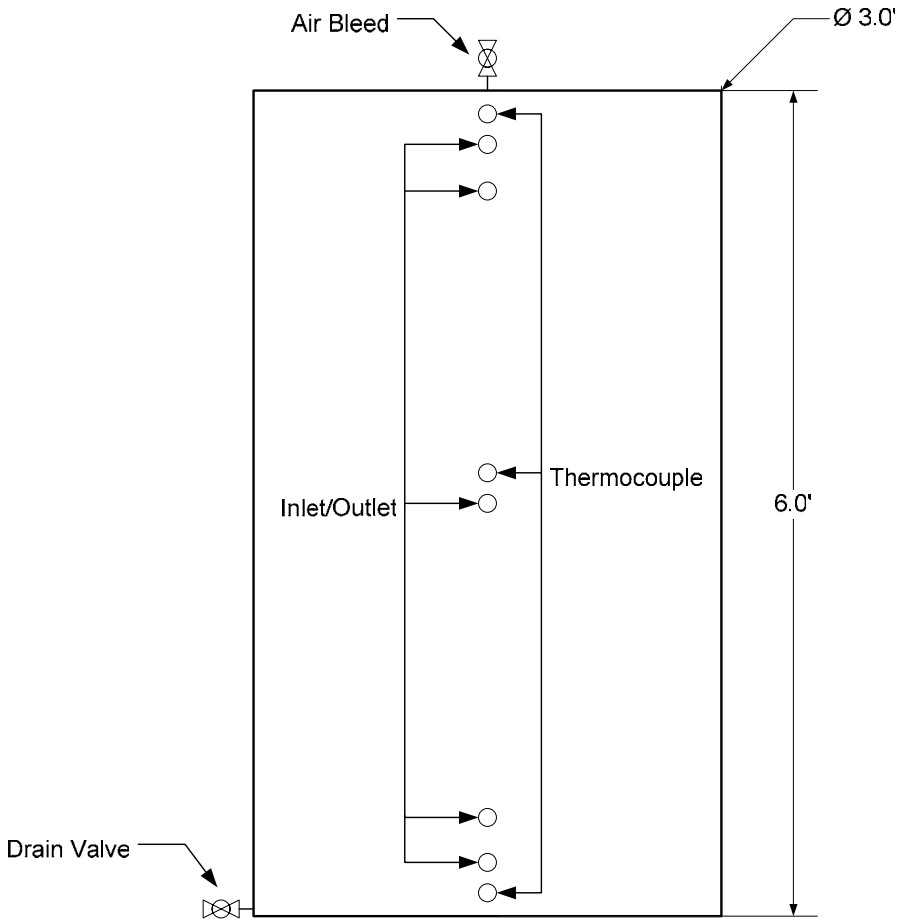

Figure 4.18 – Water Storage Tanks

The cooling mode heat pump conditions water from the top of the cold tank and returns it to the bottom of the tank. The heating mode heat pump draws cold water from the bottom and returns it to the top of the warm tank. Water is sent to the fan coil and tower from the center ports of the tanks. The water storage tanks can also be isolated from the rest of the load side of the system. For this configuration, circulating pumps 4 and 5 are not operated, and the water from the return line is run directly into the heat pumps.

5. Instrumentation and Controls

5.1 Instrumentation

The main purpose of the instrumentation and control system is to provide high-quality experimental data sets to validate system simulations and component models. To achieve this goal, three types of measurements were required: water temperature measurements, water flow rate measurements and power measurements. Temperature measurements were made using thermocouples. Vortex and paddlewheel flow meters were used to measure volumetric flow rate throughout the system. Power measurements were taken using precision watt transducers. These instruments allow for various aspects of the system to be analyzed as well as to provide data for system control.

For system simulation and component model validation, the primary metric is the experimental heat transfer rate. This is calculated as:

$$\dot{Q} = \dot{m}_w c_p \Delta T \tag{5.1}$$

Where:
$\dot{Q}$ = heat transfer rate
$\dot{m}_w$ = mass flow rate of water
c_p = specific heat of water
ΔT = temperature difference

Therefore, the general instrumentation scheme was to measure the temperature difference across each system component and the volumetric flow rate through each component as shown in Figures 5.1, 5.2 and 5.3.

The electrical power measurements provide a check for equipment power usage against the manufactures' catalog data. Electrical power information is also required in the overall heat balance of the system. Additional temperature measurements were taken

for equipment control. An example is the temperature measurements used in the water storage tank.

Each signal transmission line was labeled at the sensor and at the data acquisition unit. A three wire twisted and shielded cable was used for sensors and controls to eliminate unwanted line noise.

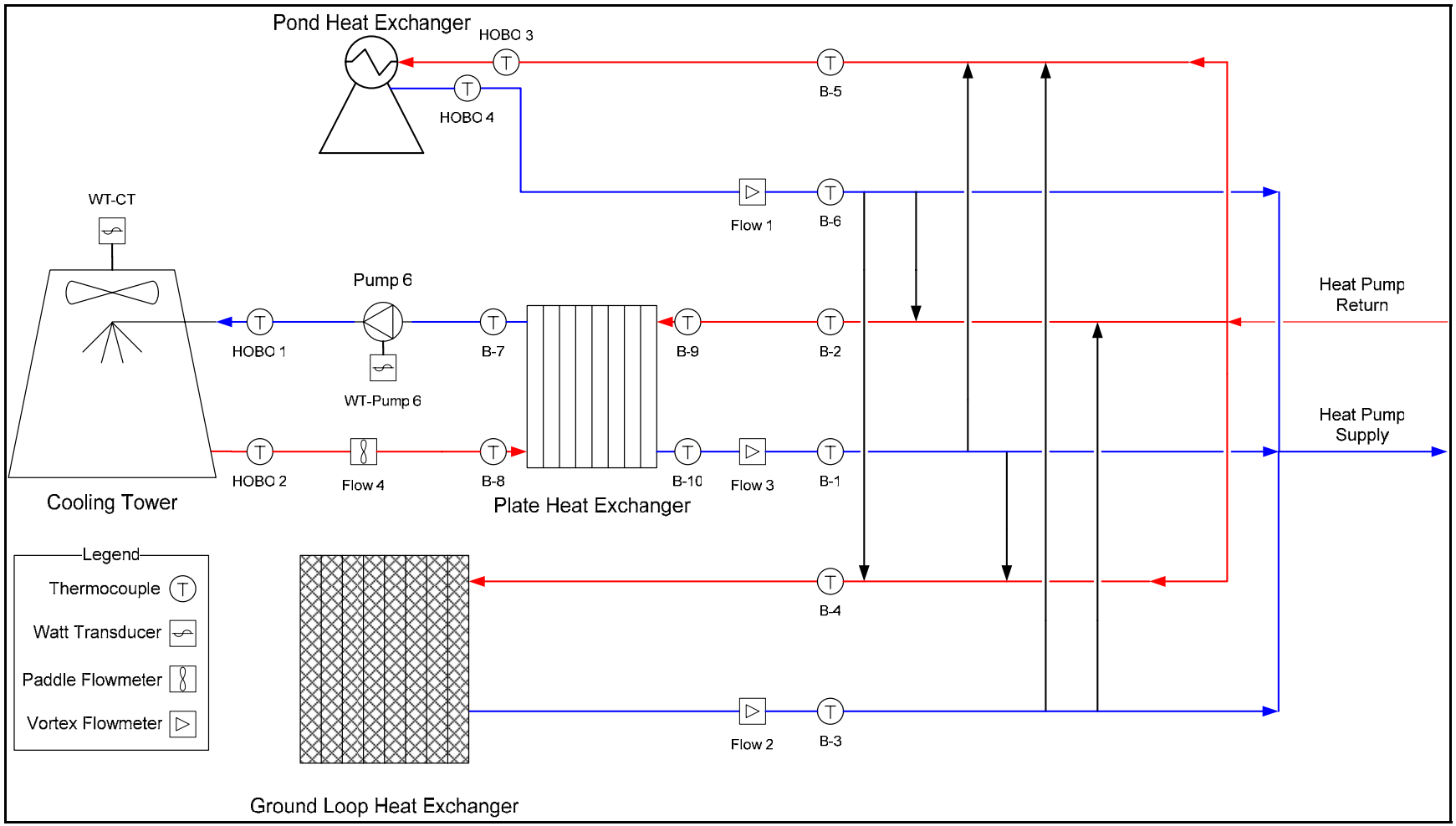

Figure 5.1 – Source Instrumentation Schematic

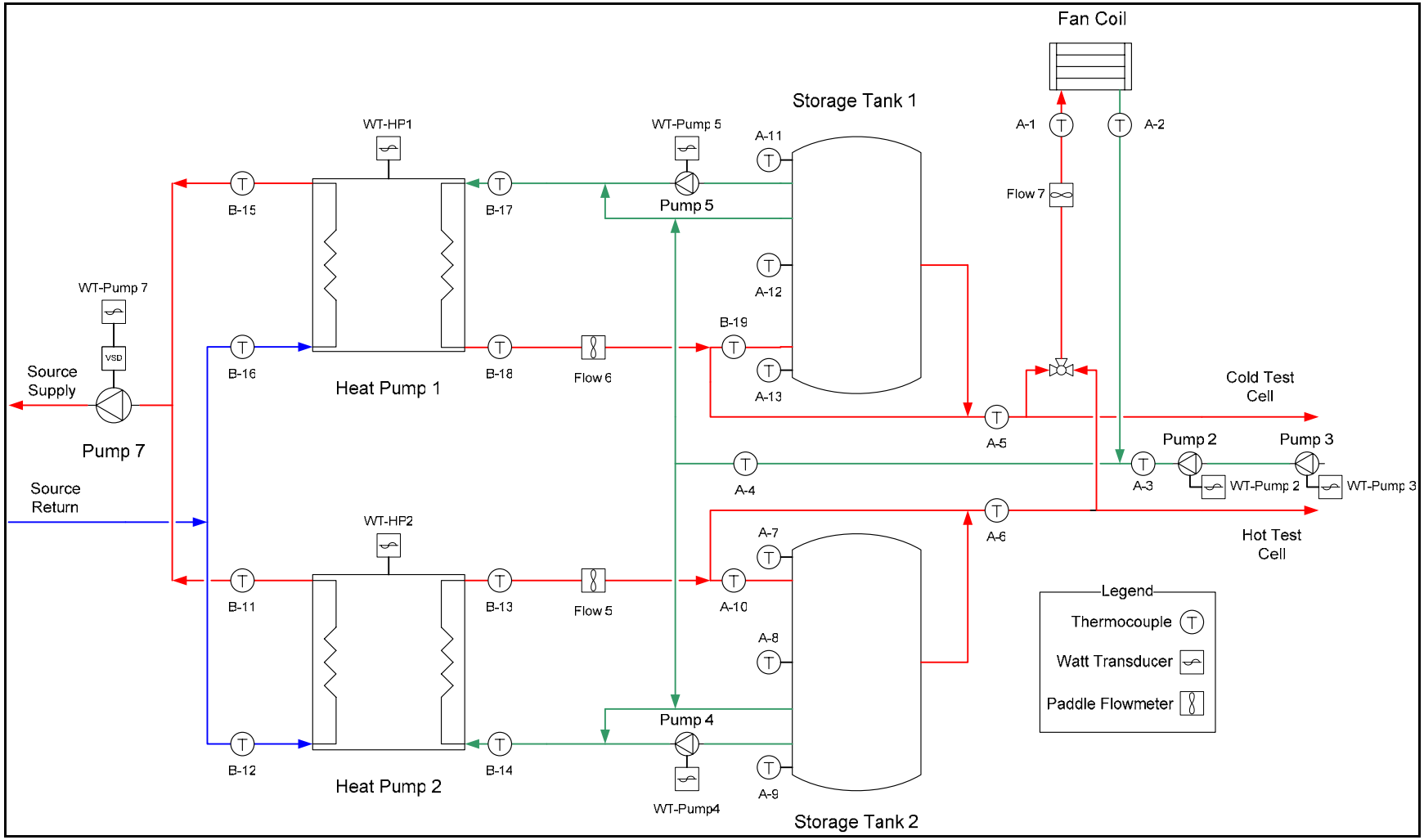

Figure 5.2 – Load and Primary Equipment Instrumentation Schematic

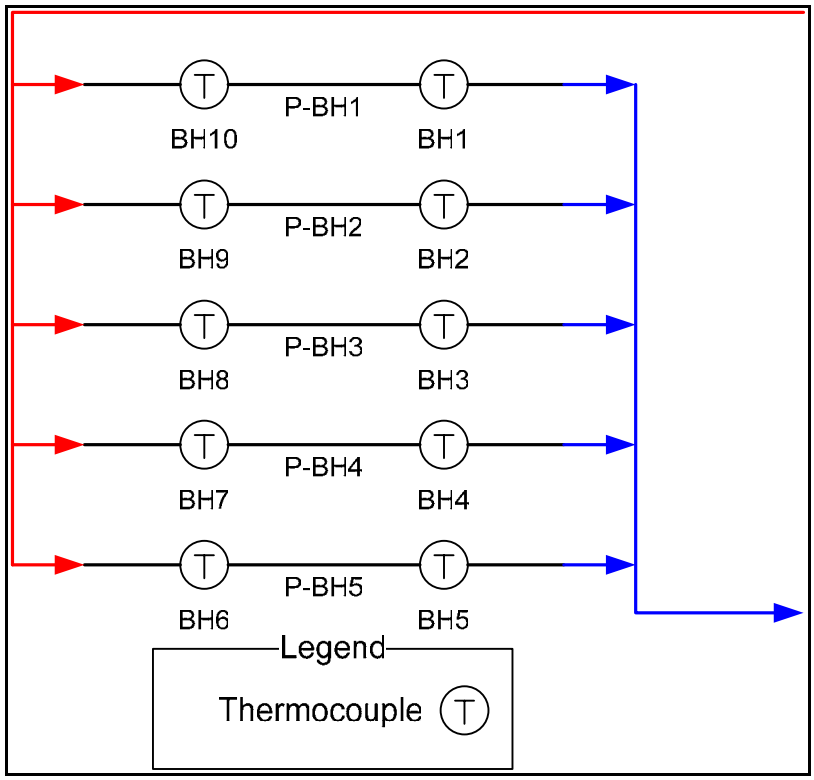

Figure 5.3 – Borehole Instrumentation Schematic

5.1.1 Data Acquisition Unit

Three Fluke/NetDAQ 2640 data loggers are used to collect temperature and DC voltage data. To facilitate thermocouple use, the Fluke/NetDAQ cold junction compensation provides an isothermal connection box so that the reference junctions are at approximately the same temperature for all thermocouples. The NetDAQ can be connected to a host computer through an isolated or general network. NetDAQ Logger software installed on the host computer allows for Dynamic Data Exchange to other Windows application for real time display. Figure 5.4 shows the data acquisition system, configured for 60 channels of data. The system can be easily extended by installing additional 20 channel NetDAQs.

Figure 5.4 – Data Acquisition System

A software program was developed to provide a graphical interface for viewing and recording incoming data. The program was developed in Excel and makes use of Dynamic Data Exchange from the NetDAQ logger software. The program includes many features that make operating the system efficient and user friendly. The interface displays a schematic of the system and the position of the instrumentation. This allows the user to quickly scan the system and make sure that it is operating properly. An example of the interface can be seen in Figure 5.5. A record feature saves the current reading values from the data logger on a time interval set by the user.

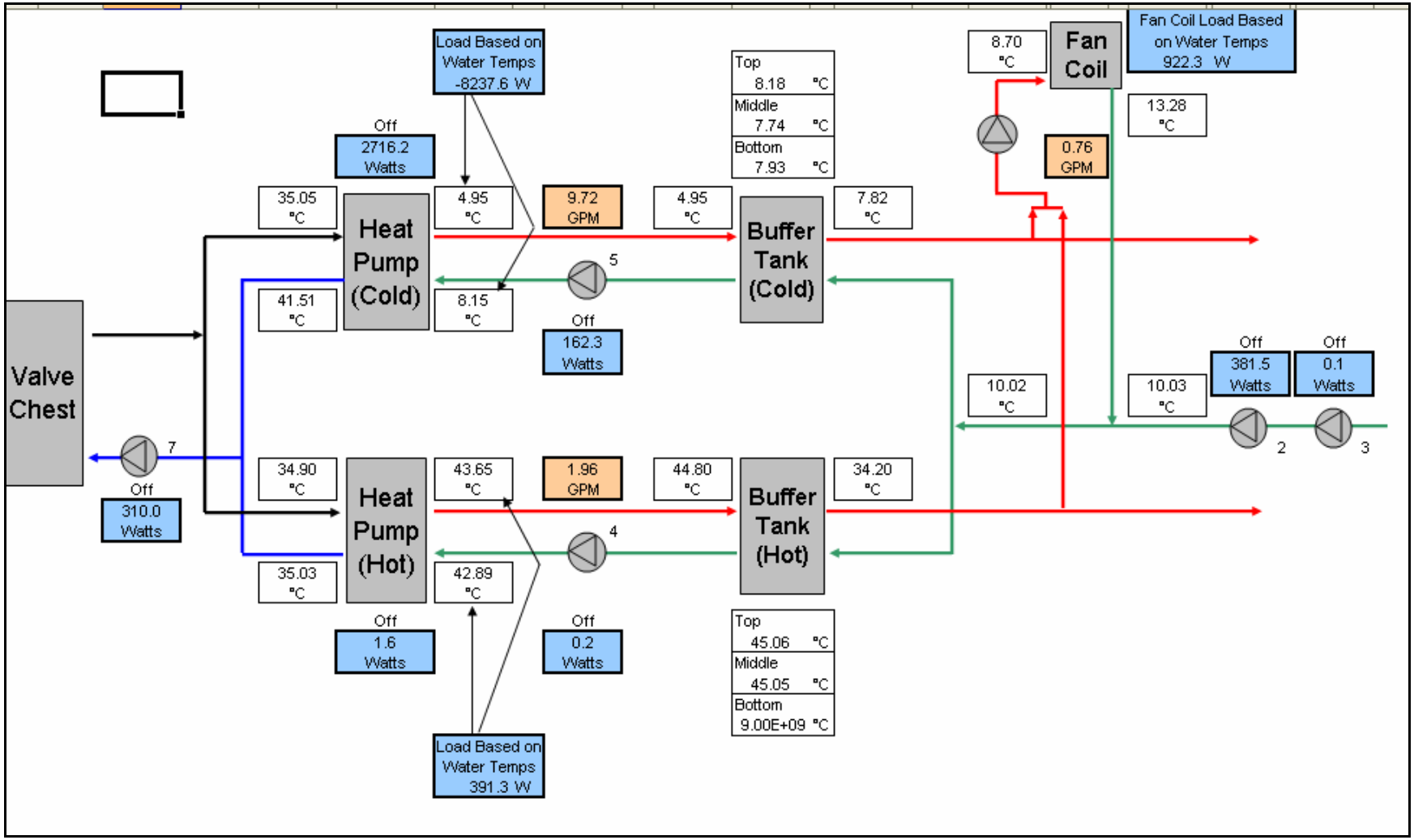

Figure 5.5 – Graphical User Interface

5.1.2 Thermocouples

Thermocouple probes are located throughout the system as shown in Figure 5.2. OMEGA HTMQSS-125G-6 immersion probes are used for water temperature measurements. These probes are a type T thermocouple and have a 6 in. (0.15 m) stainless steel protective sheath with a grounded thermocouple which increases its thermal response time. The probes are inserted into the piping system through Watts Hydronic Heating Specialties Series TP-N temperature test plugs. The test plugs consists of a neoprene washer that around the thermocouple probe.

The large storage tanks are instrumented with three thermocouple probes inserted into the tanks at the top, bottom, and middle elevations. OMEGA T-type industrial thermocouples NB1-CPSS-18G-18 were chosen for the tanks. These thermocouples contain a thermocouple grounded to a stainless steel sheath. A cast iron head with an internal terminal block is used to protect the extension wire connection.

Multi-pair thermocouple extension wire was used to gather temperature measurements from the borehole and also to facilitate organized installation of the thermocouples in the plant area. The extension wire was purchased from Technical Industrial Products (part number MPW-T-20-PP-24S). The wire is T type, 24 gauge, stranded extension grade with a polyvinyl jacket covering each wire and an outer jacket covering the entire 20 pair assembly. The assembly is also covered with an aluminized mylar shield and a ground wire. In the plant area, the multi-pair cable was attached to two 20 pair phenolic terminal strips as shown in Figure 5.6.

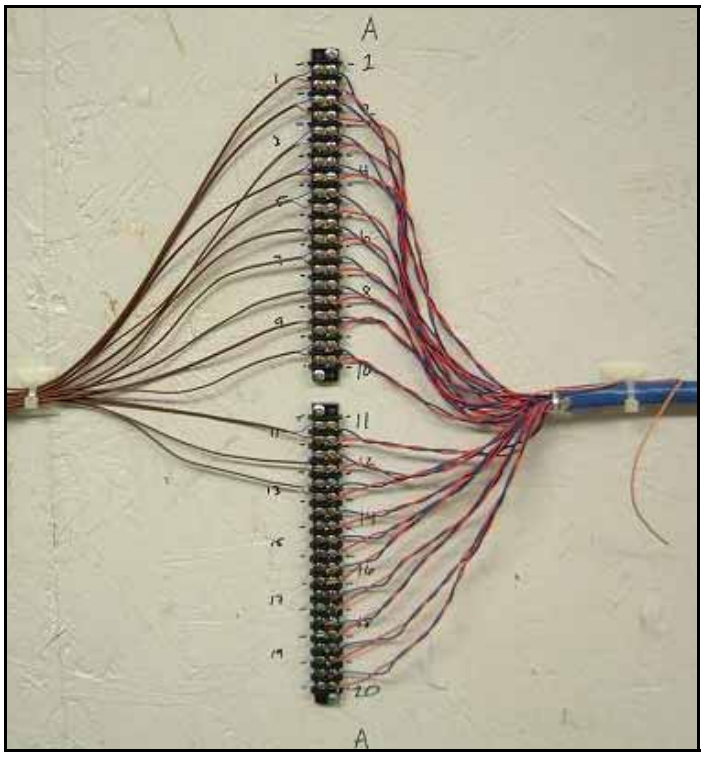

Figure 5.6 – Multi-pair Thermocouple Wire.

Pelican Wire Company T type, 24 gauge thermocouple wire with FEP insulation was used to make the final connections to the thermocouple probes. It was also used to measure the outdoor temperature.

5.1.3 HOBO Data Logger

To eliminate long lengths of thermocouple extension wire, portable HOBO H8 data loggers from Onset were chosen to measure the temperature at the pond loop heat exchanger and the cooling tower. The H8 data logger is a self contained data logger unit that can accept a variety of external sensors and has a user-selectable sampling interval. A TCM6-HC stainless steel temperature probe was selected for use with the H-8 data logger. The temperature probe has an un-calibrated accuracy of ± 0.9°F at 68°F (± 0.5°C at 20°C) with a resolution of 0.7°F at 68°F (0.41°C at 20°C).

5.1.4 Vortex Flowmeters

Three vortex flowmeters (model V1-M1-A075F25-E1-X1-15GPM from ASAHI/America) were installed in the system as shown in Figure 5.1. This model provides a 4 to 20 mA output corresponding to a flow rate from 0 to 15 gpm with an accuracy of ± 1.0% of the full-scale range and a repeatability of ± 0.25%. The 0.75-in body size allows for enough system backpressure to prevent cavitation while imposing a pressure drop of 0.8 ft of head for a flow rate of 10 gpm. To ensure accurate flow measurement, a straight length of 20 pipe diameters was installed upstream of the flowmeter and a straight length of 7 pipe diameters was installed downstream. Unions were then placed at the ends of the pipes so that the flowmeters could be easily removed for repair or replacement.

5.1.5 Paddle Wheel Flowmeters

A Gems Sensors RFA-2500 Series Continuous Output RotoFlow paddle wheel flowmeter is used in the locations as shown in Figure 5.2. This flowmeter utilizes a hall-effect sensor to measure fluid flow rate. It has a brass body that houses a magnetized composite rotor and electronics that are covered by a polysulfone lens. Fluid flow turns the rotor and produces an analog 0-10 Vdc proportional to the flow rate for each specified unit. The flow meter has an operating temperature range of -20 to 212°F (-29 to 100°C). An un-calibrated unit has an accuracy of ± 7-15% dependent on the unit size. The manufacturer recommends placing 8 in of straight pipe before the flowmeter. Each flowmeter was installed in an assembly using the same specifications previously discussed for the vortex flowmeters.

5.1.6 Watt Transducers

Watt transducers measure power input to critical system components as shown in Figure 5.2. The watt transducers are Ohio Semitronics GW5 precision units. These units were selected because they are self powered and include an internal current sensor which facilitates placement in a confined area as shown in Figure 5.7.

Figure 5.7 – Watt Transducer Box

These units have an accuracy of $\pm 0.04\%$ the full scale of the unit or $\pm 0.2\%$ of the reading maintained over a wide temperature range. Output for the models used is a 0-10 Vdc proportional to the full scale watt range. The model numbers and specifications can be seen in Table 5.1.

Table 5.1 – Watt Transducer Specifications

Unit	Model #	Watt Range	Voltage (Vac)	Amps	Phase
WT-Pump 2	GW5-001C	0-500	85-135	0-5	1
WT-Pump 3	GW5-001C	0-500	85-135	0-5	1
WT-Pump 4	GW5-001C	0-500	85-135	0-5	1
WT-Pump 5	GW5-001C	0-500	85-135	0-5	1
WT-Pump 6	GW5-001C	0-500	85-135	0-5	1
WT-Pump 7	GW5-005C	0-2000	200-280	0-5	3
WT-HP 1	GW5-020CY148	0-5000	200-280	0-25	1
WT-HP 2	GW5-020CY148	0-5000	200-280	0-25	1
WT-CT	GW5-002C	0-1000	200-280	0-5	1

5.1.7 Relative Humidity Sensor

An OMEGA HX302C relative humidity sensor measures the outdoor relative humidity. This sensor is in a sealed unit that can be installed outdoors and uses a thin film capacitor to measure humidity. The unit has a signal output of 4-20 mA for a range of 0-100% relative humidity with an accuracy of ± 2.5% at 77°F (25°C). It was installed on the plant building underneath the roof overhang to protect it from rain.

5.2 Controls

5.2.1 Overview of Controls System

The main objective in designing the control system for the test facility was to provide a flexible and programmable control system. This allows future researchers the opportunity to add new features and control schemes to the test facility. To achieve this goal, the system was designed in two parts: the hardware and software. The hardware uses a computer with a digital input/output (I/O) board to control various solid state relays. Each solid state relay completes an electrical circuit which provides power to the system equipment. An electrical safety interlock is included in the system to shut down

the system in the event that the control computer fails. The software consists of a program that is used to monitor and control the output of the I/O board. The control program interfaces with the data acquisition system discussed in section 5.1.1. Each part of the control system is described in detail in the following sections.

5.2.2 Controls Hardware

The hardware used to control the equipment in the system consists of four main components: the I/O board, control signal/power boards, solid state relays, and the timer board. Component layout is shown in Figure 5.8.

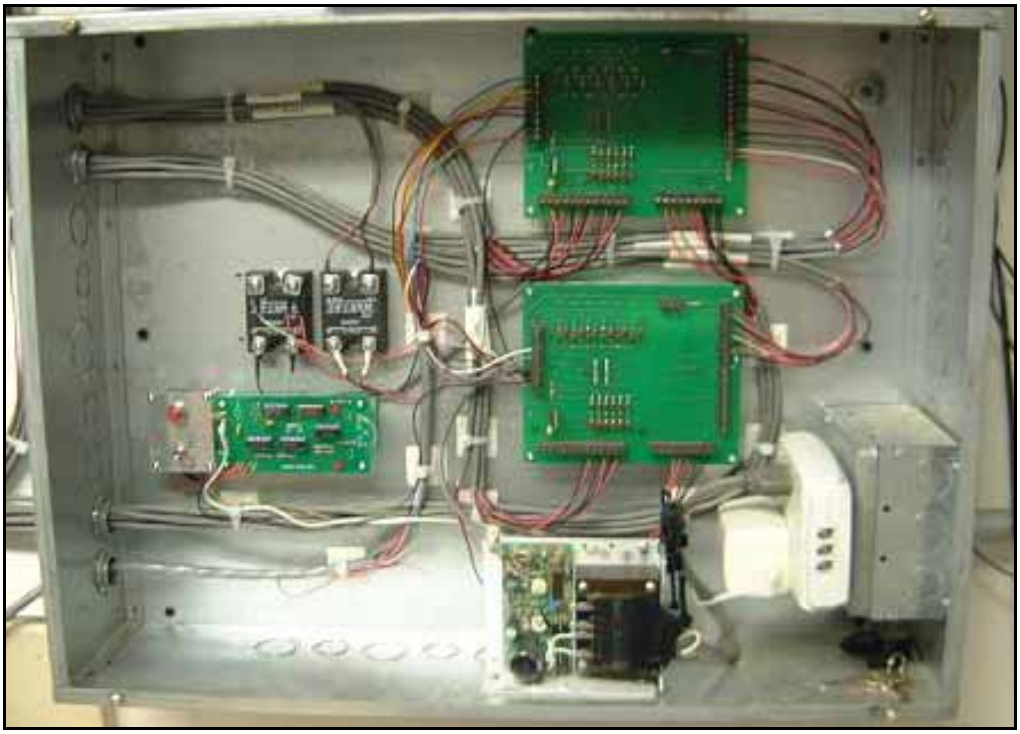

Figure 5.8 – Control Circuit Board Box

Crydom CSD2425 solid state relays were installed inline for the circulating pumps, the two heat pumps, and the cooling tower. These relays have a load operating voltage of 24-280 Vac with a current capacity up to 25 A. A control input voltage of 3.5-15 Vdc activates the relay. A Crydom DC60S7 relay is used to start the VFD and the

timer board as shown in Figure 5.9. This relay will switch a 3-60 Vdc load with an input of 3.5-32 Vdc to close the relay.

A digital I/O board, model number PCI-DIO24 board from Measurement Computing, is installed in the data acquisition computer. The I/O board is interfaced to the PCI bus of the computer, and its 24 I/O channels are accessible through the board's standard 37-pin connector. This I/O board outputs a control signal to a control signal/power board shown in Figure 5.9. The control signal/power board, as shown in Figures 5.10 and 5.11, conditions each I/O channel signal through a buffer chip (74C902) which is used to ensure that the solid state relays controlled by the I/O card receive the proper voltage and current. To safeguard against unwanted input signals, each channel is tied to a pull down resistor. This maintains each channel in the normally open position unless the channel is energized with the I/O board. To provide a quick visual check of active channels, LED's on the circuit board are lit with the output signal transmitted from the I/O board for each channel. This board also includes connections for the flowmeters and relative humidity sensor. A 24 Vdc power supply is attached to the board from which the flowmeter and relative humidity sensor can draw power. The output signal is then returned to the board and passed on to the data logger.

A timer board, as shown in Figure 5.12, monitors an event control pulse sent from the data acquisition computer every few seconds. The pulse is used to keep a model CD4040 counter reset. In the event the computer hangs, and the control pulse is not received in approximately 1.5 minutes, the counter will count up until line Q14 on the counter goes high. Q14 triggers an astable multivibrator made from the model CD4013 chip. When this occurs, the output signal of the CD4013 is latched high which opens a

solid state relay which supplies 24 Vdc to operate the control signal/power board as shown in Figure 5.9. With no input power to the signal/power board, all digital outputs are forced to ground through pull down resistors and the circuits for all equipment are opened, interrupting power. The latch on the timer board must be manually reset with a momentary switch on the timer board to resume normal operation. Another double pole single throw switch allows a 'test' mode which disables the timer board for troubleshooting and a 'run' mode for normal operation.

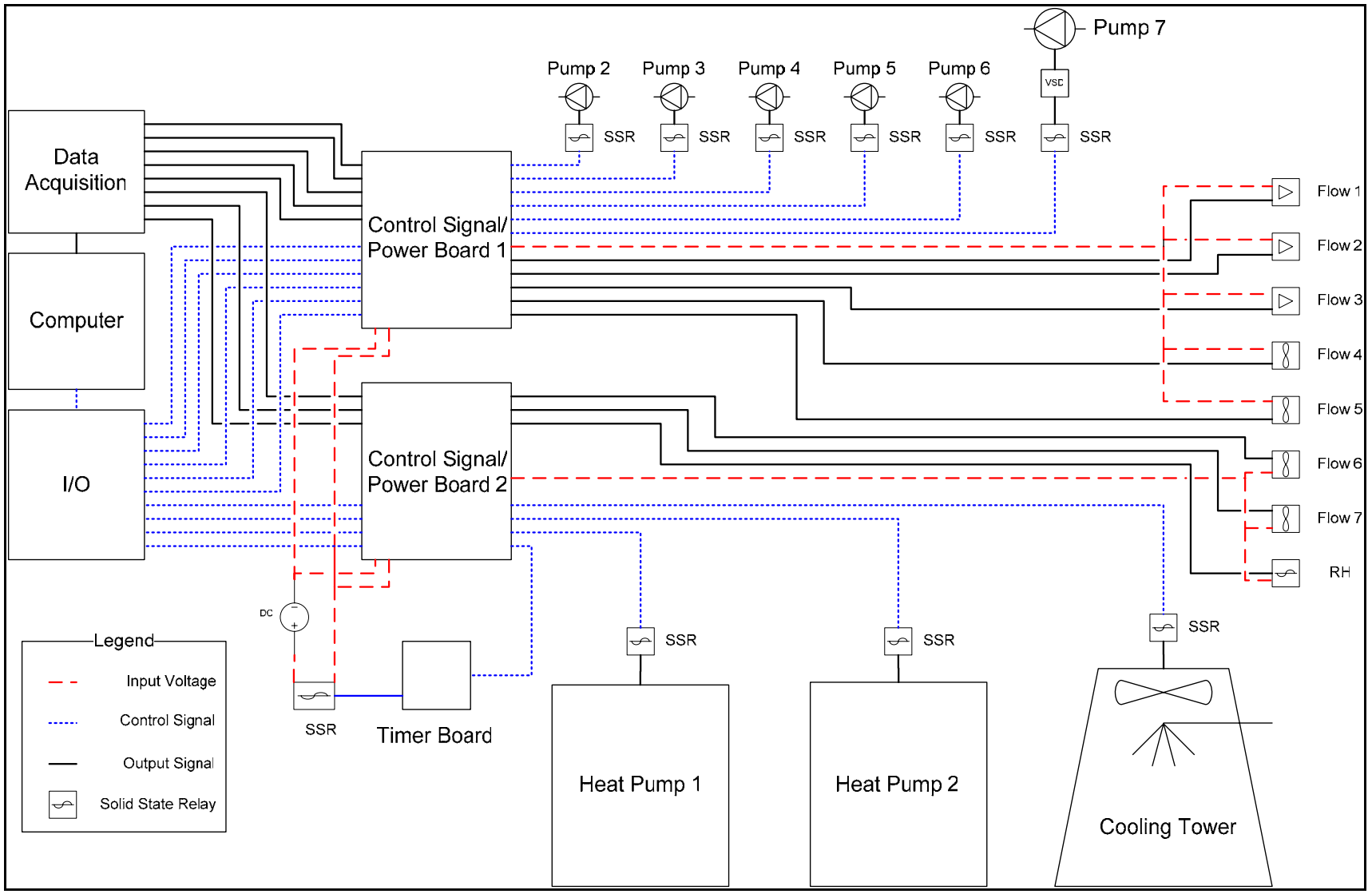

Figure 5.9 – Control Hardware Wiring Schematic

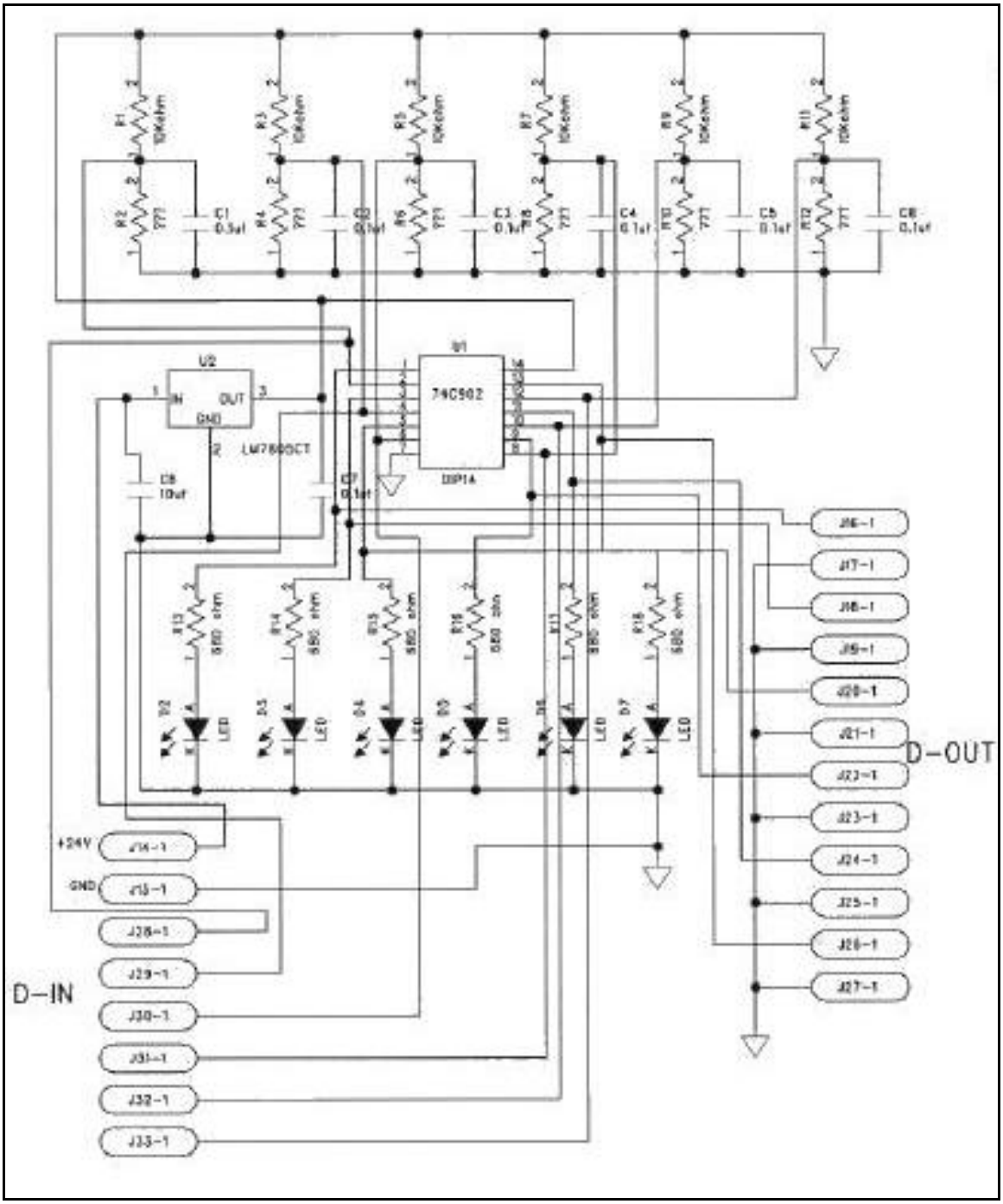

Figure 5.10 – Control Signal/Power Board Schematic (1)

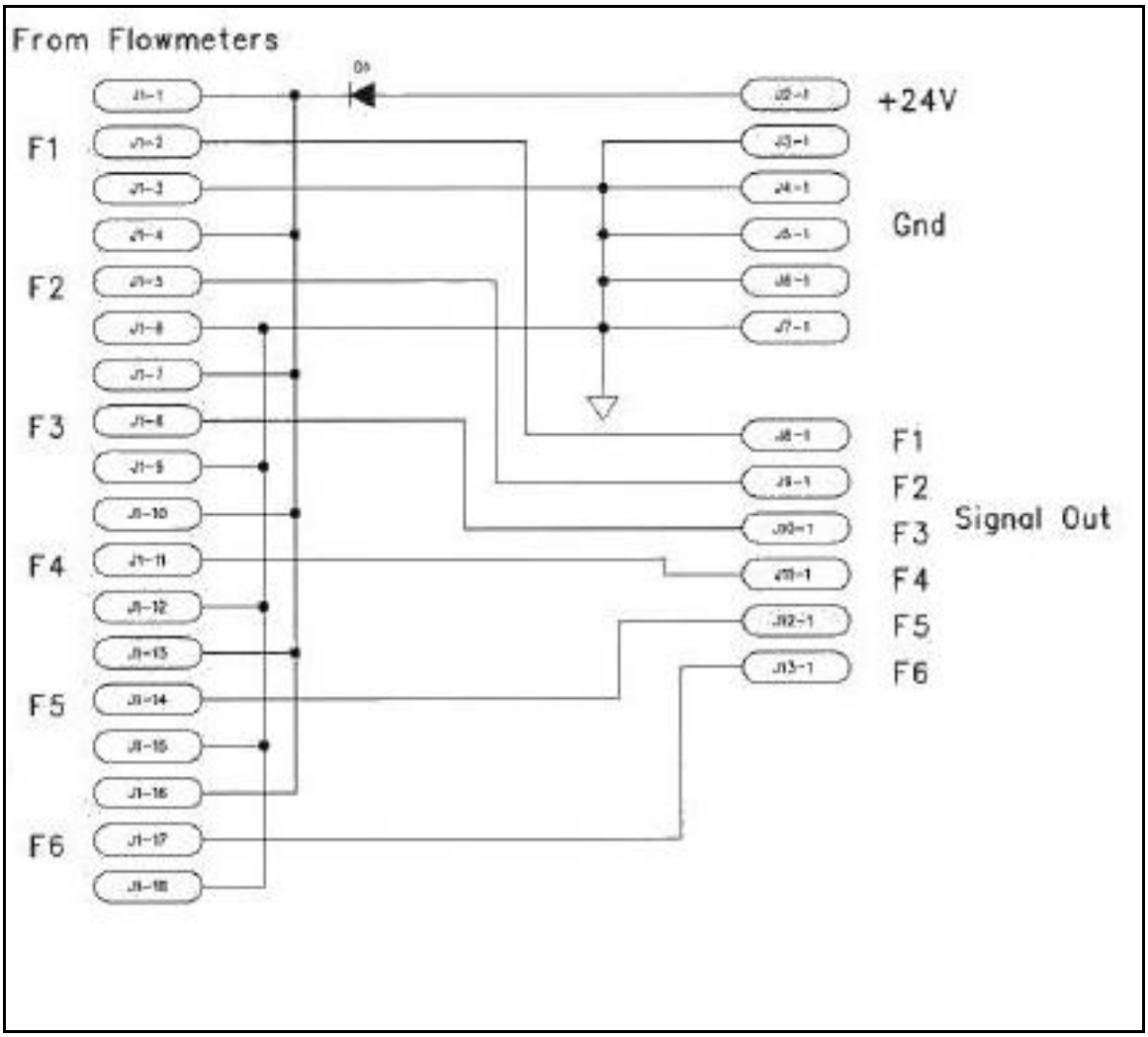

Figure 5.11 – Control Signal/Power Board Schematic (2)

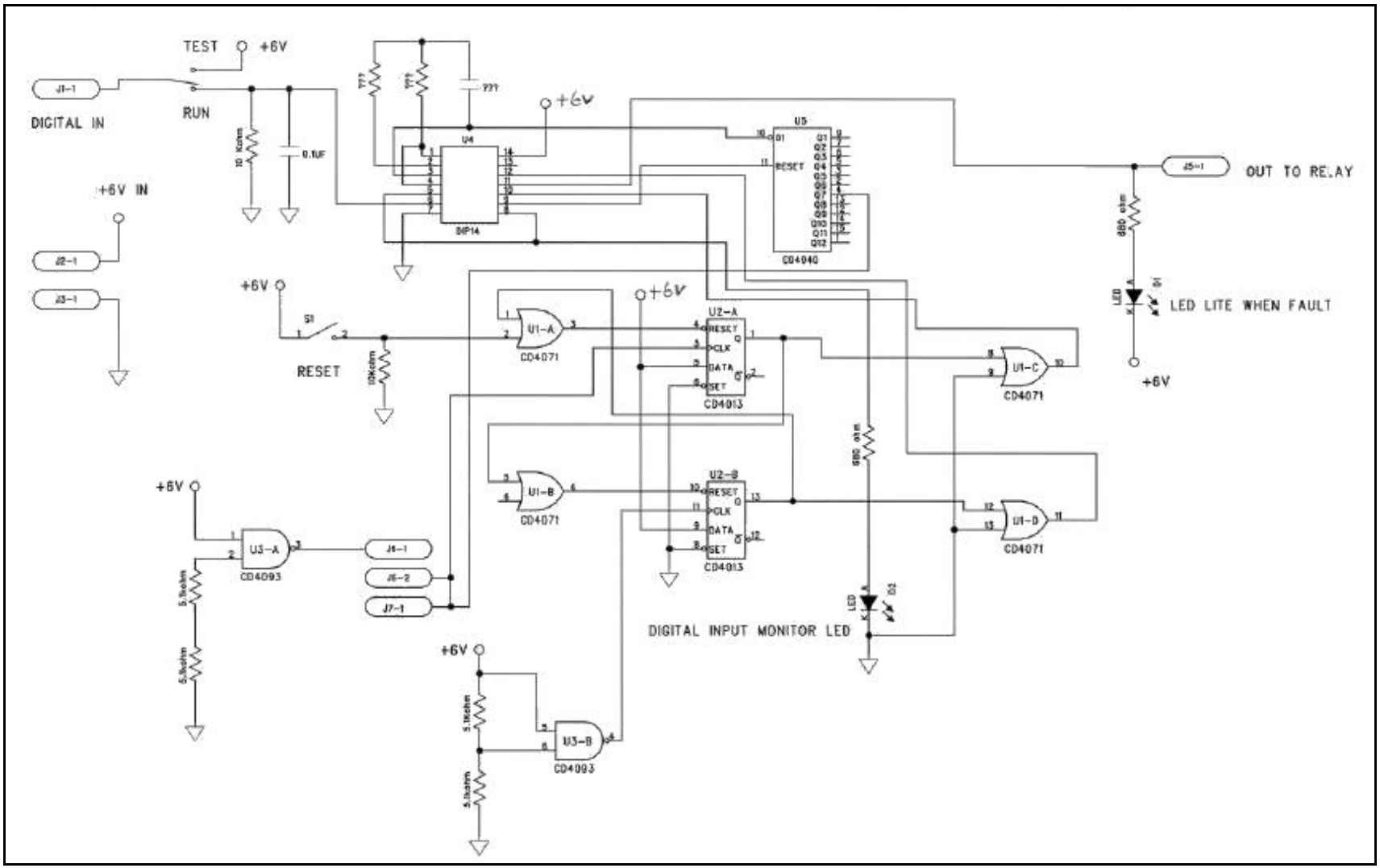

Figure 5.12 – Timer Board Schematic

6. Instrumentation Calibration and Uncertainty Analysis

The uncertainty in calculated results is related to the primary uncertainty for each independent variable. This is based on the method of Kline and McClintock (1953) which state:

$$e_R = \sqrt{\left(\frac{\partial R}{\partial x_1} e_1\right)^2 + \left(\frac{\partial R}{\partial x_2} e_2\right)^2 + \ldots + \left(\frac{\partial R}{\partial x_n} e_n\right)^2} \qquad (6.1)$$

Where:
R is the calculated results, $R = R(x_1, x_2, .. x_n)$
e_R is the uncertainty interval in the result
e_i is the uncertainty interval in the i^{th} variable
$\frac{\partial R}{\partial x_i}$ is the sensitivity of the result to a single variable, x_i

In the following sections this method is applied to primary temperature and flowrate measurements and calculated heat transfer rates.

6.1 Instrumentation Calibration and Uncertainty

An in-situ calibration was performed on the thermocouples and flowmeters installed in the facility. The sensors and instruments were calibrated with operating flow conditions, wire lengths and datalogger connections. In-situ calibration curves were generated and an uncertainty analysis was performed for each type of instrument as discussed in the following sections.

6.1.1 Thermocouples

Thermocouples were calibrated using a constant temperature water bath with an operating range of -40 to 302°F (-40 to 150°C) and a temperature stability of ± 0.09°F (0.05°C). The user can set the temperature of the water bath to within 0.18°F (0.1°C).

For calibration purposes the temperature range used was 32 to 140°F (0 to 60°C) with temperature increments of 27°F (15°C).

Each of the thermocouples was placed into the water bath after it had stabilized at a set point temperature for 30 minutes. The channels of each thermocouple were scanned and recorded by the NetDAQ over a period of 10 seconds. Simultaneously values were recorded from a reference thermistor probe. The values for each channel along with the reference thermistor were then average over the 10 second time period. This procedure was repeated for the remaining calibration points.

The NetDAQ logger allows the user to apply a linear correction to each channel. The linear correction takes the form:

$$y = m \cdot x + b \tag{6.2}$$

Where:
x = un-calibrated data logger reading
m = slope coefficient
b = offset coefficient

The calibration data for each thermocouple channel was used to perform a least squares fit on the m and b coefficients. The coefficients were then applied to each channel and a new set of temperatures determined. Table 6.1 shows the results from an error analysis between the corrected and reference temperature points. Data from the analysis shows that the linear correction provided an excellent fit to the reference temperature points.

Table 6.1 – Thermocouple Calibration Results

Channel	*m*	*b*	High	Low	Average	RMS
A1	0.998	-0.135	0.24	0.00	0.08	0.12
A2	0.993	-0.179	0.19	0.00	0.09	0.12
A3	0.994	-0.197	0.13	0.00	0.07	0.09
A4	0.992	-0.242	0.13	0.02	0.07	0.09
A5	0.989	-0.233	0.08	0.00	0.04	0.05
A6	0.990	-0.193	0.12	0.02	0.08	0.09
A7	0.990	-0.219	0.09	0.01	0.05	0.06
A8	0.995	-0.244	0.12	0.01	0.06	0.07
A9	0.987	0.041	0.11	0.01	0.06	0.08
A10	0.991	0.110	0.06	0.01	0.04	0.05
A11	0.993	0.258	0.16	0.02	0.07	0.09
A12	0.994	0.037	0.22	0.01	0.09	0.12
A13	0.993	0.130	0.12	0.01	0.06	0.07
B1	0.992	0.007	0.05	0.01	0.03	0.03
B2	0.990	0.042	0.05	0.02	0.03	0.03
B3	0.990	0.075	0.05	0.01	0.03	0.03
B4	0.990	0.022	0.06	0.00	0.03	0.04
B5	0.989	-0.002	0.02	0.00	0.01	0.02
B6	0.990	0.003	0.04	0.01	0.02	0.02
B7	0.990	0.015	0.06	0.00	0.02	0.03
B8	0.991	-0.051	0.02	0.00	0.01	0.01
B9	0.991	-0.086	0.03	0.00	0.02	0.02
B10	0.995	0.017	0.05	0.00	0.03	0.03
B11	0.991	0.336	0.09	0.03	0.05	0.06
B12	0.995	-0.097	0.04	0.00	0.02	0.03
B13	0.990	0.230	0.07	0.03	0.05	0.05
B14	0.993	-0.019	0.06	0.01	0.04	0.04
B15	0.993	-0.034	0.06	0.00	0.03	0.04
B16	0.990	0.376	0.08	0.01	0.04	0.05
B17	0.993	0.015	0.05	0.01	0.03	0.04
B18	0.993	-0.006	0.05	0.01	0.02	0.03
B19	0.997	-0.044	0.06	0.01	0.03	0.04
B20	0.985	0.728	0.12	0.01	0.05	0.06
BH1	0.988	0.023	0.06	0.01	0.04	0.04
BH2	0.991	-0.137	0.09	0.00	0.04	0.04
BH3	0.991	-0.250	0.11	0.02	0.05	0.06
BH4	0.991	-0.134	0.09	0.01	0.05	0.05
BH5	1.020	-0.541	0.24	0.01	0.11	0.12
BH6	0.991	-0.144	0.06	0.01	0.04	0.04
BH7	0.991	-0.122	0.09	0.00	0.04	0.05
BH8	0.993	-0.122	0.05	0.01	0.03	0.03
BH9	0.991	-0.044	0.07	0.01	0.05	0.05
BH10	0.993	0.040	0.04	0.01	0.03	0.03

The water bath reference temperature was calculated as the average of a Hart Scientific 1504 Thermometer readout and a Hart Scientific 5610 reference thermistor probe. The 1504 is a high-accuracy digital thermometer readout designed to be used with various thermistor or RTDs and has a temperature resolution of 0.0001°F (0.0001°C) and a temperature accuracy of:

$$e_{T1504} = \pm 0.01°C, \text{ measuring between 0 and } 75°C$$

The 5610 reference thermistor probe is a 6 in. (0.15 m) immersion probe with a stainless steel protective sheath. The probe comes with a NIST-traceable calibration curve and has a temperature accuracy of:

$$e_{T5610} = \pm 0.015°C, \text{ measuring between 0 and } 100°C$$

The total uncertainty in the reference temperature measurement is then:

$$e_{TRef} = \pm\sqrt{(0.01)^2 + (0.015)^2} = \pm 0.018°C$$

For the HOBO sensor, the total uncertainty for the reference temperature measurement is smaller than the resolution of the data logger which is:

$$e_{THOBO} = \pm 0.41°C, \text{ at } 20°C$$

With the values from the cold temperature bath averaged over a time period, a repeatability test was performed using two thermocouple probes at three points throughout the calibration range. The thermocouple probes were placed into the water bath for a one minute period while the data logger recorded on a one second interval. Each thermocouple was then removed for 20 seconds and returned to the water bath. This process was repeated three times for each of the temperature set points. The temperature data was then average and analyzed over the three time periods. Table 6.2 shows the time average values obtained from the data.

Table 6.2 – Repeatability Temperature (°C)

	Probe 1	Probe 2	Probe 1	Probe 2	Probe 1	Probe 2
Test 1	0.27	0.15	30.33	30.22	60.36	60.22
Test 2	0.25	0.18	30.32	30.22	60.35	60.23
Test 3	0.25	0.14	30.33	30.22	60.36	60.27

Studying the data shows an error due to the repeatability of temperature measurements. This error can add to the uncertainty of the temperature measurements and can be defined as the largest temperature difference between repeated tests. With this criterion, the repeatability error is:

$$e_{T\_repeat} = \pm 0.04°C$$

Figure 6.1 shows the raw test data for a set point temperature. Temperature points measured for each of the thermocouples bounced around a range of $\pm$ 0.1°C. With the current data acquisition system, data points are recorded at a user specified interval instead of time averaging the values between each logging event. This introduces further error into the calibration giving:

$$e_{T\_stability} = \pm 0.1°C$$

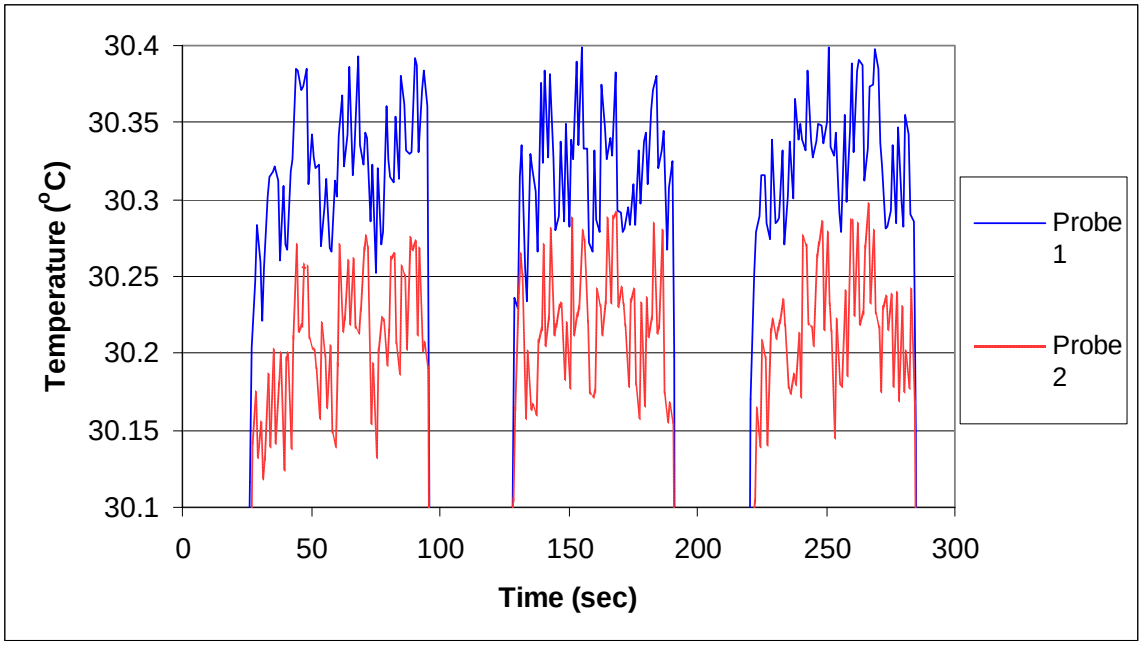

Figure 6.1 – Temperature Stability

Adding the total uncertainty for the Fluke temperature measurement gives:

$$e_{TFluke} \approx \sqrt{\left(e_{TRef}\right)^2 + \left(e_{T\_repeat}\right)^2 + \left(e_{T\_stability}\right)^2} \approx \sqrt{(0.018)^2 + (0.04)^2 + (0.1)^2} \approx 0.11°C$$

For the HOBO datalogger the total uncertainty is:

$$e_{THOBO} \approx \sqrt{\left(e_{TRef}\right)^2 + \left(e_{T\_repeat}\right)^2 + \left(e_{T\_stability}\right)^2 + \left(e_{THOBO}\right)^2}$$

$$e_{THOBO} \approx \sqrt{(0.018)^2 + (0.04)^2 + (0.1)^2 + (0.41)^2} \approx 0.42°C$$

6.1.3 Flowmeters

The flowmeters are calibrated in-situ using a stopwatch, bucket, and precision weight scale. Performing the tests in-situ accounts for the dynamics of the system at each flowmeter and increases the accuracy achieved during calibration. First, the empty bucket is placed on the weight scale and is zeroed. One person then starts the data logger that scans the channel to which the flowmeter is connected. An outlet valve to the piping system is then adjusted until the desired flow rate is reached. The stopwatch and water

flow is started simultaneously and the bucket is filled to a predetermined point. Once this point is reached, the stopwatch and water flow is stopped and the bucket is weighed and the value recorded. The recorded information for each point is then used to calculate the actual flow rate given by the equation:

$$\dot{V} = \frac{m_w \cdot 448.98}{t \cdot \rho_w} \tag{6.3}$$

Where 448.98 is a unit conversion factor and:
$\dot{V}$ = volumetric flow rate of water, gpm
m_w = mass of water, lbm
t = time, seconds
ρ_w = density of water, lbm/ft^3

The values recorded for the data logger are averaged for each calibration point. The linear correction given by Equation 6.2 is used and least squares fit performed on the calibration data to obtain the *m* and *b* coefficients for each flowmeter. Table 6.3 shows an error analysis performed on the corrected flow rate values to ensure that the linear correlation matched the measured flow rates. The results of this analysis show that the linear correlation provides a good fit to the measured data.

Table 6.3 – Flowmeter Calibration Results

Channel	*m*	*b*	High	Low	Average	RMS
Flow 1	2.133	-4.312	3.33	0.03	0.70	1.01
Flow 2	2.133	-4.407	1.68	0.001	0.64	0.81
Flow 3	1.744	-3.470	4.69	0.07	0.89	1.34
Flow 4	2.379	1.782	4.69	0.03	1.48	1.93
Flow 5	2.347	1.894	4.27	0.11	1.10	1.61
Flow 6	2.238	1.590	1.86	0.07	0.69	0.87
Flow 7	0.957	0.732	5.25	0.09	1.95	2.57

The scale used for calibration was an A&D EP-20KA precision industrial balance. This balance has a resolution of 0.005 lbs with an accuracy of:

$$e_{m_w} = \pm 0.01$$

A stop watch with a resolution of 0.01 seconds was used to record the time. An estimated accuracy for the time measurement due to human error is:

$$e_t = \pm 0.5$$

The accuracy of voltage measurements associated with the Fluke/NetDAQ 2640 dataloggers is:

$$e_{Vfluke} = \pm\ 0.042\% + 3.9\ \text{mV}$$

The total uncertainty in the flowrate measurement can then be found by calculating the partial derivatives in terms of m_w and t for equation 6.3, which are:

$$\frac{\partial \dot{V}}{\partial m_w} = \frac{448.98}{t \cdot \rho_w}$$
$$\frac{\partial \dot{V}}{\partial t} = -\frac{448.98 \cdot m_w}{t^2 \cdot \rho_w}$$

Therefore, the uncertainty in flow rate is:

$$e_{\dot{V}} \approx \pm \sqrt{\left(\frac{448.98}{t \cdot \rho_w} \cdot 0.01\right)^2 + \left(\frac{-448.98 \cdot m_w}{t^2 \cdot \rho_w} \cdot 0.5\right)^2 + \left(0.00042 \cdot V_{Fluke} + 0.0039\right)^2} \quad (6.4)$$

Where:
V_{Fluke} = voltage measurement at Fluke, Vdc

A second order polynomial was fit to the calculated uncertainty of equation 6.4 for the range of calibrated flow rates. This allows the uncertainty to be easily calculated for any flow rate. Two equations are given for the different flowmeters, as they each have a specified uncertainty.

$$e_{\dot{V}\_Paddle} = 0.00217\left(\dot{V}\right)^2 - 0.00042\left(\dot{V}\right) + 0.00525 \quad (6.5)$$

$$e_{\dot{V}\_Vortex} = 0.00191\left(\dot{V}\right)^2 - 0.00008\left(\dot{V}\right) + 0.00044 \quad (6.6)$$

Where:
$\dot{V}$ = flow rate of water, gpm

6.1.4 Watt Transducer

The watt transducers installed in the system measure the power used by the cooling tower, circulating pumps, and heat pumps. These watt transducers are calibrated from the factory and are NIST traceable. This accuracy is decreased with the uncertainty added by the Fluke/NetDAQ logger which is:

$$e_{Vfluke} = \pm 0.042\% + 3.9 \text{ mV}$$

The Fluke/NetDAQ uncertainty can then be converted for any instrument that uses an output voltage signal to correspond to a measurement range. A general equation for this conversion is given by:

$$e_{VFluke} = \frac{\left(0.00042 \cdot V_{Fluke} + 0.0039\right) \cdot \Delta Range}{\Delta V} \tag{6.7}$$

Where:
V_{Fluke} = voltage measurement at Fluke, Vdc
Δ_{Range} = measurement range of instrument
ΔV = output signal range

The power drawn by the constant speed circulating pumps are measured with an Ohio Semitronics GW5-001C watt transducer. This transducer has an accuracy of $\pm$ 0.2 W, and an output signal of 0 to 10 Vdc for a 0 to 500 W range. Therefore, the largest uncertainty introduced from the data logger is:

$$e_{VFluke} = \frac{\left(0.00042 \cdot 10 + 0.0039\right) \cdot 500}{10} = 0.405 \text{ W}$$

The total uncertainty for this watt transducer is:

$$e_{W001} = \pm\sqrt{\left(0.20\right)^2 + \left(0.405\right)^2} = \pm 0.452 \text{ W}$$

An Ohio Semitronics GW5-002C watt transducer is used to measure the power used by the cooling tower. This transducer has an internal sensor that is accurate to within ± 0.4 W. The output signal of the transducer is 0 to 10 Vdc for a 0 to 1000 W range. The uncertainty introduced from the data logger for this measurement is:

$$e_{VFluke} = \frac{(0.00042 \cdot 10 + 0.0039) \cdot 1000}{10} = 0.810 \text{ W}$$

The total cooling tower uncertainty is therefore:

$$e_{W002} = \pm\sqrt{(0.40)^2 + (0.810)^2} = \pm 0.903 \text{ W}$$

The power for the variable speed circulation pump is measured with an Ohio Semitronics GW5-005C watt transducer. It has an accuracy of ± 0.8 W, with an output signal of 0 to 10 Vdc for a 0 to 2000 W range. An uncertainty introduced from the datalogger is:

$$e_{VFluke} = \frac{(0.00042 \cdot 10 + 0.0039) \cdot 1000}{10} = 1.620 \text{ W}$$

The total uncertainty for the variable speed pump is:

$$e_{W005} = \pm\sqrt{(0.80)^2 + (1.620)^2} = \pm 1.807 \text{ W}$$

The heat pumps use an Ohio Semitronics GW5-020C to measure the power drawn during operation. The internal sensor for this transducer is accurate to within ± 2.00 W. The transducer has an output signal of 0 to 10 Vdc with a measurement range of 0-5000 W. The uncertainty introduced from the data logger for this measurement is:

$$e_{VFluke} = \frac{(0.00042 \cdot 10 + 0.0039) \cdot 5000}{10} = 4.050 \text{ W}$$

The total uncertainty in power measurement for the heat pumps is:

$$e_{W020} = \pm\sqrt{(2.00)^2 + (4.050)^2} = \pm 4.517 \text{ W}$$

6.1.5 Relative Humidity Sensor

The relative humidity for the outdoor air is measured with an OMEGA HX302C. The thin film capacitor for this sensor is accurate to within ± 2.5% RH. The sensor output is 4 to 20 mA signal that corresponds to 0 to 100% RH. The output current is sent through a fixed precision 500 ohm resistor. This converts the output signal to a Vdc range of 2 to 10. The data logger introduces an uncertainty of:

$$e_{VFluke} = \frac{(0.00042 \cdot 10 + 0.0039) \cdot 100}{8} = 0.101\% \text{ RH}$$

The total uncertainty for the humidity measurement is:

$$e_{RH} = \pm\sqrt{(2.5)^2 + (0.101)^2} = \pm 2.502\% \text{ RH}$$

6.2 Calculated Heat Transfer Rates

The heat transfer rate is calculated from the measurements of flow rate and the inlet and outlet temperature across various components and pipe sections. The equation takes the form:

$$\dot{Q} = 0.0631 \cdot \rho_w \dot{V} c_p \Delta T \qquad (6.8)$$

Where 0.0631 is a unit conversion factor and:
$\dot{Q}$ = heat transfer rate, W
ρ_w = density of water, kg/m^3
$\dot{V}$ = volumetric flow rate of water, gpm
c_p = specific heat of water, kJ/kg-^{0}C
ΔT = air temperature difference, T_o-T_i

The uncertainty for temperature is obtained in Section 6.1.1 for both the Fluke and HOBO data loggers. Since the uncertainties in temperature are the same at both the inlet and outlet, the uncertainty in the temperature difference is:

$$e_{\Delta T} = \pm\sqrt{(0.11)^2 + (0.11)^2} = \pm 0.16°\text{C}$$

$$e_{\Delta T-HOBO} = \pm\sqrt{(0.42)^2 + (0.42)^2} = \pm 0.59°\text{C}$$

Evaluating the partial derivatives of $\dot{Q}$ in terms of $\dot{V}$ and ΔT gives:

$$\frac{\partial \dot{Q}}{\partial \dot{V}} = 0.0631 \cdot \rho_w c_p \Delta T$$
$$\frac{\partial \dot{Q}}{\partial \Delta T} = 0.0631 \cdot \rho_w c_p \dot{V}$$

Substituting the results into equation 6.8 and using the uncertainty calculated from equations 6.5 and 6.6, the uncertainty for the heat transfer rate is:

$$e_{\dot{Q}} = \pm\sqrt{\left(0.0631 \cdot \rho_w c_p \Delta T \cdot e_{\dot{V}}\right)^2 + \left(0.0631 \cdot \rho_w c_p \dot{V} \cdot e_{\Delta T}\right)^2} \qquad (6.9)$$

7. Experimental Results

7.1 System Performance and Heat Balance

Data was obtained from experiments performed over 24 hour periods and analyzed to validate system performance. Heat transfer rates through system components were determined and compared to catalog data where applicable. Heat losses through the system were also calculated.

7.1.1 Heat Pump

Source side heat transfer rates, load side heat transfer rates and compressor power can be obtained from heat pump instrumentation. This allows for analysis of transient and steady-state operation and the calculation of an overall heat balance for the heat pumps. Each heat pump is thermostatically controlled by the tank temperature. Heat pump 1 was operated in cooling mode, and the data obtained from the experiment can be seen in Figures 7.1 and 7.2.

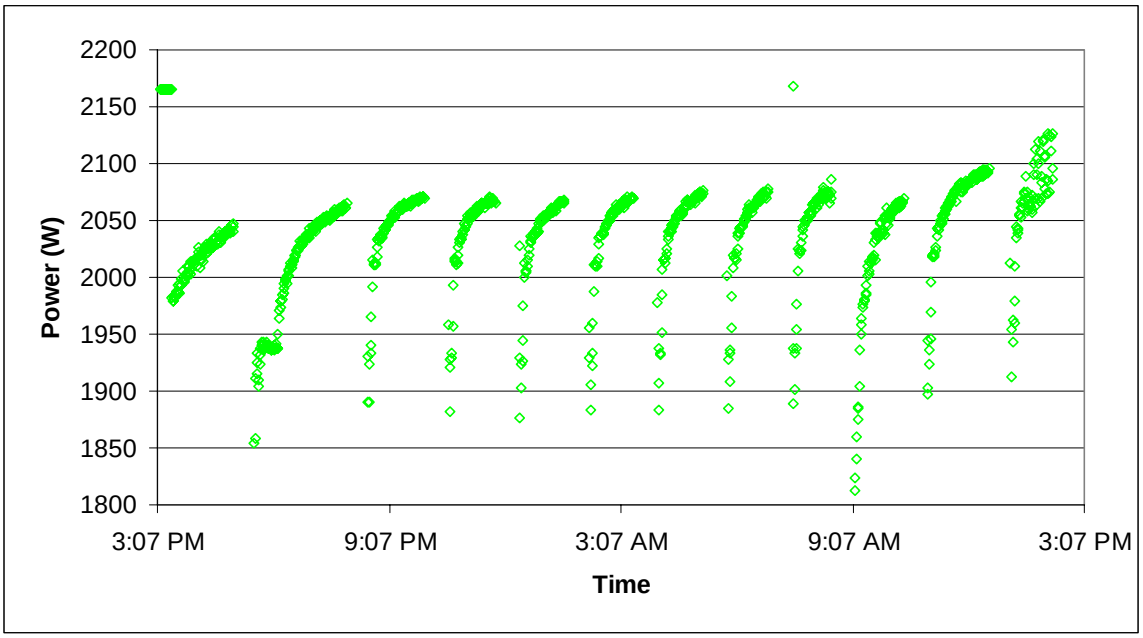

Figure 7.1 – Power Usage for Heat Pump 1

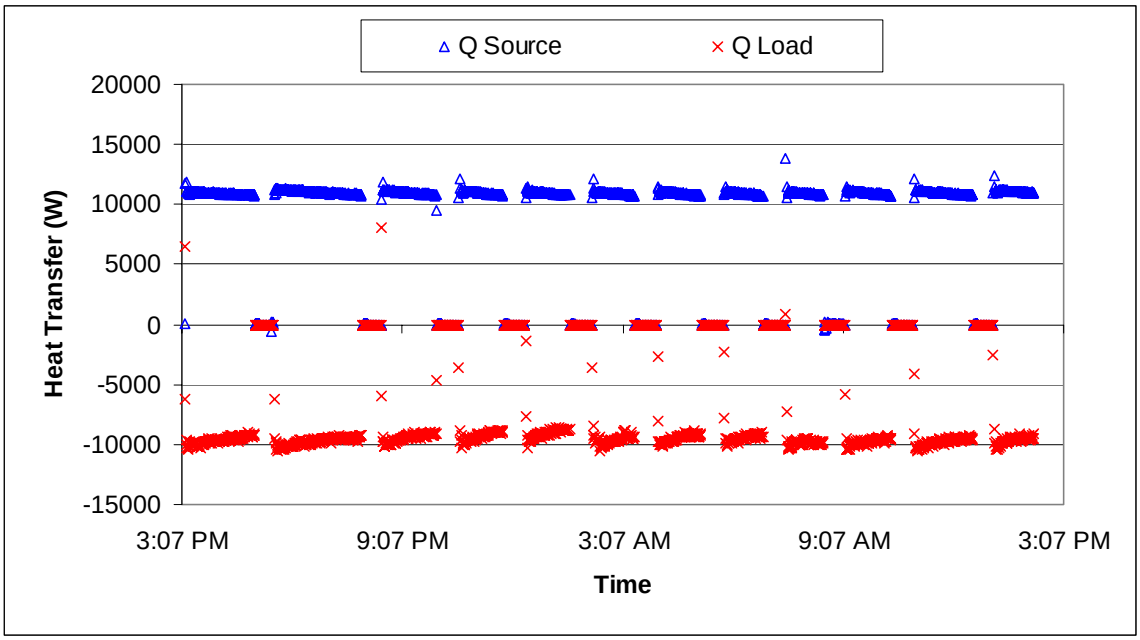

Figure 7.2 – Heat Pump 1 Heat Transfer Rate

Figure 7.2 shows how the heat pump cycles according to the control program. The heat pump is operated until the user setpoint temperature for the storage tank is reached. Once this temperature is reached, the heat pump and circulating pumps are turned off.

Figures 7.3, 7.4 and 7.5 show the typical transient operation for heat pump 1. These transient points can have a significant impact on the overall system performance and cause simulation results to be inaccurate. This is due to measured heat transfer rates or power usage below or above the steady state values obtained after the system has operated for a short time. Currently most system simulation programs use steady-state models and either neglect the transient effect or use a degradation factor to correct for the start-up transient. These models tend to over predict both the heat transfer rate and the energy use. By capturing the transient data, the experimental facility will support the development and validation of more realistic heat pump models.

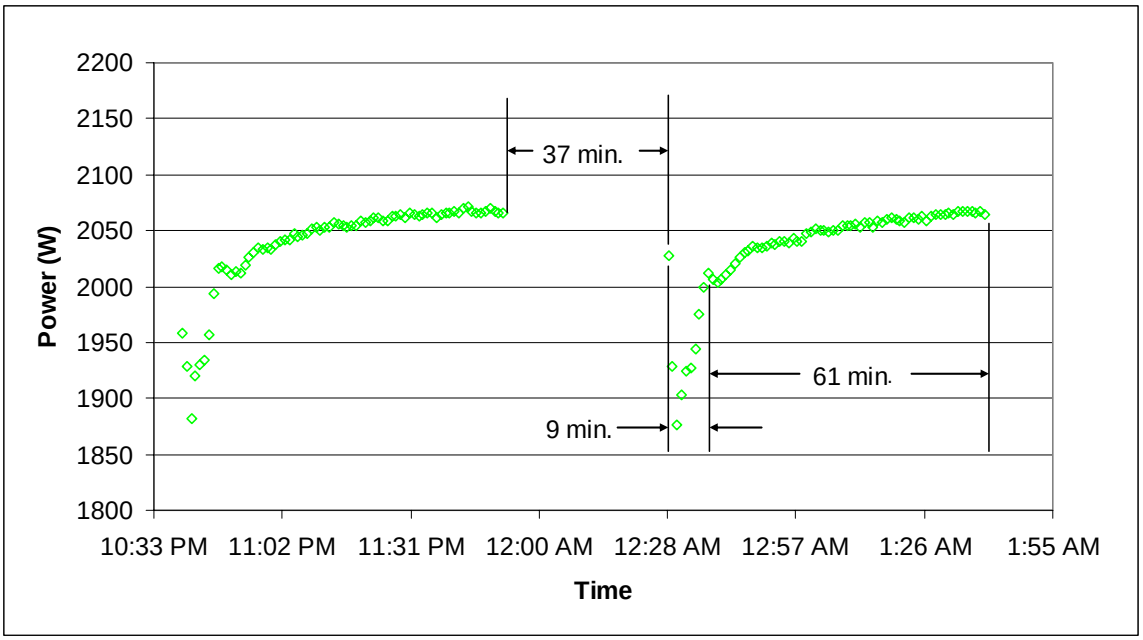

Figure 7.3 – Transient Power Usage for Heat Pump 1

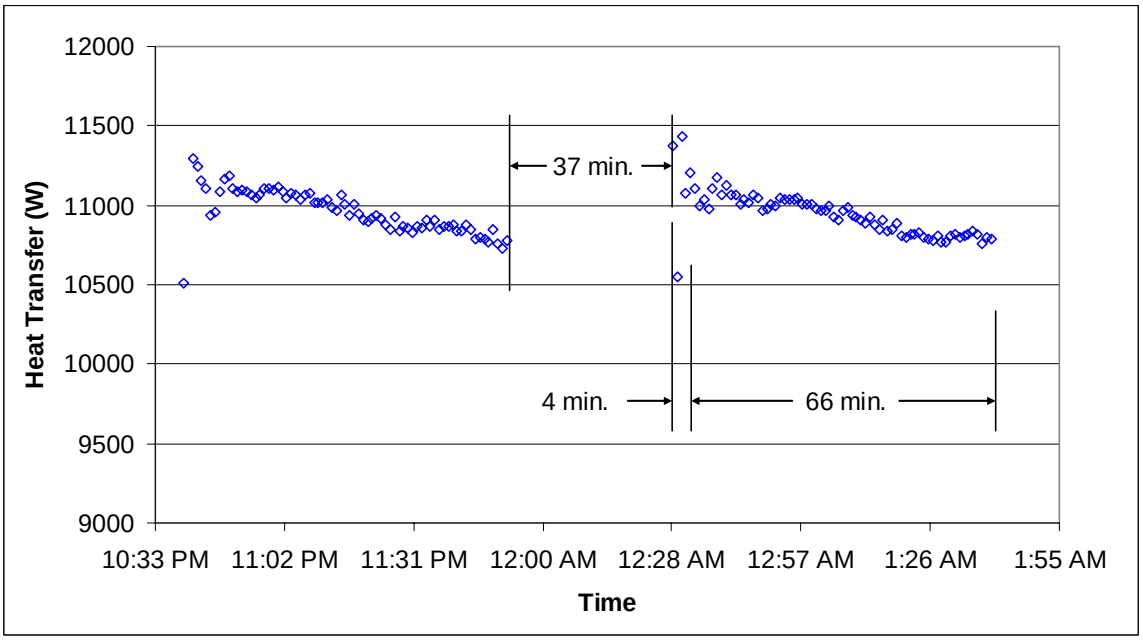

Figure 7.4 – Transient Heat Transfer for Source Side on Heat Pump 1

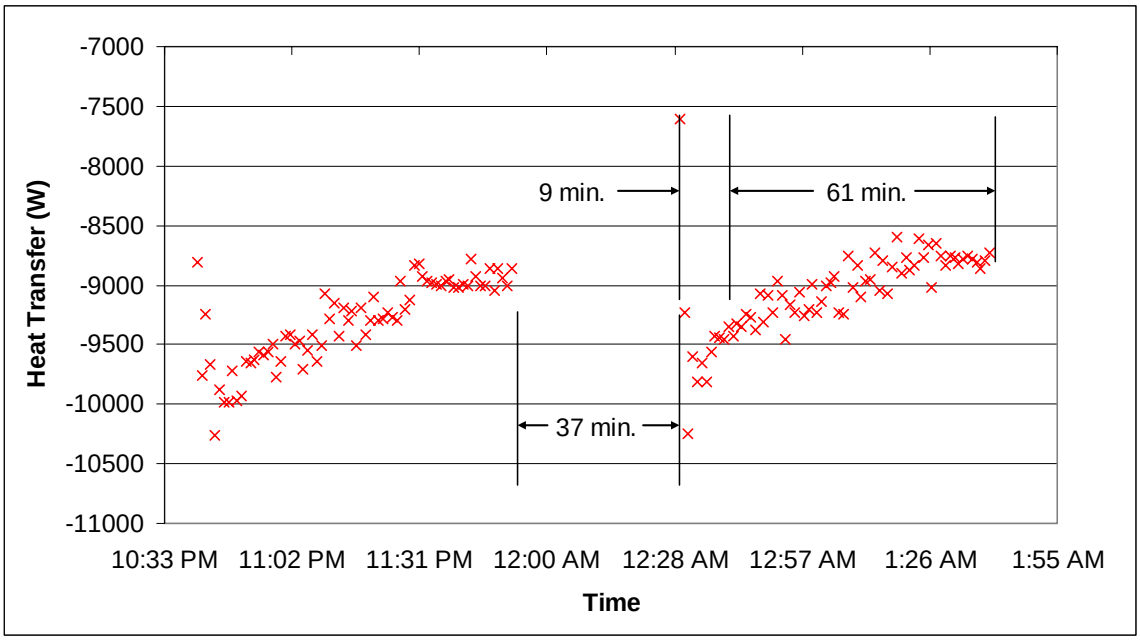

Figure 7.5 – Transient Heat Transfer for Load Side on Heat Pump 1

Figure 7.3, 7.4 and 7.5 show that the heat pump can take 4 to 9 minutes to approach a steady state condition. This is a significant portion of the overall 70 minute cycle time. A particularly interesting trend in all the figures is the varying power consumption and heat transfer that takes place as the heat pump continues to operate. A closer look at the data in Figure 7.6 reveals that the trend is correct for a decreasing tank temperature. As the heat pump operates, the temperature of the water entering the load side decreases and the temperature of the water entering the source side increases. This increases the power drawn by the heat pump compressor.

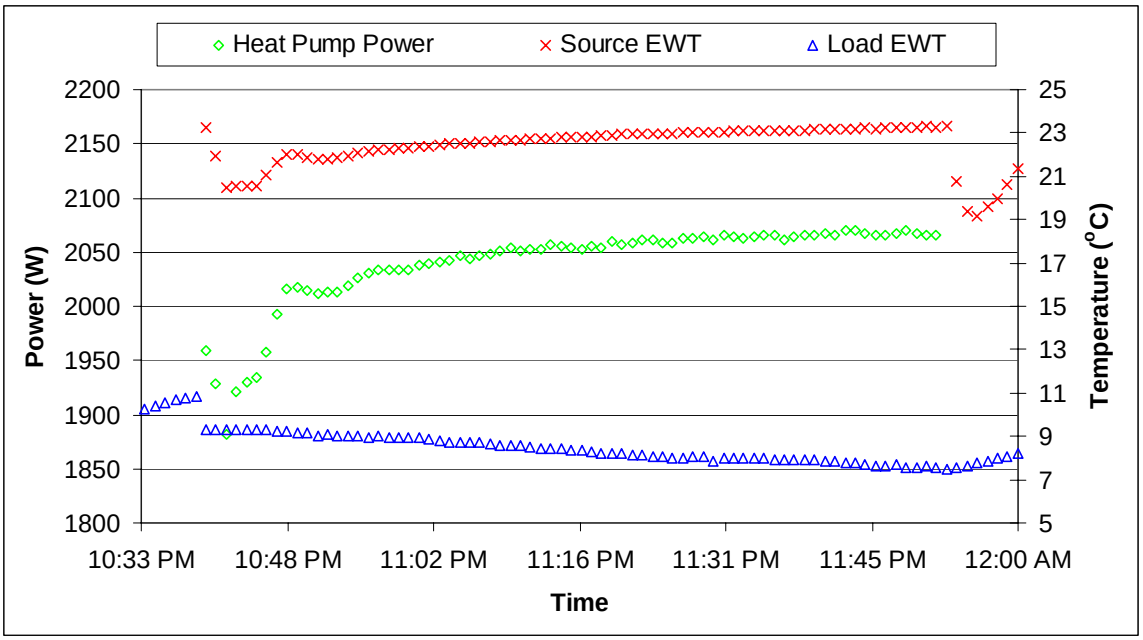

Figure 7.6 – Heat Pump Power Usage

When the cooling tower is operated, the heat pump power consumption is even greater. Figure 7.7 shows the power consumption for the heat pump when the cooling tower is in operation plotted with the outside air temperature. Of particular interest is the sinusoidal pattern observed in the power measurement. The cooling tower uses ambient air to evaporatively cool the source side fluid. As the outside air temperature decreases, the source loop fluid temperature decreases. This causes the heat pump to consume less power to maintain heat transfer rates through the load side. During the day, the outside air temperature increases causing the source fluid loop temperature to increase. As the loop temperature increases, the heat pump power consumption increases to maintain heat transfer rates through the load side.

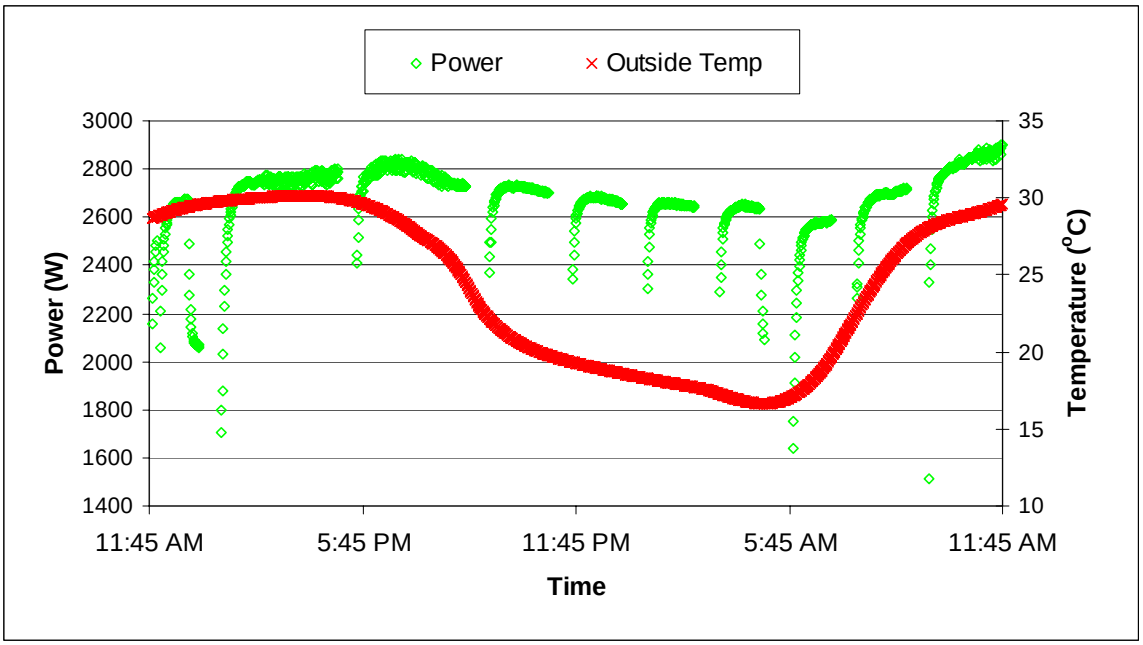

Figure 7.7 – Heat Pump 1 during Cooling Tower Operation

The results for heat pump 2 are similar to the results obtained for heat pump 1. The heat pump, controlled by the tank thermostat, warmed the water to the setpoint temperature. The transient effects of the system matched the results found from heat pump 1. Operating results for heat pump 2 can be seen in Figures 7.8 and 7.9.

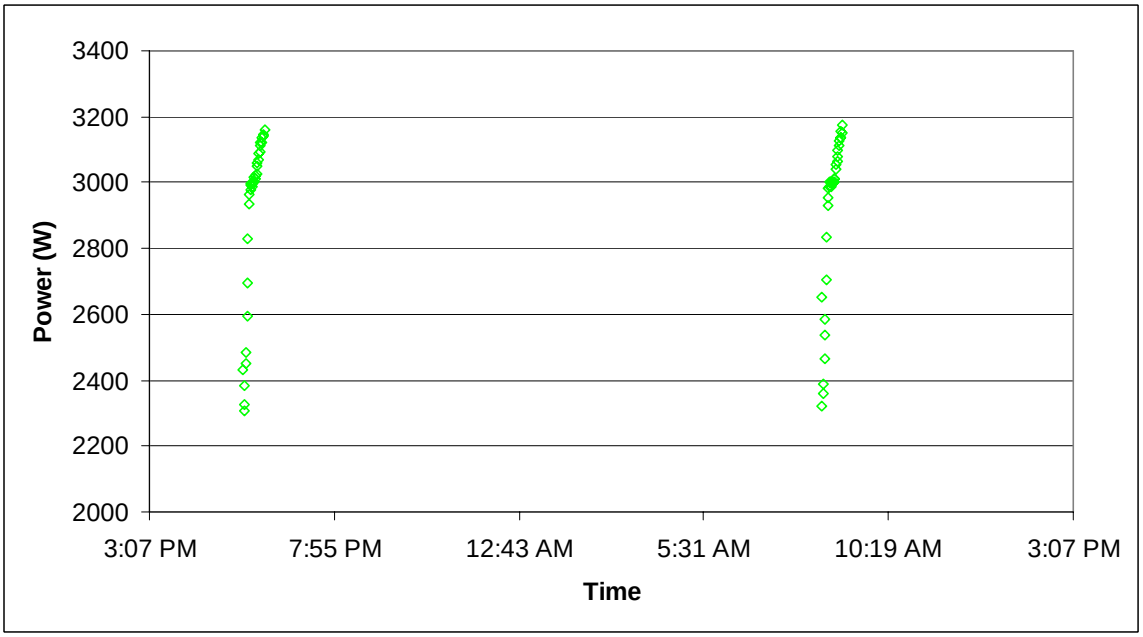

Figure 7.8 – Power Usage for Heat Pump 2

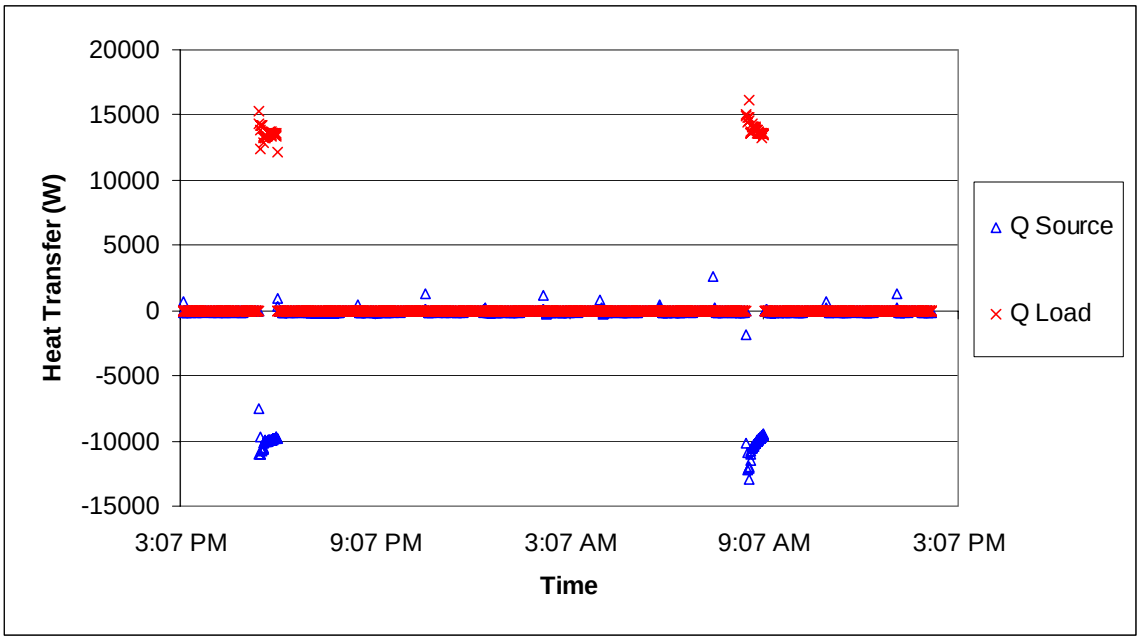

Figure 7.9 – Heat Pump 2 Heat Transfer Rate

In most residential systems the heat pump operates with a short run-time cycle which can increase the operating efficiency. This trend is shown in Figure 7.10 and 7.11 with the transient performance of a heat pump operating in heating and cooling mode utilizing a GLHE. Upon start-up the water circulating through the heat pump is near the surrounding ground temperature which increases the efficiency of the heat pump. By the time the system reaches steady-state operation 10 minutes have elapsed which is approximately the cycle time for a normal residential system.

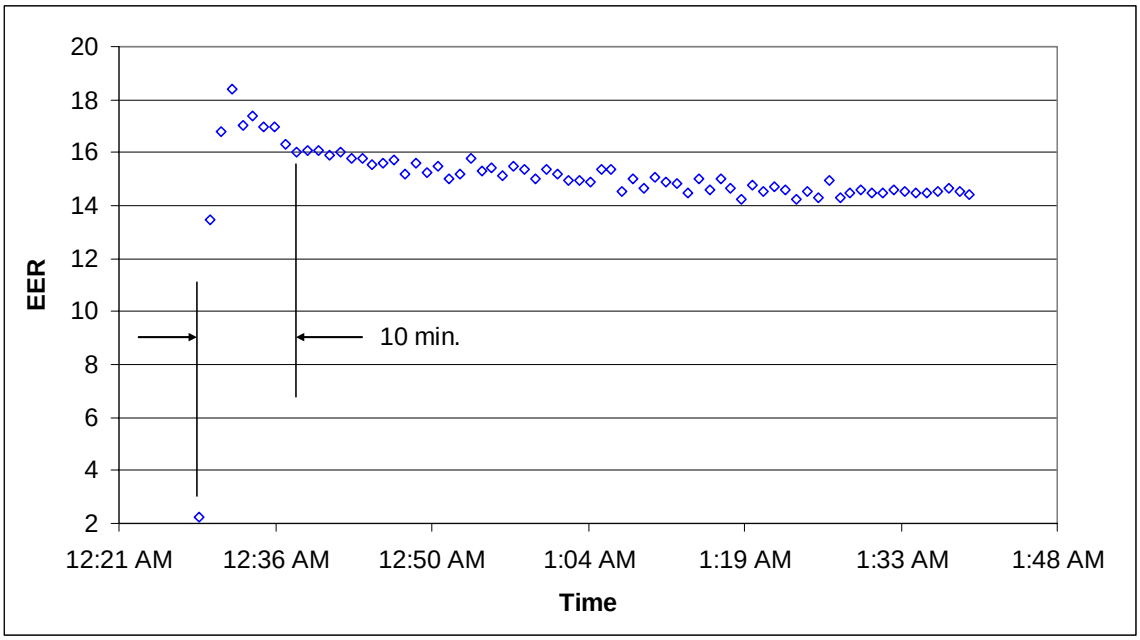

Figure 7.10 – Heat Pump 1 EER

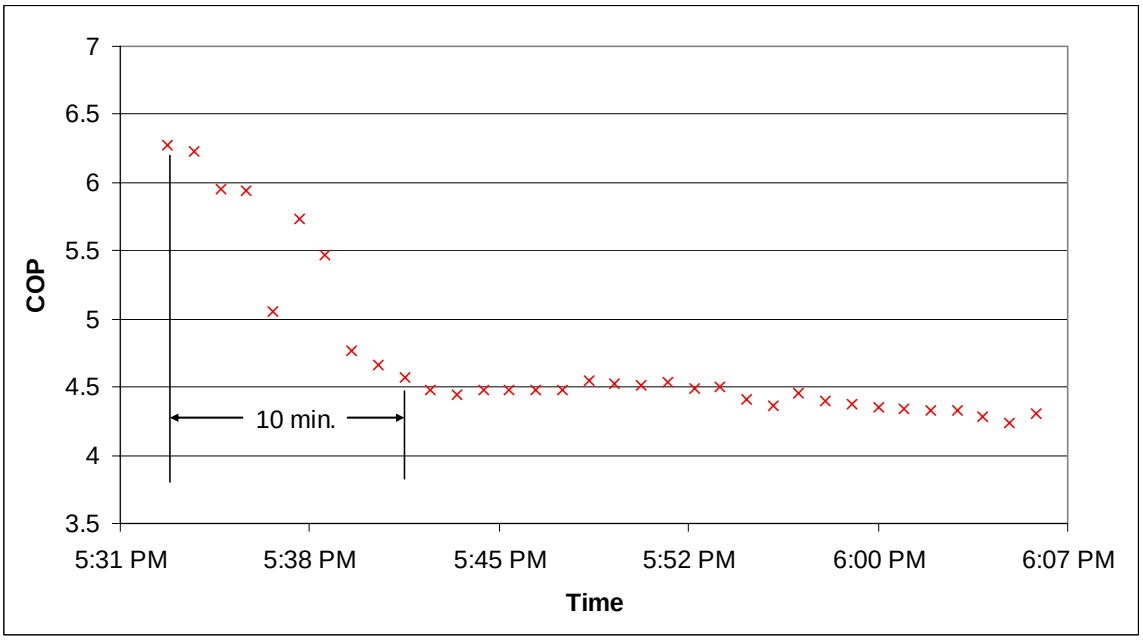

Figure 7.11 – Heat Pump 2 COP

A heat balance across each heat pump was calculated in order to check the calculated uncertainty in the temperature and flow rate measurements. This heat balance equations for heating and cooling are:

$$\dot{Q}_{Balance-Heating} = \dot{Q}_L - W - \dot{Q}_S = 0 \qquad (7.1)$$

$$\dot{Q}_{Balance-Cooling} = \dot{Q}_S - W - \dot{Q}_L = 0 \tag{7.2}$$

The predicted uncertainty for this calculated error is:

$$e_{Balance} = \pm\sqrt{\left(e_{\dot{Q}-L}\right)^2 + \left(e_{\dot{Q}-S}\right)^2 + \left(e_{w020}\right)^2} \tag{7.3}$$

Where $e_{\dot{Q}-L}$ and $e_{\dot{Q}-S}$ are calculated according to Equation 6.9. To obtain a percentage for the heat balance and the uncertainty, each was divided by the side into which the heat pump power was added to give the following:

$$\%_{Heating} = \frac{\dot{Q}_{Balance-Heating}}{\dot{Q}_L} \tag{7.4}$$

$$\%_{Cooling} = \frac{\dot{Q}_{Balance-Cooling}}{\dot{Q}_S} \tag{7.5}$$

$$\%_{e_{Heating}} = \frac{e_{Balance-Heating}}{\dot{Q}_L} \tag{7.6}$$

$$\%_{e_{Cooling}} = \frac{e_{Balance-Cooling}}{\dot{Q}_S} \tag{7.7}$$

The results for a short steady state period can be seen for both heat pumps in Figures 7.12 and 7.13.

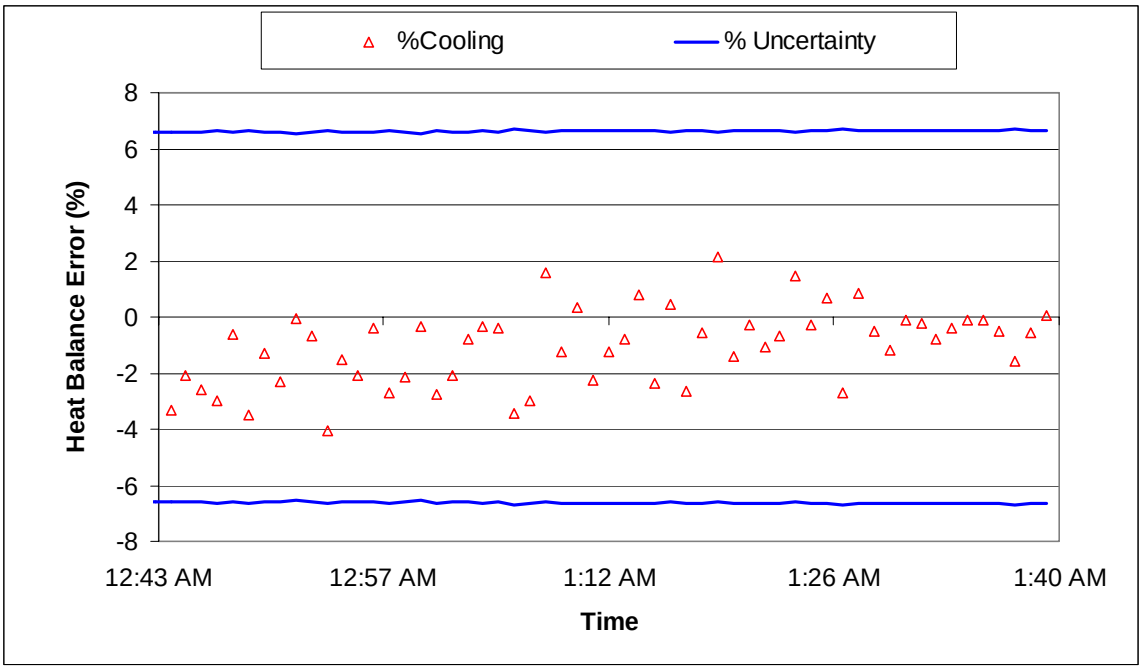

Figure 7.12 – Heat Balance Across Heat Pump 1

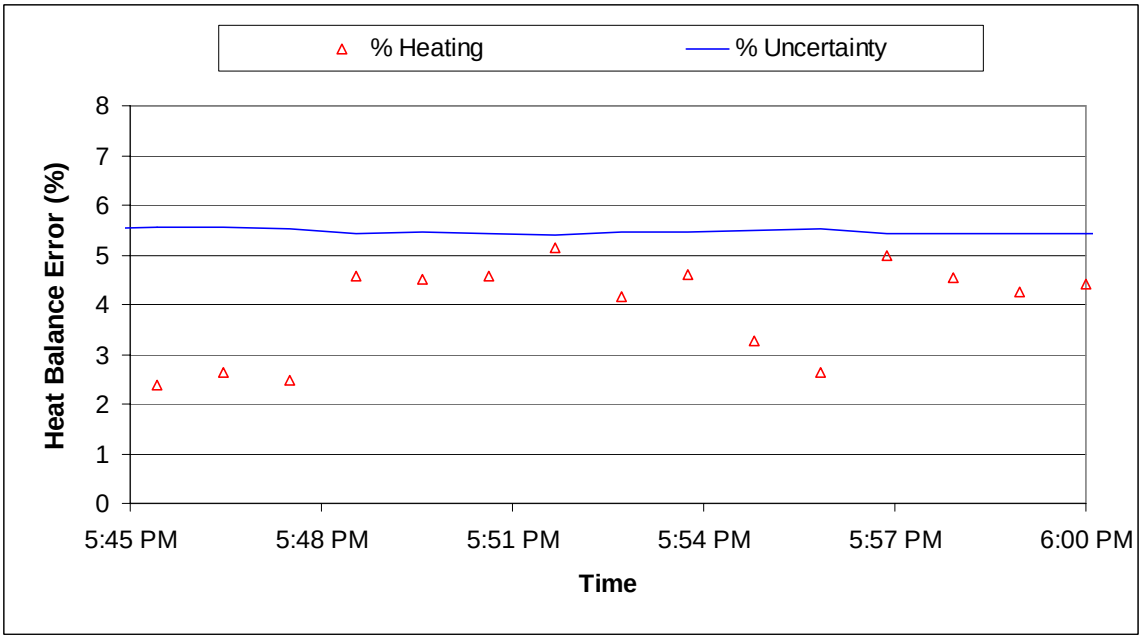

Figure 7.13 – Heat Balance Across Heat Pump 2

As seen from the figures above, the heat balance for the heat pumps is within the calculated uncertainty interval for the measurements.

There does appear to be a slight systematic error associated with the heat pump 1 measurements and a significant systematic error associated with heat pump 2

measurements. Table 7.1 shows the measured data at steady state compared to catalog data operating at the same conditions. The measured data is shown to be systematically low.

Table 7.1 – Heat Pump Catalog Comparison

	Heating			Cooling		
	Catalog	Measured	% Error	Catalog	Measured	% Error
Load Capacity (W)	13700	13500	1.5	9400	9000	4.3
Source Capacity (W)	10500	10000	4.8	11600	10900	6.0
Input Power (W)	3200	3000	6.3	2250	2050	8.9

One measurement not taken, internal piping and compressor shell heat transfer, could at least partially account for the systematic error. Additional control and instrumentation of the heat pump enclosure (cabinet) would be required to improve the heat balances shown in Figures 7.12 and 7.13.

7.1.2 Storage Tanks

The data obtained for the load side measurements was analyzed to determine if the primary equipment was operating to the design specifications. This includes observing the storage tanks to make sure that the controls maintain the user specified set points. Heat pump 1 was set to operate in cooling mode to condition storage tank 1 and heat pump 2 was to operate in heating mode to condition storage tank 2. The chilled water tank was set to maintain a temperature between 7 and 9°C while a set point of 43 and 45°C was used for the hot water tank. The mid-elevation thermocouple in each tank was used as the reference temperature monitored by the control program. The temperatures for each tank are shown in Figures 7.14 and 7.15.

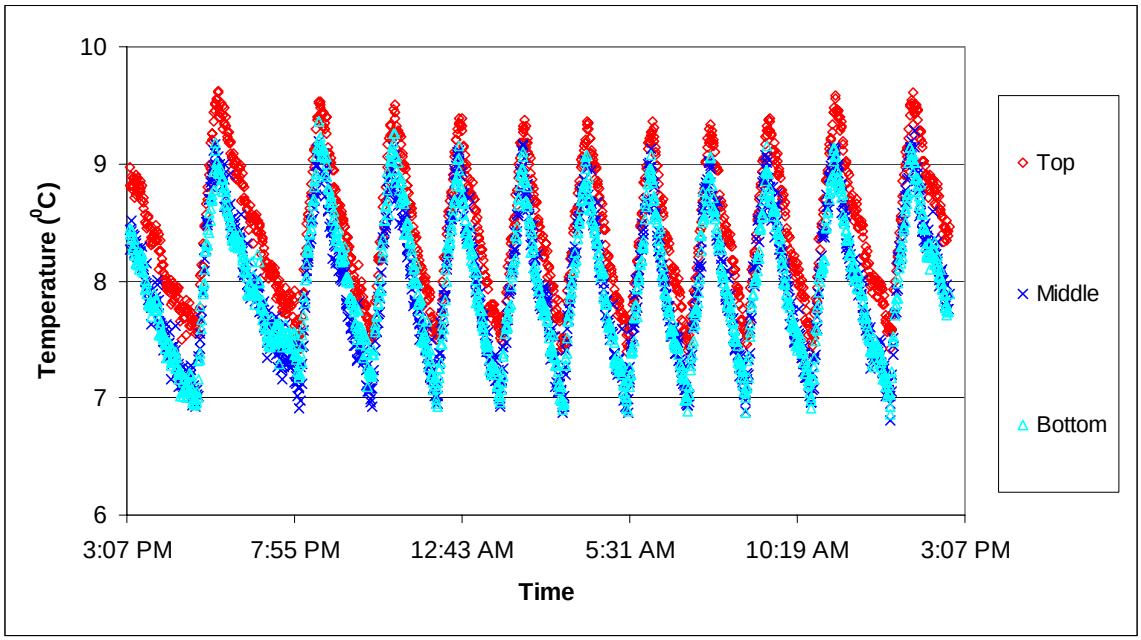

Figure 7.14 – Chilled Storage Tank Temperatures

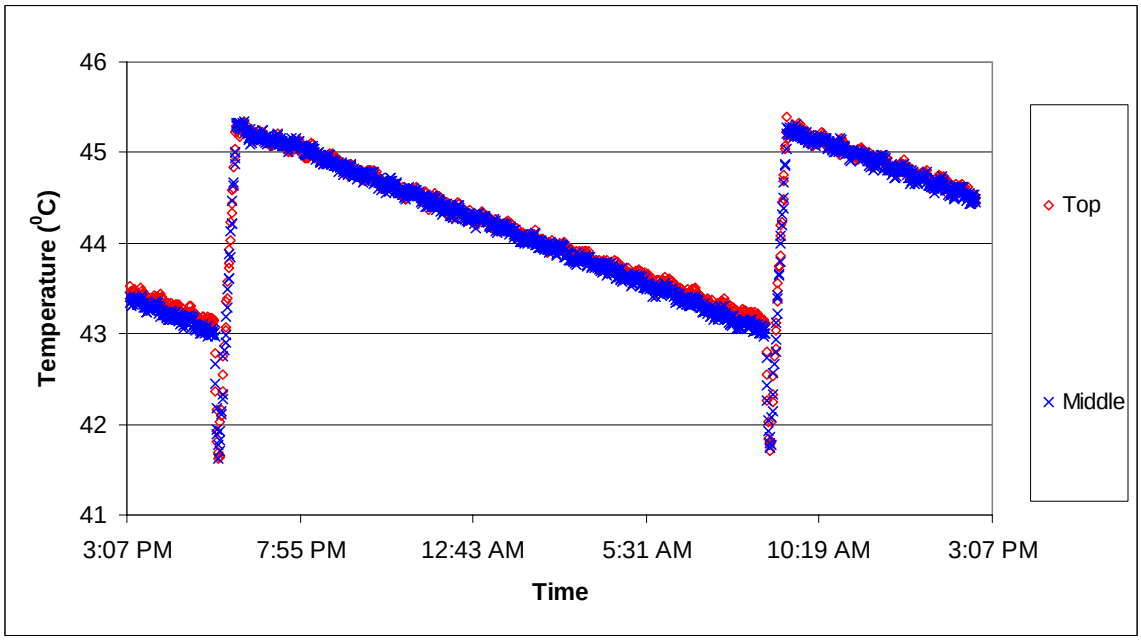

Figure 7.15 – Hot Storage Tank Temperatures

As shown in the figures above, the tanks can be controlled (by cycling the heat pumps) to maintain between their setpoint range. The chilled water tank heat pump cycles more frequently because of the loads being drawn for the fan coil and test cell. The temperatures at the three elevations in the tank show approximately 0.4°C of

stratification with warmer temperatures at the top and cooler temperatures near the bottom. The hot water tank temperature initially drops upon startup of the heat pump. Water circulated back into the tank is initially cooler than the water at the top of the tank. This is an artifact of the 'no-load' condition on the tank. Upon heat pump start-up, water that has been stagnated in the pipes for over twelve hours is pumped into the tank. Once this water is well mixed with the tank water, the entire tank is quickly heated.

One important consideration is the tank heat loss to the ambient air. The linear change in hot tank temperature between heat pump cycles, is due entirely to heat loss to the surroundings. This heat loss is calculated from the experimental data as:

$$\dot{Q} = \frac{V \cdot \rho_w \cdot c_p \cdot \Delta T \cdot 1000}{t} \tag{7.8}$$

Where 1000 is a unit conversion factor and:
$\dot{Q}$ = heat transfer rate, W
V = tank volume, m^3
ρ_w = density of water, kg/m^3
c_p = specific heat of water, kJ/kg-°C
ΔT = tank temperature difference, $T_{t=0}$-$T_{t=i}$
t = time, sec

The tank resistance was then found by:

$$R = \frac{\left(T_{\text{tank}} - T_{ambient,air}\right) \cdot A}{\dot{Q}} \tag{7.9}$$

Where:
R = thermal resistance, m^2–°C/W
$\dot{Q}$ = heat transfer rate, W
A = surface area of tank, m^2

The resistance was calculated for the hot water tank and found to be approximately 0.7 m^2–°C/W. Since the insulated tank walls are identical for both tanks, this thermal resistance may also be used to estimate heat gain to the chilled water tank.

7.1.3 Pond Loop Heat Exchanger

The pond heat exchanger was operated using a flow rate of 12 gpm. This would give a flow rate of 6 gpm through each heat pump. Figure 7.16 shows the calculated heat transfer across the pond heat exchanger. The remote HOBO data logging unit discussed in Chapter 5 measured inlet and outlet water temperature at the pond loop heat exchanger. These water temperature measurements are then used in Equation 6.8 to calculate the source side heat transfer rate. Load side temperature measurements are made with thermocouples probes located at the inlet and outlet pipes into the plant.

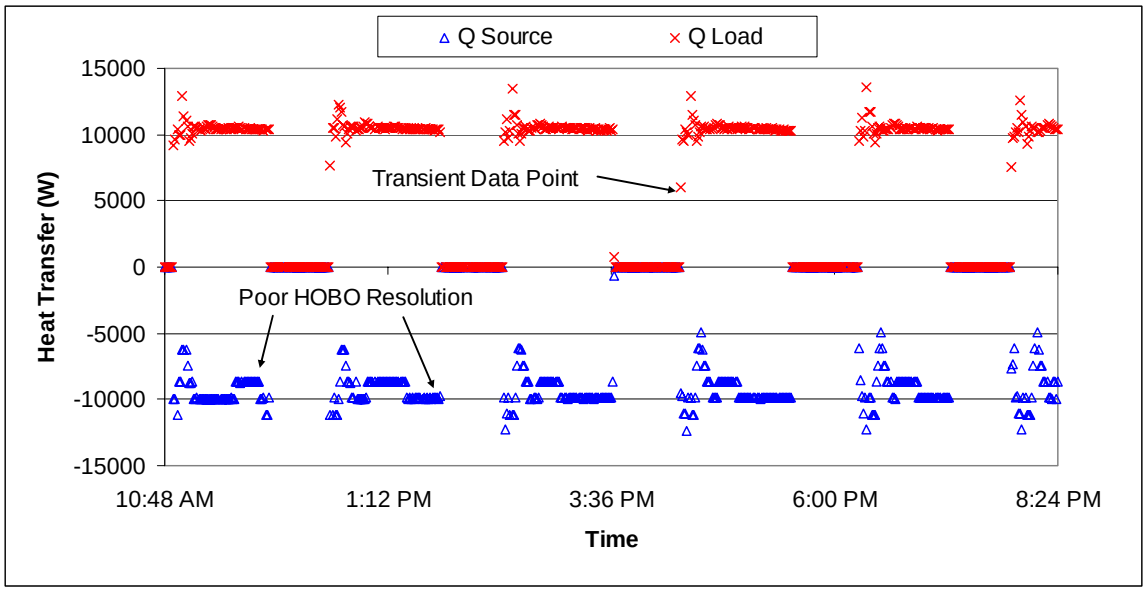

Figure 7.16 – Pond Heat Exchanger Heat Transfer

Figure 7.17 shows the 1200 W increase in the heat transfer rate for a single cycle during steady-state operation. This large increase is due to the 0.4°C resolution of the HOBO datalogger. The overall temperature difference ($\approx 3°C$) is small enough so that a 0.4°C change in the reported temperature represents a large change in the heat transfer rate. The uncertainty in the temperature measurement, results in an average uncertainty in the heat transfer rate of approximately 20% during steady-state operation. This is

unacceptably high for model development and validation. It is recommended that the remote Hobo dataloggers to upgraded to a higher resolution dataloggers.

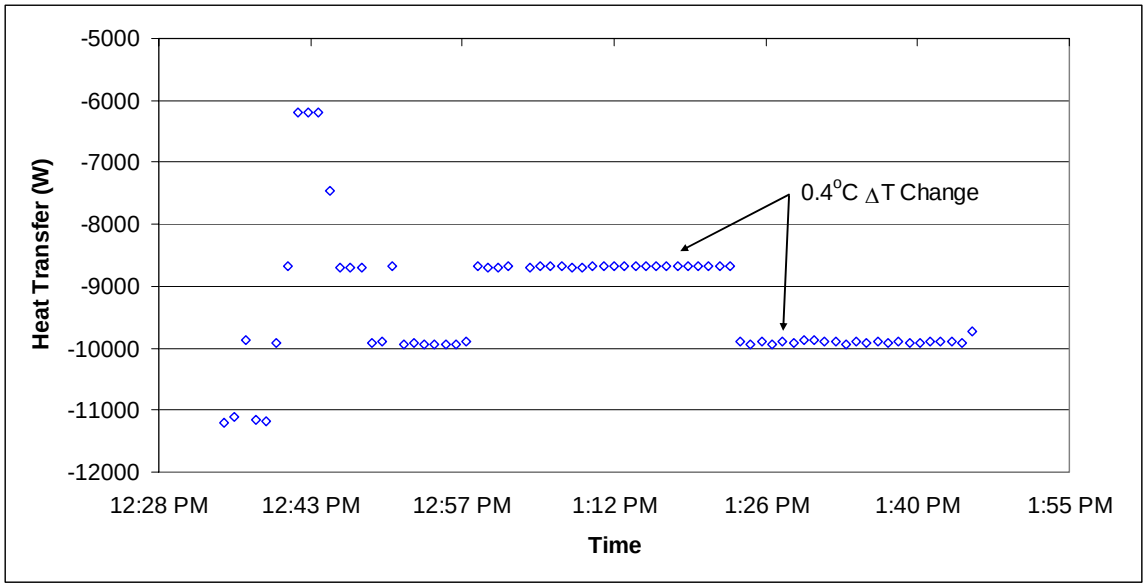

Figure 7.17 – Heat Transfer Temperature Sensitivity

Another consideration for model development and simulation validation is the relatively long transients for each cycle. As shown in Figure 7.18, the transient time accounts for almost a third of the total time the system is operational. The supply to the pond heat exchanger included 500 ft (152.4 m) of buried, uninsulated pipe which would increase the time required for the system to reach steady state. The typical time for steady state conditions to be reached is a function of the pipe wall, the conductivity and initial temperature of the surrounding ground, and the system flowrate.

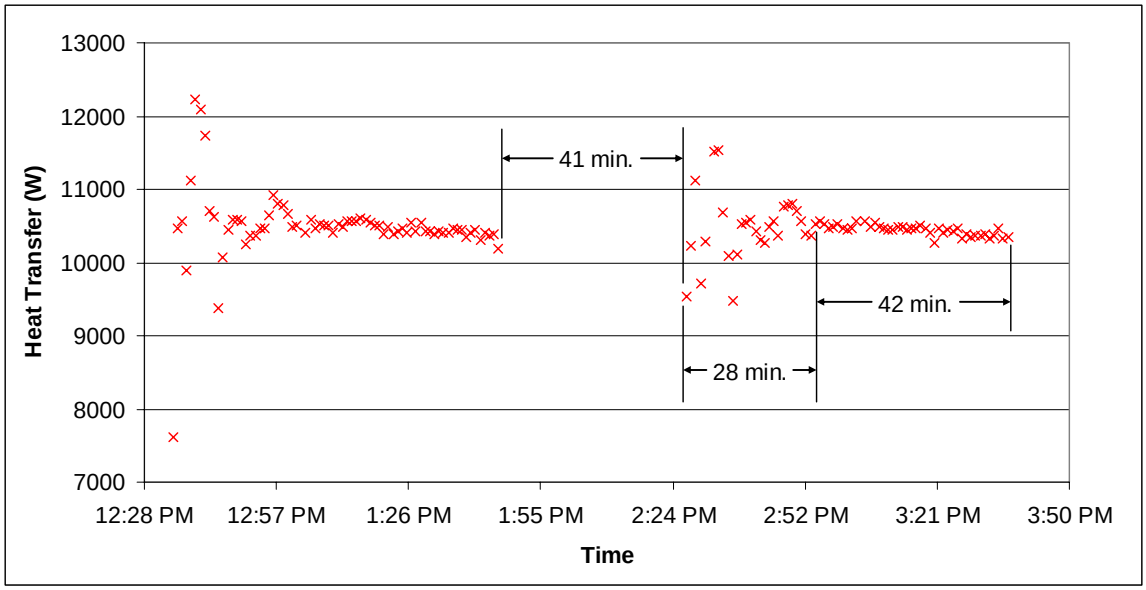

Figure 7.18 – Pond Transient Effects

7.1.4 Cooling Tower

The cooling tower was operated at a flow rate of 12.4 gpm on the heat pump side of the plate heat exchanger and 9.3 gpm on the cooling tower side. The cooling tower and its' associated circulating pump were operated so that the cooling tower fan and circulation pump are turned on anytime one of the heat pumps is in operation.

A HOBO datalogging unit was also used for this remote datalogging operation. Water temperature measurements were taken at ports on the inlet and outlet of the cooling tower. As shown in Figure 7.19, the measurement problem associated with the HOBO datalogging (discussed in the previous section) affects the tower heat transfer measurement as well.

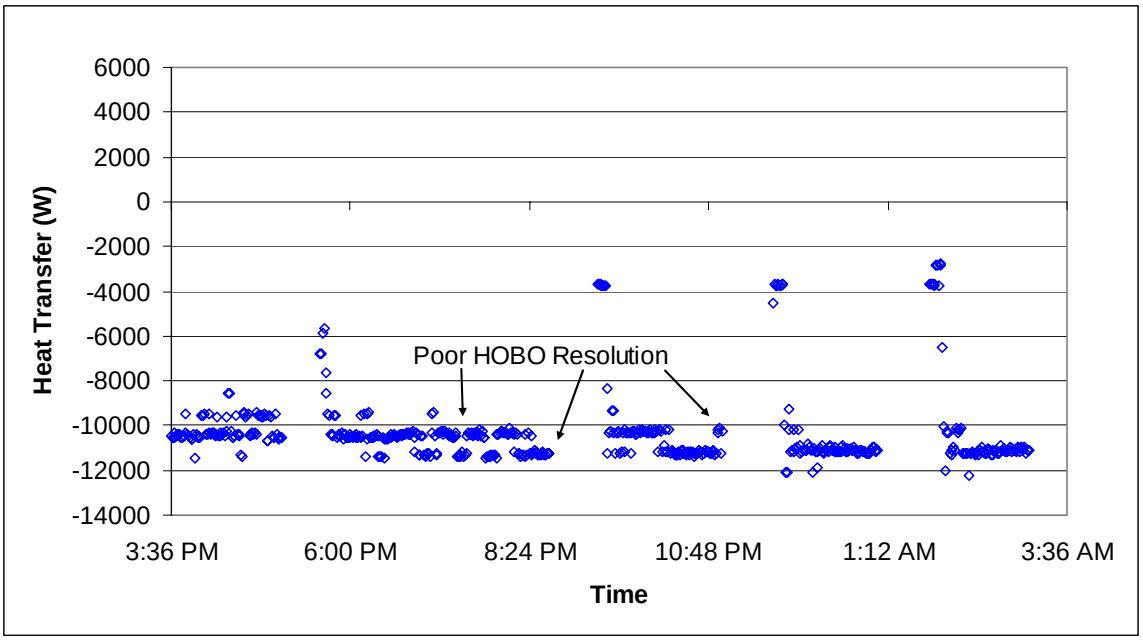

Figure 7.19 – Cooling Tower Heat Transfer

The uncertainty associated with the cooling tower heat transfer can be seen in Figure 7.20. It shows that after the cooling tower has reached steady state operation, an uncertainty greater than 12% can be expected in the heat transfer rate.

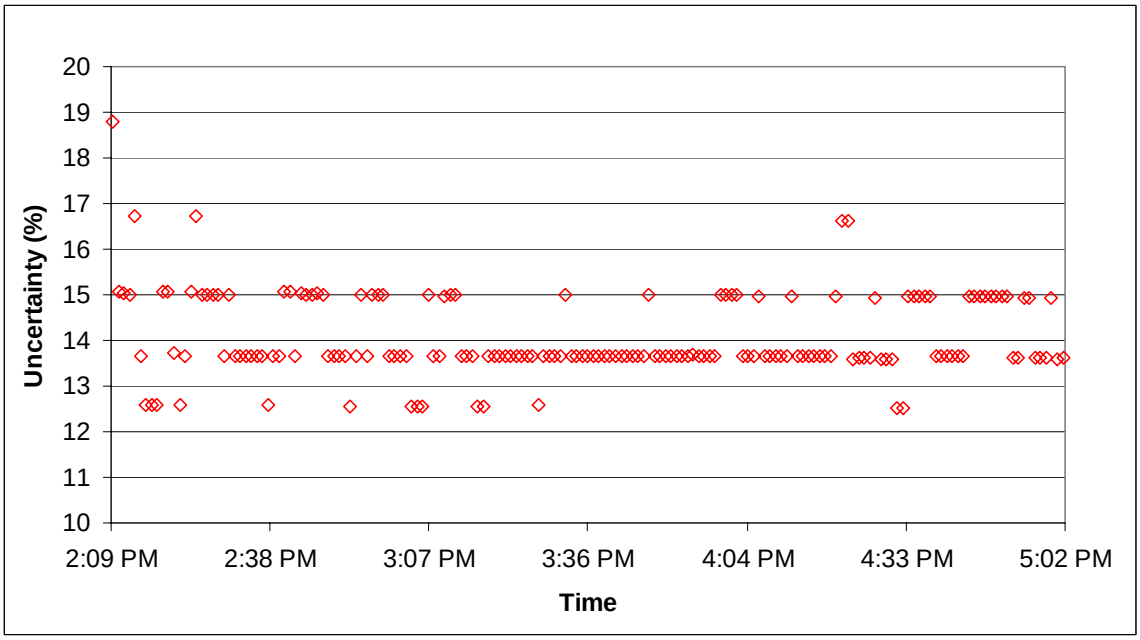

Figure 7.20 – Cooling Tower Heat Transfer Uncertainty

The heat transfer across the plate heat exchanger closely matches the design value of 36,000 BTU/hr (10.55 kW). Trends seen in Figure 7.21 closely match the cooling tower heat transfer.

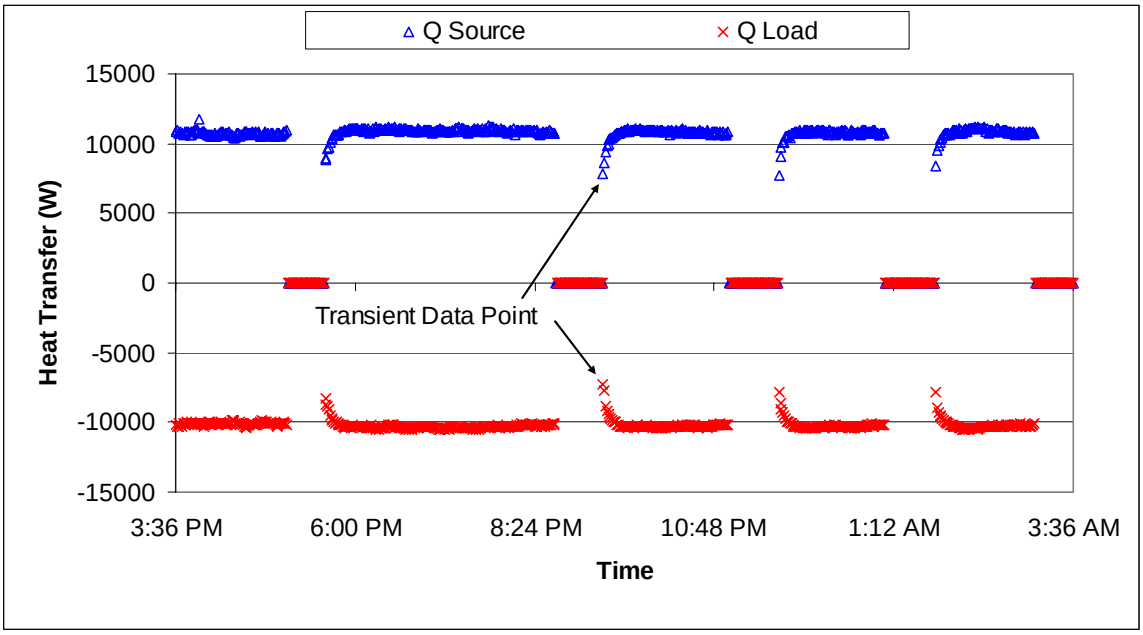

Figure 7.21 – Plate Heat Exchanger Heat Transfer

The data shows longer cooling tower run times during the daylight hours. This is due to higher outdoor temperatures, which create a larger load on the system and also lower the sensible heat transfer through the cooling tower. Figure 7.22 shows the typical transient response time of the tower. The cooling tower reaches steady-state operation after approximately 11 minutes. This time period is dominated by the buried pipe on the cooling tower side of the heat exchanger.

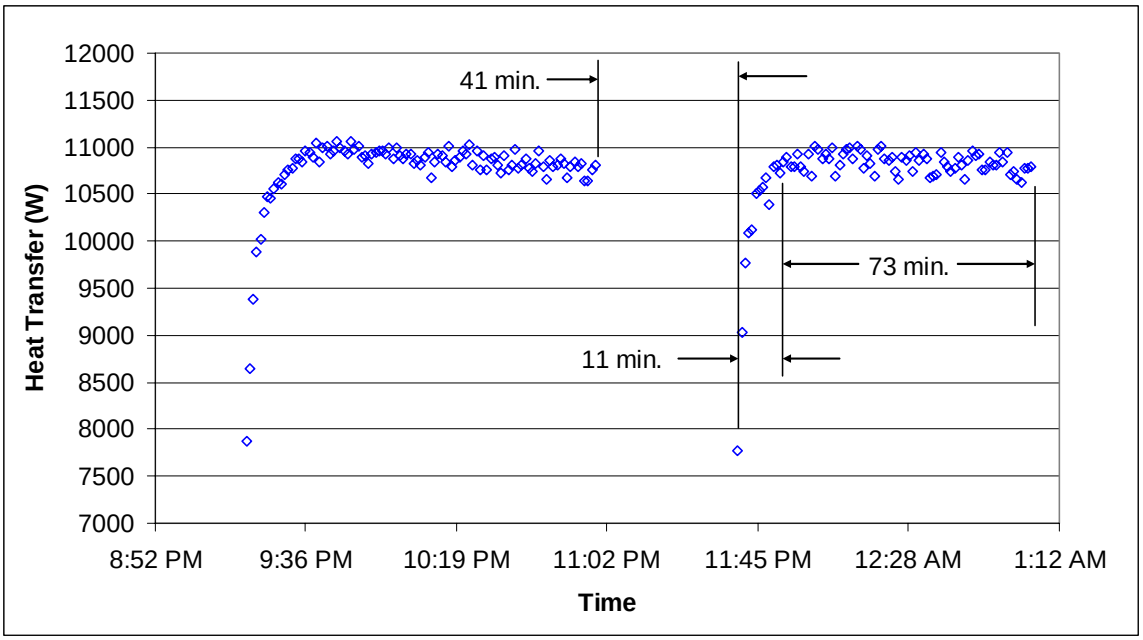

Figure 7.22 – Cooling Tower Transient Effects

The plate heat exchanger heat transfer rate data shows that the source side heat transfer rate is systematically higher than the load side. The error in the heat balance is shown in Figure 7.23.

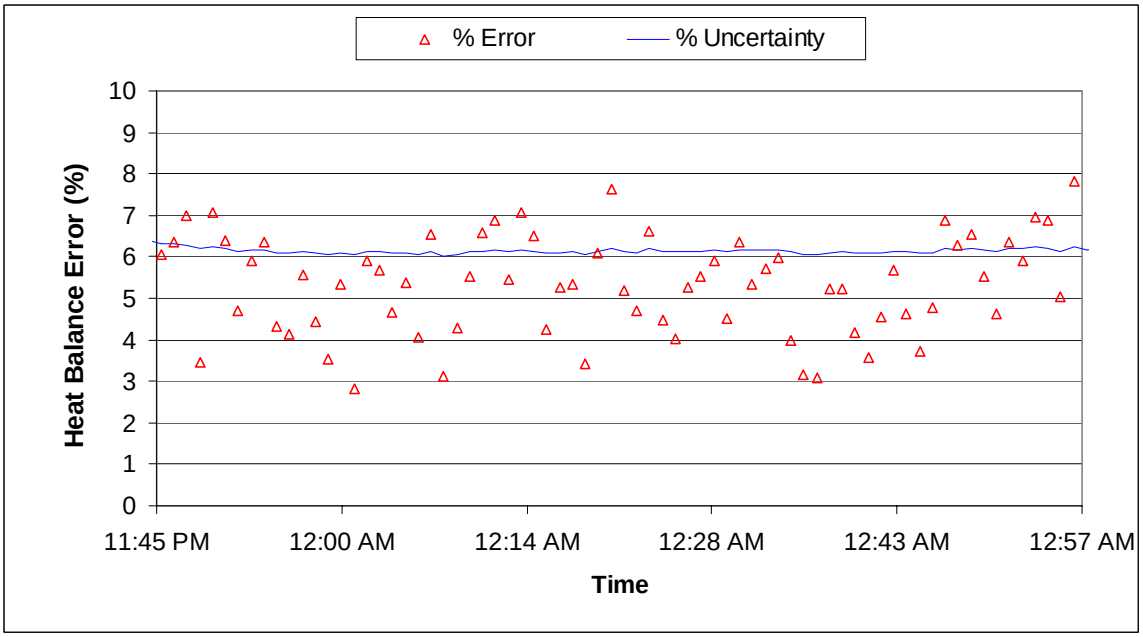

Figure 7.23 – Plate Heat Exchanger Heat Balance

As shown, approximately 70% of the measured points are within the uncertainty interval. The systematic shift can be accounted for by heat loss to the ambient air. On the source side, average temperature difference between the water circulating and the ambient air is negligibly small. On the load side however, this difference is +11°C. The large temperature difference on the load side results in a heat loss to the plant building and accounts for the systematic error in the measured calculated heat balance. This error can be significantly reduced by insulating the heat exchanger.

7.1.5 GLHE

The GLHE was tested with the four vertical boreholes in operation. A flow rate of 12.4 gpm through the source system was set by adjusting the VFD. This would result in a flow rate of approximately 3 gpm through each borehole and 6.2 gpm through each heat pump. The heat transfer results for each borehole are shown in Figures 7.24-7.27.

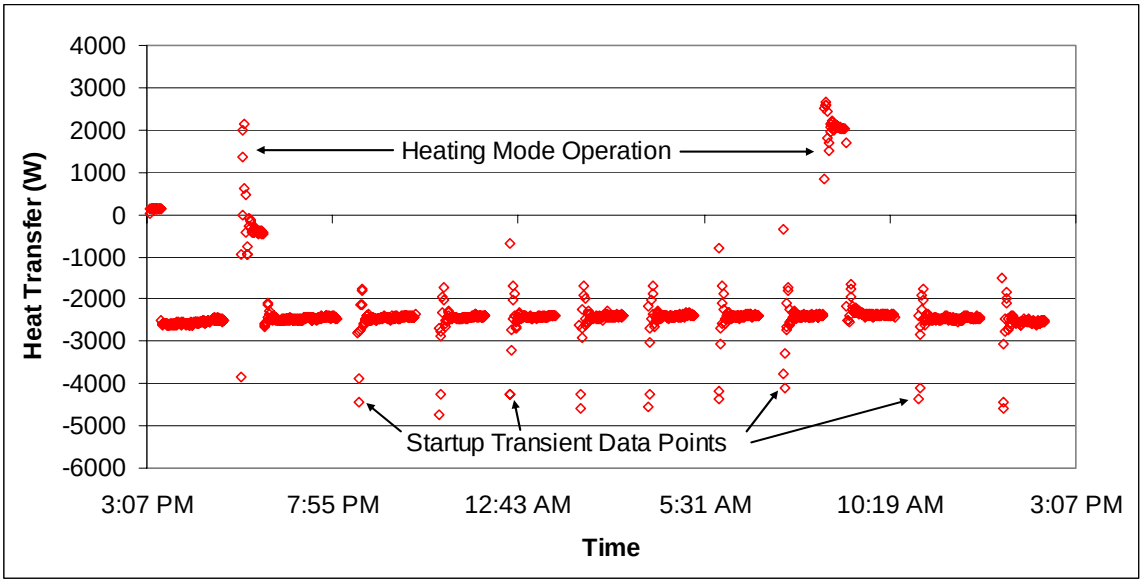

Figure 7.24 – Borehole 1 Heat Transfer

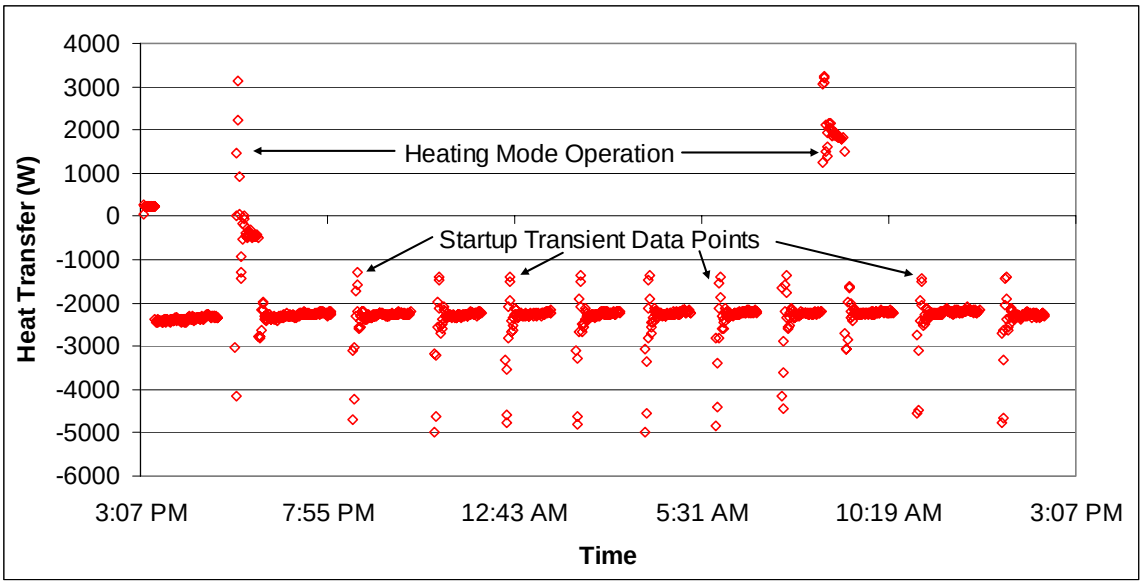

Figure 7.25 – Borehole 2 Heat Transfer

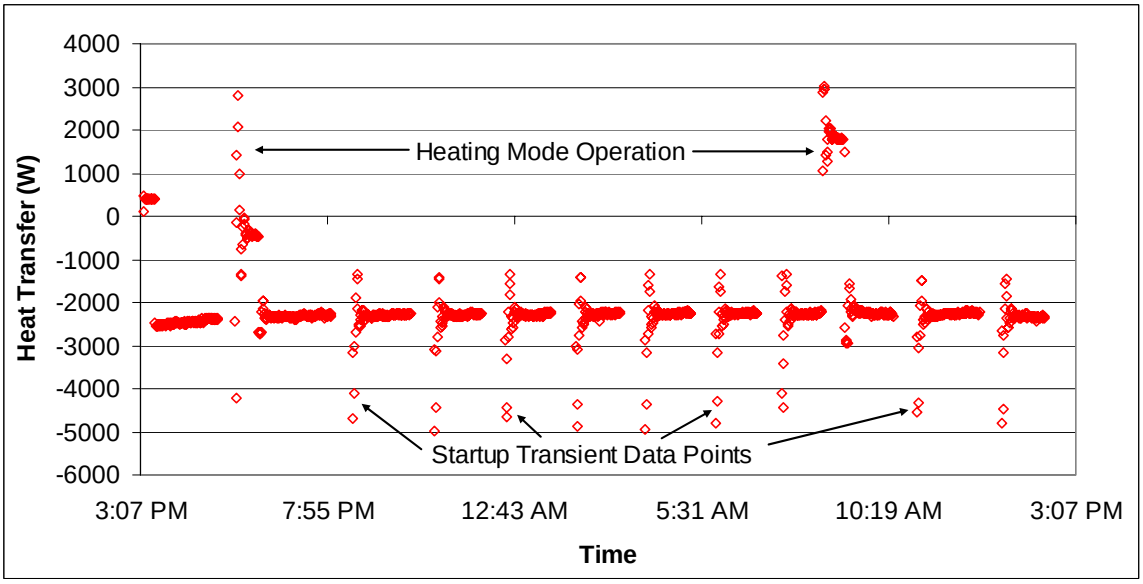

Figure 7.26 – Borehole 3 Heat Transfer

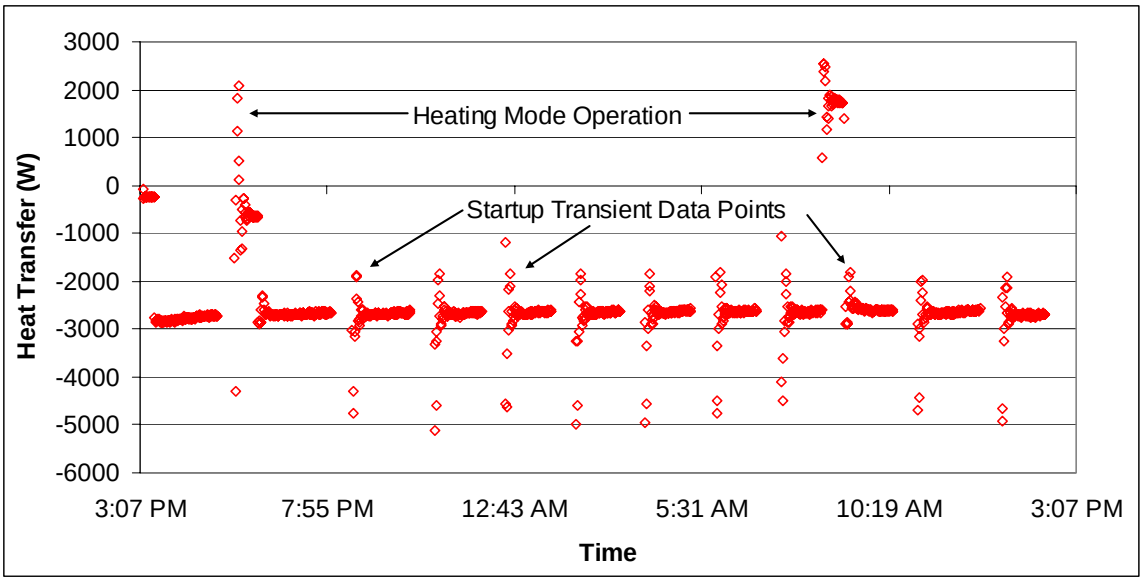

Figure 7.27 – Borehole 4 Heat Transfer

The heat transfer rate for each borehole exhibits the same general pattern and cycles with the heat pumps. As shown, the heat pump operates in heating mode two times during the test resulting in a positive heat transfer rate. The heat pump operating in cooling mode cycles 12 times during the same twenty four hour period.

An interesting feature of the figures is the magnitude of the transient heat transfer rate spike, which can be nearly twice the steady state value. Figure 7.28 shows that the high heat transfer rates are obtained in the first couple of minutes because the water temperature at the top of the borehole is heated to near ambient temperature. The exiting water temperatures are low since the water has been sitting in the borehole and is close to the ground temperature. The values then go from a high to a low heat transfer rate because the water being circulated through the boreholes is closer to the ground temperature so the temperature drop across the borehole is low.

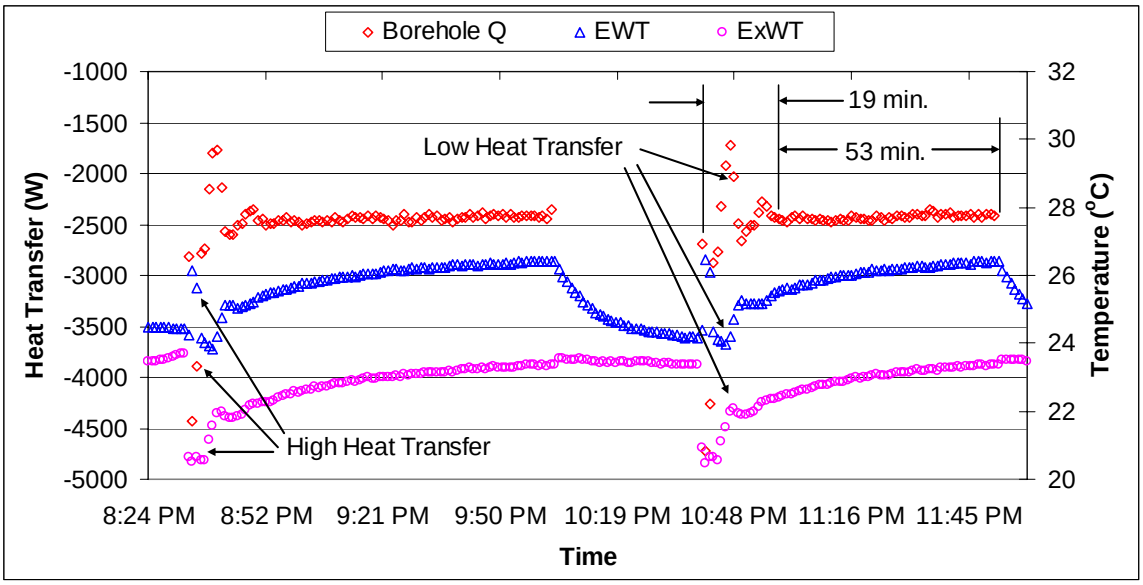

Figure 7.28 – GLHE Transient Effects

The transient time of 19 minutes is similar to the time found for the pond loop. This is because of the long pipe length that the water has to travel. The uncertainty for the heat transfer was also calculated and can be seen in Figure 7.29. It shows the calculated uncertainty as a percentage of the heat transfer rate from the borehole at near steady state conditions.

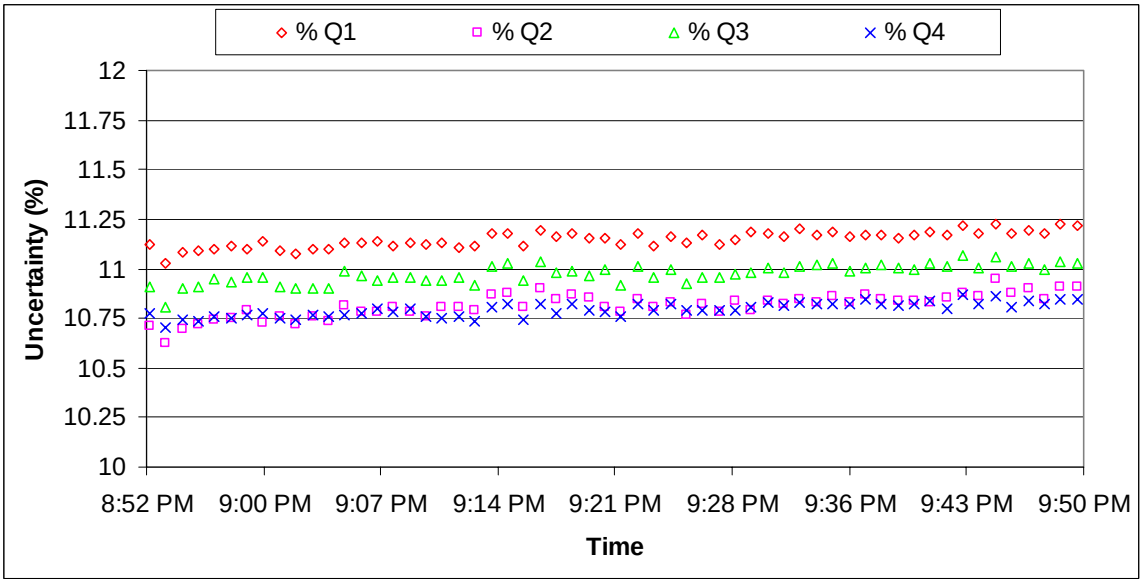

Figure 7.29 – GLHE Uncertainty

7.2 Borehole In-situ Tests

7.2.1 Undisturbed Ground Temperature

As shown in the literature review, the undisturbed ground temperature is an important parameter in determining the thermal properties of a ground loop heat exchanger. The method of lowering a temperature sensor into a water filled borehole (Gehlin and Nordell, 2003) was used to estimate the undisturbed ground temperature. The temperature sensor was a thermocouple calibrated to ± 0.18°F (0.1°C) attached to a Fluke Hydra Data Logger. Temperatures were measured at 10 ft (3.048 m) increments. The temperature profile for borehole 3 as shown in Figure 7.30 represents the typical temperature profile for an undisturbed borehole.

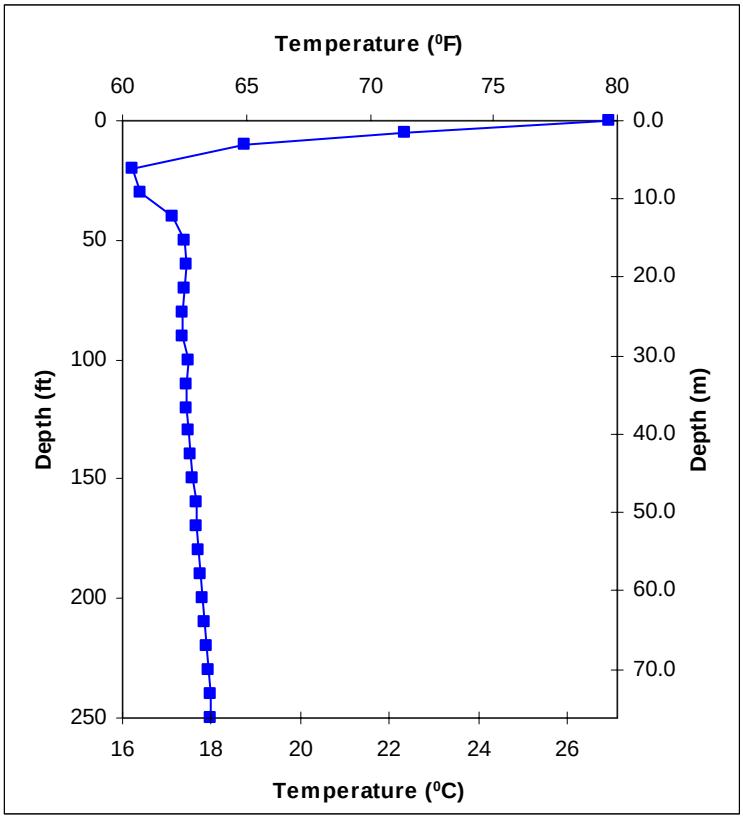

Figure 7.30 – Temperature Profile Along Borehole

The temperature profile for each borehole tested was similar with a small variation in average temperature. The average temperature was calculated from 10 ft (3.048 m) below the surface to the bottom of each borehole. The first 10 ft (3.048 m) of the borehole are affected by ambient conditions such as air temperature and rain. An average temperature was calculated as, 63.1°F (17.3°C), 63.3°F (17.4°C), 62.8°F (17.1°C), for borehole 1, 2, and 3 respectively.

7.2.2 In-situ Results

In-situ tests were performed on each borehole following the procedure presented by Austin (1998). Data from the tests were used to estimate the thermal conductivity of the grout and soil as well as the borehole thermal resistance. Heat input to the water, the mass flow rate as well as water inlet and outlet temperatures were measured. An example of the temperature results obtained from an in-situ test is shown in Figure 7.31.

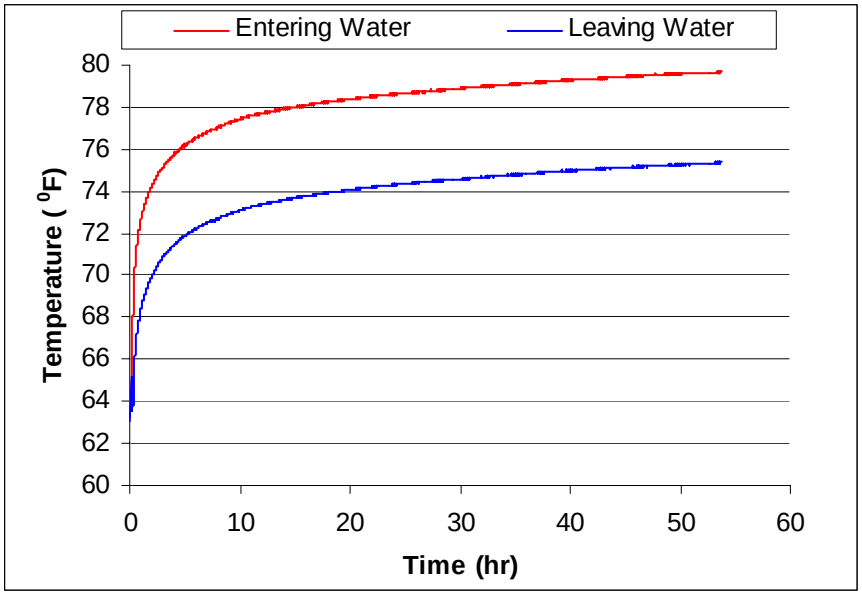

Figure 7.31 – In-situ Results for Borehole #3

The data from the in-situ tests for each borehole were then analyzed to ensure that ambient conditions did not affect the results. Inadequate insulation of the test apparatus

resulted in a fluid temperature oscillation that coincided with the ambient air temperature as shown in Figure 7.32.

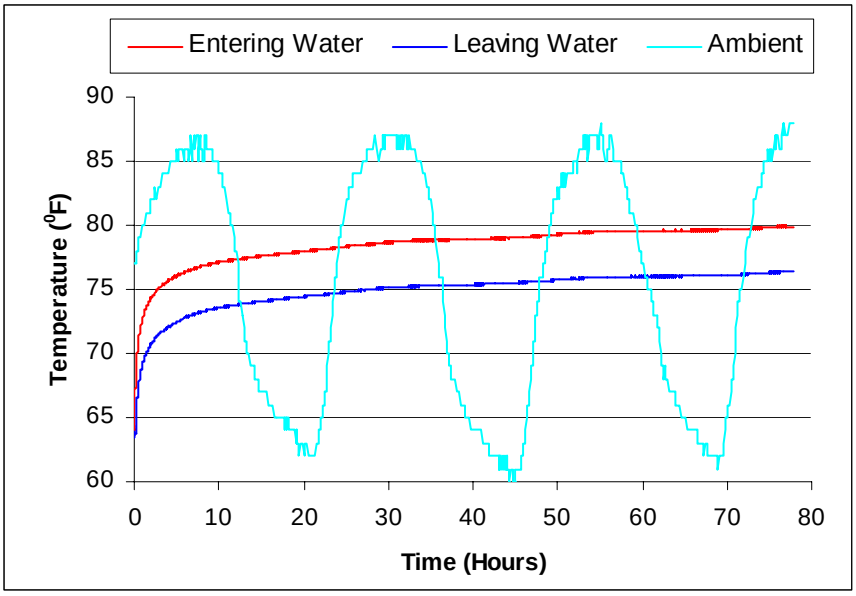

Figure 7.32 – In-situ Results with Improper Insulation

Tests were performed for a minimum of 50 hours as recommended by Austin (1998). To further verify that the results obtained for each test were good, a heat balance was performed. The results from the heat balance are shown in Table 7.2.

Table 7.2 – In-situ Test Error Comparison Results

Error	1	2	3	4	5
Average %	3.62	1.05	1.10	8.97	7.46
RMS	3.74	1.30	1.36	9.09	7.90
Max %	6.48	7.16	4.42	12.09	17.37

As shown the power input based on the temperature difference compares well with the heat input measured by current and amperage transducers. This shows that any extra heat input into the system by outside conditions is negligible and that the data will accurately represent the borehole properties.

The Geothermal Properties Measurement program (Shonder and Beck, 2000) developed at Oakridge National Laboratory was used to estimate the soil and grout

conductivity as well as the borehole resistance. This program uses the data recorded from an in-situ test along with the U-tube diameter, borehole diameter, borehole depth, deep earth temperature, and the soil and grout volumetric heat capacity. All of these parameters were known except for the soil and grout volumetric heat capacity, which can vary from an average range of 20 to 40 (Btu/ft^3-°F). A sensitivity analysis was preformed using the program and the corresponding values for the first borehole can be found in Table 7.3.

Table 7.3 – Sensitivity Analysis of Volumetric Heat Capacity

Soil Volumetric Heat Capacity (Btu/ft^3-^{o}F)	Grout Volumetric Heat Capacity (Btu/ft^3-^{o}F)	RMS of Model	Thermal Conductivity of Soil (Btu/hr-ft-^{o}F)	Thermal Conductivity of Grout (Btu/hr-ft-^{o}F)	Borehole Resistance (hr-ft-^{o}F/Btu)
20	20	0.135	1.45	0.69	0.26
20	30	0.135	1.53	0.69	0.26
20	40	0.158	1.59	0.69	0.26
30	20	0.119	1.41	0.64	0.28
30	30	0.096	1.50	0.64	0.28
30	40	0.098	1.57	0.64	0.28
40	20	0.129	1.37	0.62	0.29
40	30	0.097	1.45	0.61	0.29
40	40	0.088	1.53	0.61	0.29

As shown in the table, varying the grout thermal heat capacity changes the estimated thermal conductivity of the soil but has little effect on the borehole resistance. Changing the soil heat capacity changes the thermal conductivity of the grout and the borehole resistance.

From this data, it was decided to estimate the thermal conductivity and borehole resistance using an average capacity of 30 for both the soil and grout. This value was chosen because Austin (1998) found that changing the volumetric heat capacity changed the design length of a borehole by less than 10% and would give a conservative result.

The results for each vertical borehole are given in Table 7.4 using an average value of 63.1°F (17.3°C) for the undisturbed ground temperature.

Table 7.4 – Thermal Conductivity and Borehole Resistance of Vertical Boreholes

Borehole	Thermal Conductivity of Soil (Btu/hr-ft-^{o}F)	Thermal Conductivity of Grout (Btu/hr-ft-^{o}F)	Borehole Resistance (hr-ft-^{o}F/Btu)
1	1.50	0.63	0.28
2	1.55	0.63	0.28
3	1.37	0.62	0.28
4	1.46	0.69	0.25

7.3 System Modeling Considerations

7.3.1 System Pressure Drop Characteristics

An important part of performing any system simulation is the ability to accurately predict the power usage for a particular configuration or operating point. This is especially true for EnergyPlus which does not model the flow characteristics of a system. The user is required to enter the equipment power usage for circulating pumps and fans. Without system flow characteristics, it is difficult to estimate the correct power usage for the equipment at the true operating conditions.

For this reason the design spreadsheet mentioned in section 4.1 was modified by adding every fitting, pipe length and piece of equipment. The pressure drop for each source component and four different hybrid configurations were calculated for a range of flowrates. Figure 7.33 shows the various system curves. The GLHE included only two vertical boreholes so that the system would be undersized and used for moderate loads.

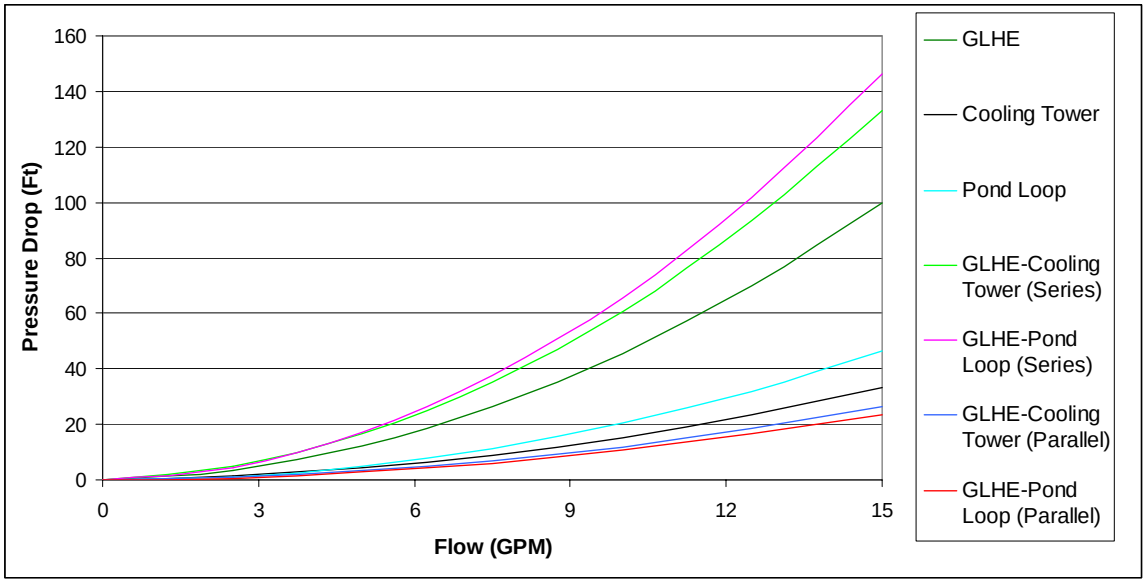

Figure 7.33 – System Pressure Drop Characteristics

As expected the series combination of the source components creates the largest pressure drop through the system followed by the individual components and then parallel combination. Each system curve was then modeled as a second order polynomial so that the pressure drop in the system could be determined without the design spreadsheet. The polynomial equation is given below:

$$\Delta P = a\dot{V}^2 + b\dot{V} + c \tag{7.10}$$

Where:
ΔP = pressure drop, Ft. of Head
$\dot{V}$ = volumetric flow rate of water, gpm
a = coefficient
b = coefficient
c = coefficient

The values for the coefficient can be found in Table 7.5.

Table 7.5 – System Pressure Drop Coefficients

Configuration	a	b	c
GLHE	0.420	0.348	-0.056
Cooling Tower	0.134	0.186	0.004
Pond Loop	0.212	-0.094	0.030
GLHE-Cooling Tower (Series)	0.556	0.517	0.000
GLHE-Pond Loop (Series)	0.633	0.246	0.000
GLHE-Cooling Tower (Parallel)	0.109	0.098	0.038
GLHE-Pond Loop (Parallel)	0.104	0.014	0.038

7.3.2 Source System Pumping Characteristic

With the system characteristics being calculated, the circulating pump needs to be modeled. The pump model needs to be able to accurately determine the pressure drop in the system for a certain flow rate and calculate the pump power. Since the source side pump is a variable speed pump and can operate under varying conditions, the circulating pump model presented in (Brandemuehl et al. 1992) was used to model the circulating pump. This circulation pump model allows for the estimation of the pressure drop given a volumetric flow rate and can estimate the power consumption. Another benefit is the model accounts for variable speed pumps.

First a dimensionless flow variable is defined:

$$\phi = \dot{V} / \left(N \cdot d^3 \right) \tag{7.11}$$

Where:
$\dot{V}$ = volumetric flow rate of water, m^3/s
N = rotational speed, rev/s
d = density, m

Then a dimensionless pressure rise is defined as:

$$\psi = \Delta P / \left(\rho \cdot N^2 \cdot d^2 \right) \tag{7.12}$$

Where:
ΔP = pressure rise across pump, Pa
ρ = impeller diameter, kg/m^3

The efficiency is defined as:

$$\eta = \dot{V} \cdot \Delta P / \dot{W} \tag{7.13}$$

Where:
$\dot{W}$ = pump power, W

The values for ψ and η can then be estimated from catalog data as a forth order polynomial function of ϕ as given below:

$$\psi = a_0 + a_1\phi + a_2\phi^2 + a_3\phi^3 + a_4\phi^4 \tag{7.14}$$

$$\eta = b_0 + b_1\phi + b_2\phi^2 + b_3\phi^3 + b_4\phi^4 \tag{7.15}$$

Catalog data was gathered for the main circulating pump used on the source side of the system. The data points were collected with a finer grid closer to the lower flow rate range where the pump would be operating. Table 7.6 shows the coefficients developed from these catalog points.

Table 7.6 – Pump Model Coefficients

a_0	a_1	a_2	a_3	a_4
5.79	42.3	-3406	60774	-1226291
b_0	b_1	b_2	b_3	b_4
0.06	38.1	-239	-30782	482037

To verify that the model is accurately representing the circulating pump, the results from the model were compared against the catalog data and can be seen in Figure 7.34 and 7.35.

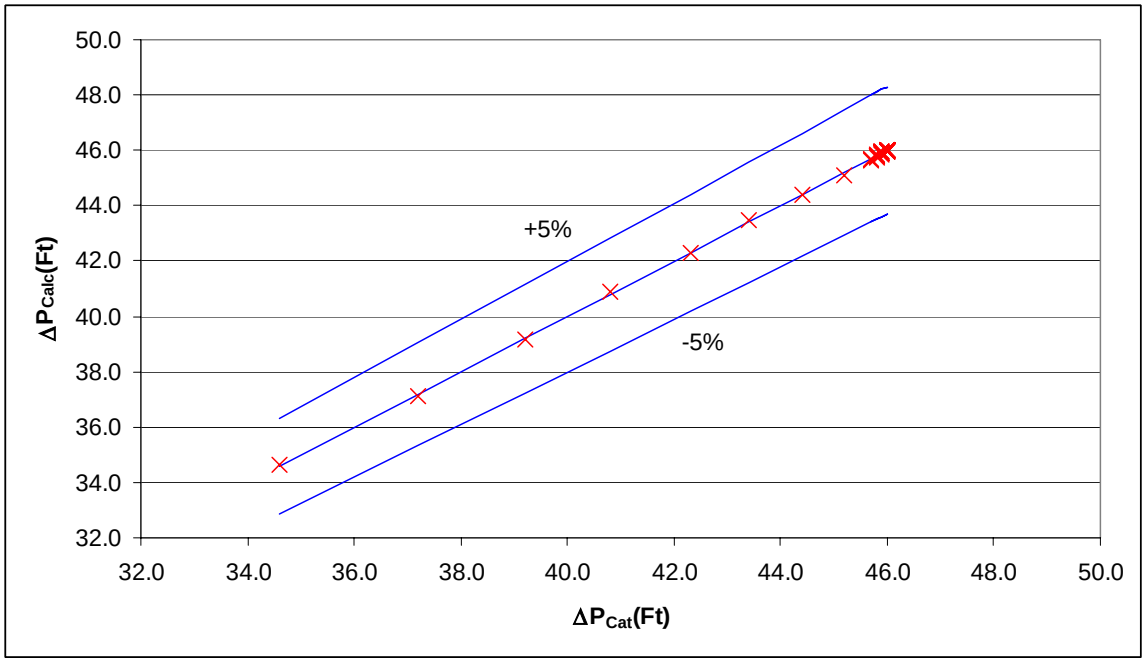

Figure 7.34 – Model vs. Catalog Comparison

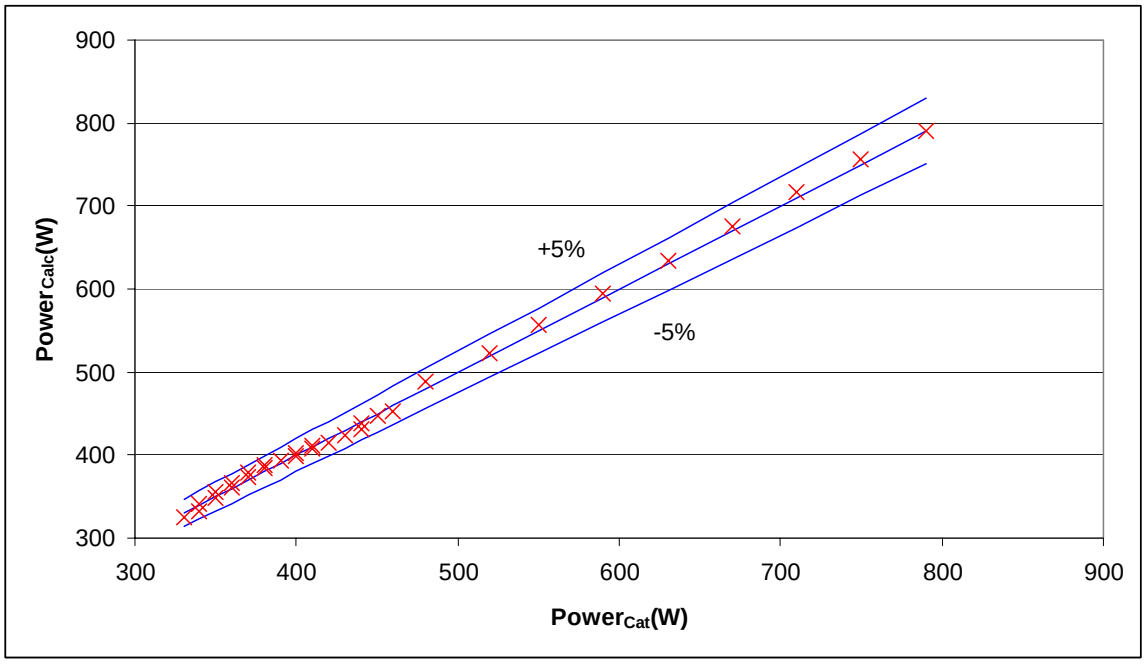

Figure 7.35 – Model vs. Catalog Comparison

As seen from the figures the model agrees very well with the catalog data. Both the power and pressure drop values produced by the model are within 5% of the catalog data.

The pump model and system characteristic curves were then used to estimate the power input for the circulating pump for different flow rates and source configurations. Table 7.7 shows the results obtained from this estimation compared to measured data for the operating system.

Table 7.7 – Pump Power Validation

Configuration	Flow (gpm)	Model Power (W)	Measured Power (W)	Error %
GLHE	6.2	90	198	54
	10.1	369	588	37
Cooling Tower	9.1	63	162	61
	12.0	141	278	49
Pond Loop	9.7	110	233	53
	12.8	262	528	50
GLHE-Cooling Tower (Series)	6.2	137	286	52
	7.2	209	400	48
GLHE-Pond Loop (Series)	5.9	130	249	48
	7.0	205	406	50
GLHE-Cooling Tower (Parallel)	10.2	63	143	56
	14.1	162	274	41
GLHE-Pond Loop (Parallel)	10.7	62	174	64
	14.7	159	342	53

The results from this experiment show a systematically large error between the model results and the measured data. A voltmeter was used to verify the output signal from the watt transducer and to eliminate possible errors with the Fluke/NetDAQ datalogger. To eliminate the possibility of a damaged watt transducer, the unit was replaced. The measured power usage for the new transducer matched the previous unit measurements. An ammeter was placed around each phase leg to measure the current. This value along with the voltage measured across each leg was used to calculate the power used by the operating pump. Results from this test matched the measurements obtained from the watt transducers. Correct installation of the watt transducer was verified by the manufacturer.

The pump manufacturer was then contacted to determine if the pump was operating properly and to ensure that the catalog data used in the model development was accurate. After a brief discussion it was determined that the pump was operating correctly and the error would not be due to the VFD which has an efficiency of approximately 97%. One possible source of error suggested is that the catalog data was generated with a circulating pump operating at 230Vac. While the facility operates at 208Vac, the manufacturer indicated that this should not create an error of this magnitude in the power usage. It was mentioned that the shaft bearings for the pump could be damaged, creating a drag on the motor and causing larger power usage. The manufacturer stated that this problem would worsen and eventually cause the pump to seize. It is recommended that during a system maintenance period, this issue be pursued further with the pump manufacturer.

Table 7.8 shows the pump model coefficients obtained from a least squares fit of the measured power data. Estimated power from the model was compared to the measured data as shown in Figure 7.36. The model was able to estimate power usage at higher pump rpm and flowrates.

Table 7.8 – Measured Pump Model Coefficients

b_0	b_1	B_2	b_3	b_4
-2.66	1711	-382210	37009076	-1305746117

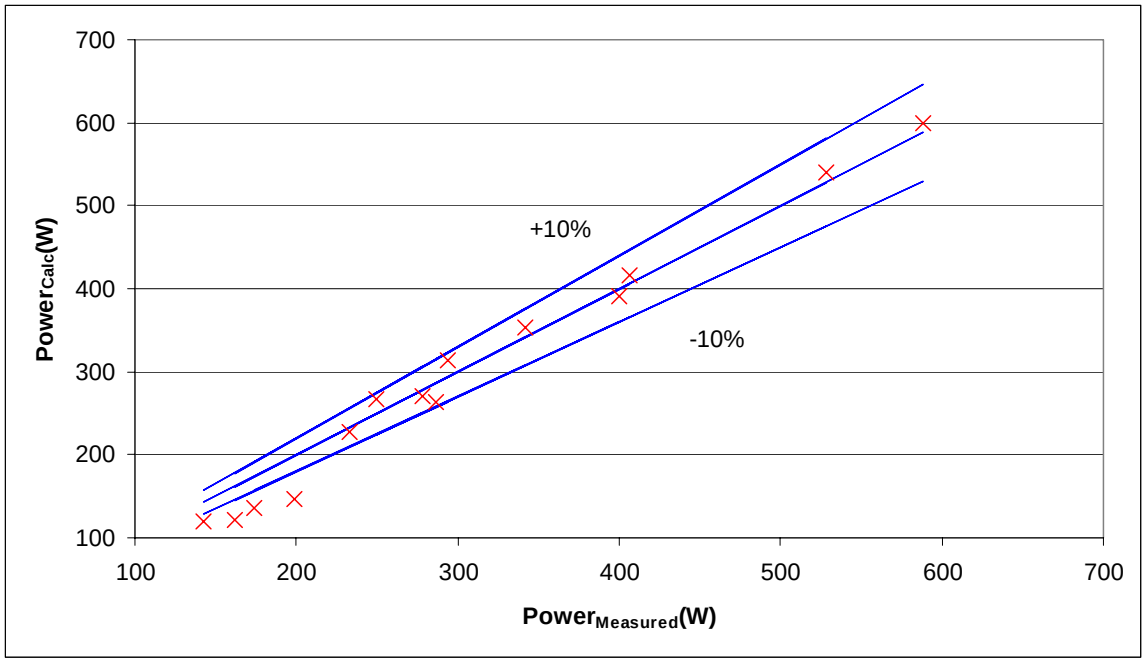

Figure 7.36 – Model vs. Measured Power Comparison

7.3.3 Circulation Piping Thermal Heat Transfer

Heat gain or loss from the circulation piping can be significant and may introduce significant error in the simulation if unaccounted for. For this reason, thermocouples were placed in the circulation pipe on the supply and return lines in the plant building and at each component. This allows the heat transfer rates from the un-insulated pipes to be measured.

Data gathered for the cooling tower and pond heat exchanger was analyzed to determine the heat transfer from the supply and return pipes. Figures 7.37-40 show the results for a steady cycle time with the heat pump. The uncertainty associated with this measurement is rather large as shown by the error bars attached to each data point.

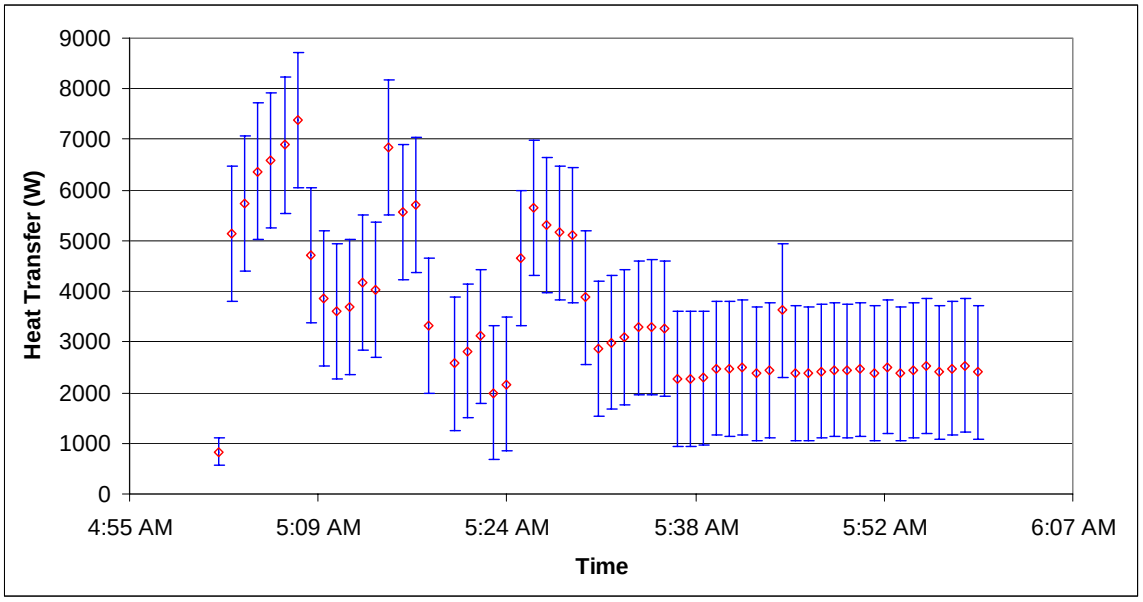

Figure 7.37 – Pond Loop Supply Pipe Heat Transfer

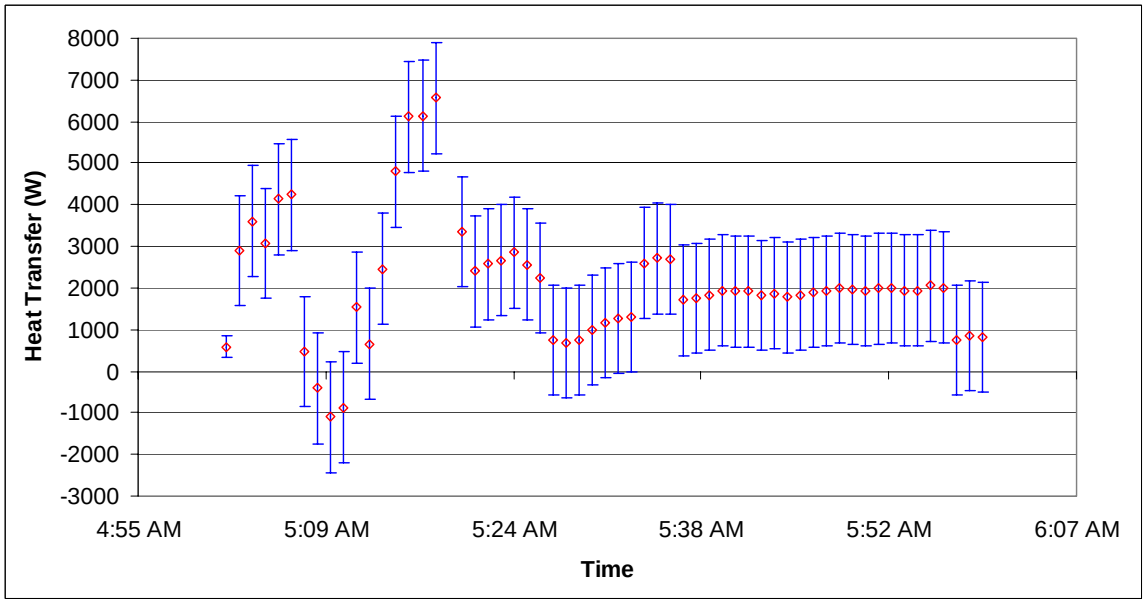

Figure 7.38 – Pond Loop Return Pipe Heat Transfer

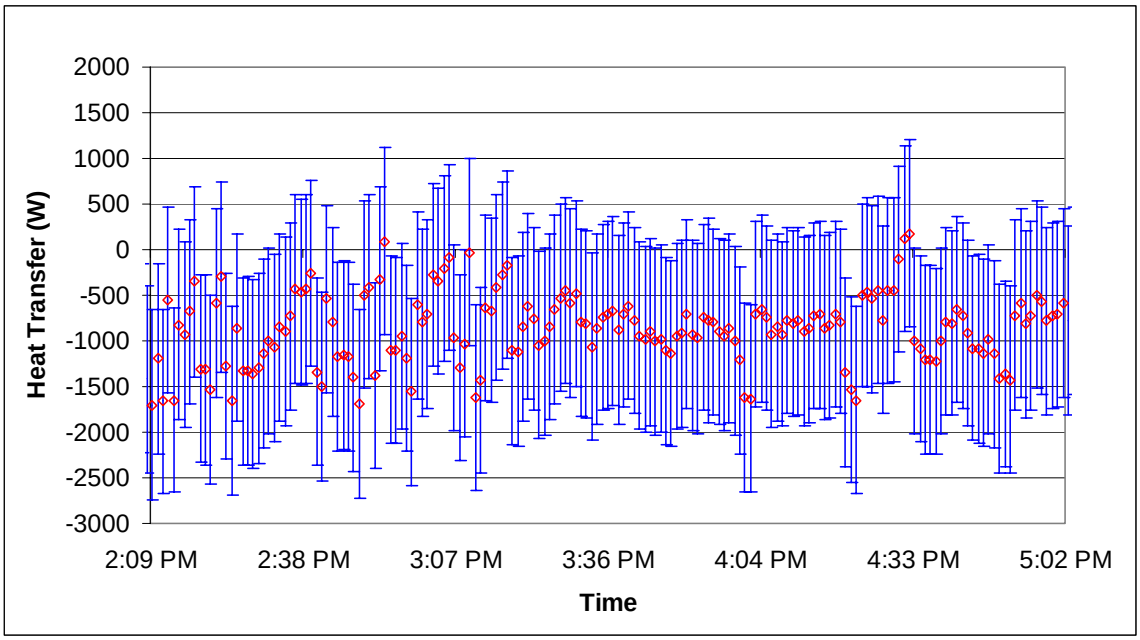

Figure 7.39 – Cooling Tower Supply Pipe Heat Transfer

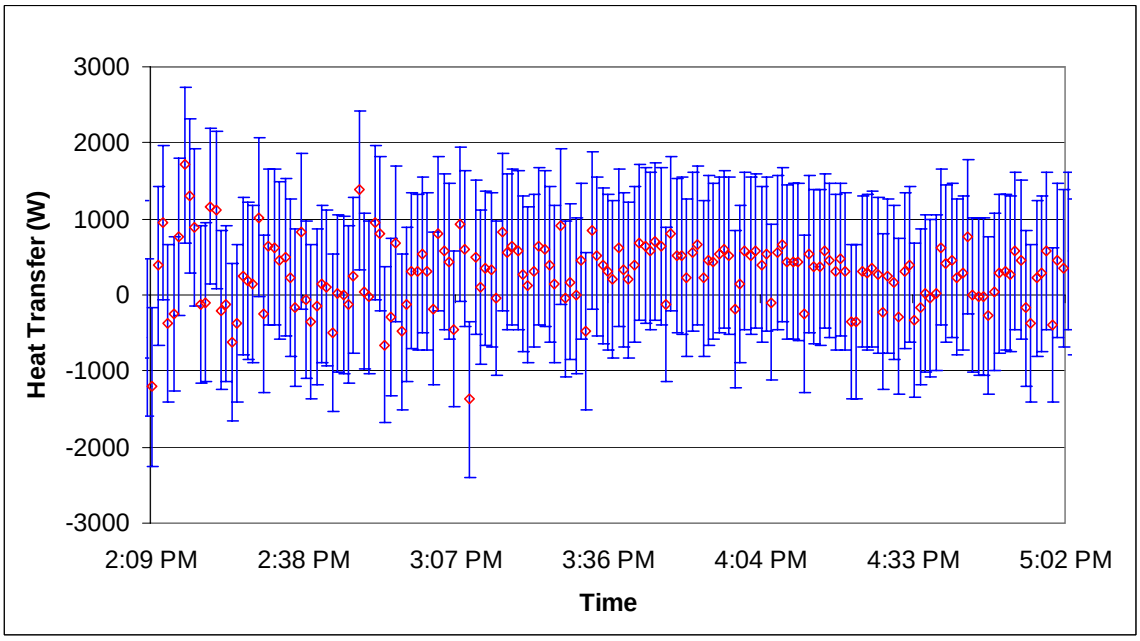

Figure 7.40 – Cooling Tower Return Pipe Heat Transfer

As shown in the figures, the heat transfer through the pipes can be quite large. The pond loop piping exhibits a greater heat transfer rate than the cooling tower due to the increased length of the buried pipe. The high uncertainty is, due primarily to the

accuracy of the HOBO data loggers. Upgrading these data loggers as previously recommended would significantly improve the accuracy of these calculations.

The temperature drop through the circulation piping for the GLHE was less than the uncertainty in the measurement, so the heat loss from these pipes could not be calculated with the current instrumentation. The relatively high flow rate and short length of these pipes results in an estimated heat loss that is typically less than 5% of the ground loop heat transfer rate.

8. Conclusions and Recommendations

8.1 Conclusions

Using current design techniques, an HGSHP experimental facility was constructed to validate existing and develop new HGSHP models for energy simulation programs. This facility included three independent source components: a ground loop heat exchanger, a pond loop heat exchanger, and an evaporative cooling tower. A range of source side configurations can be tested under variable flowrates, loads, and temperatures.

Sufficient instrumentation was installed to allow calculation of heat transfer rates, flow rates and power inputs at both the system and the component level. In addition, sufficient control hardware was installed to allow development of control algorithms and operating strategies for HGSHP systems.

Instrumentation was calibrated *in situ* to minimize measurement error. Calibration coefficients were listed along with an uncertainty analysis for each measurement. An uncertainty analysis was also performed for the calculated heat transfer rate.

Experiments were performed to demonstrate system performance and validate the calculated measurement uncertainties. Several conclusions were drawn from the results of these experiments.

- System control hardware and software operated as designed for the case of simple setpoint control of the heat pumps. Each heat pump was operated to maintain the setpoint temperatures of the hot and chilled water tanks.

- Measured temperatures, flow rates and power input showed an error in the heat pump energy balance of less than 5.0%. This was well within the predicted uncertainty of 5.7% for the heat pump energy balance. The plate heat exchanger energy balance error was also within the estimated uncertainty for the calculation.
- Transient operation was shown to have a significant impact on the overall system performance. The heat pump transient of approximately 9 minutes was estimated as 13% of the duty cycle for part load cooling operation. The cooling tower loop transient of 11 minutes was 13% of the duty cycle, and the pond loop transient of 28 minutes was 40% of the duty cycle for the part load cooling experiments.
- In-situ calibration of thermocouples and flowmeters resulted in an estimated uncertainty of ±0.11°F for temperature measurements with the Fluke NetDAQ dataloggers and an estimated uncertainty of ±0.42°C for temperature measurement with existing HOBO data loggers. The uncertainty associated with the HOBO loggers was unacceptably large and they are recommended for replacement in the following section. Flow measurement uncertainty is a function of the calibration time, weight, and voltage. For a flow rate of 10 gpm, the measurement uncertainty is approximately ±0.2 gpm.
- The GLHE transient response behaves as expected. Large heat transfer rates are obtained in the first couple of minutes because the water temperature at the top of the borehole is heated to near ambient temperature. The exiting water temperatures are low since the water has been sitting in the borehole and is close to the ground temperature. The heat transfer rate then decreases because the water being circulated through the boreholes is closer to the ground temperature

so the temperature drop across the borehole is low. After a short time period, the heat input from the heat pumps increases the input water temperature through the borehole and the heat transfer increases.

- Proper insulation is critical for the accurate measurement of borehole thermal properties. Inadequate insulation of the test apparatus results in a fluid temperature oscillation that coincides with the ambient air temperature. This unmeasured heat transfer can affect the estimated thermal conductivity of the borehole.
- The heat transfer rate from the uninsulated piping in a system can be a significant source of heat loss or gain. The experimental data showed that as much as 3000 W can be transferred in the installed system.

8.2 Recommendations and Future Work

Although this thesis presents a state-of-the-art experimental facility for HGSHP systems, the author suggests the following to improve facility performance:

- Replace the H-8 HOBO datalogger that measures the pond loop heat exchanger inlet and outlet temperature. The current datalogger has a temperature resolution which creates an unacceptable uncertainty in the measured heat transfer rate. A HOBO U-12 is recommended by the author to replace the H-8 remote datalogger. The U-12 can utilize the temperature probe used with the H-8 but increases the resolution to 0.03°C at 20°C. After calibration the accuracy of the temperature measurement would be increased from 0.42°C to 0.11°C.
- Convert the HOBO temperature measurements used at the cooling tower inlet and outlet to thermocouple probes. The two thermocouple probes could be attached to

the extra Fluke NetDAQ channels in the GLHE manhole. A potential problem with this setup is the requirement of an additional Fluke/NetDAQ datalogger.

- Use the remaining 8 thermocouples channels in the GLHE manhole to increase instrumention on the cooling tower. Thermocouples can be placed on the entering and leaving air screen of the cooling tower to give dry bulb temperatures to facilitate cooling tower model validation.
- Install a vortex flowmeter on the source side of each heat pump to increase the accuracy of measured flowrate into each heat pump.
- Modify the flowmeter calibration procedure to lengthen the flow measurement time well beyond the recommended 90 second minimum. Recalibrate the flowmeters using a flow measurement time of 100 seconds or more.
- Enclose each heat pump in and insulated, sealed cabinet with a single air inlet and a single air outlet. Measure air inlet and outlet conditions as well as the air flow rate. Using these measurements estimate the heat transfer rate from the heat pump to the surroundings. This estimate will significantly improve the overall heat balance on the heat pump.
- The current method of purging the cooling tower requires a significant time period to ensure that air is removed from the system. Installing a purge and isolation valve on the return piping line next to the cooling tower would facilitate purging.
- A pond loop heat exchanger component model needs to be developed that accounts for both pond thermal stratification and natural convection.

Development of this model would require additional pond instrumentation including a pond thermocouple grid around the heat exchanger.

- Work in conjunction with the manufacturer to determine the source of error found in the power measurement for the main circulation pump.

References

ASHRAE, (1995b). *Commercial/Institutional Ground-Source Heat Pump Engineering Manual*. Caneta Research, Inc., American Society of Heating, Refrigeration and Air-Conditioning Engineers, Inc., Atlanta, GA.

Austin III, W. A. (1998). Development of an In-Situ System for Measuring Ground Thermal Properties. Master's thesis. Oklahoma State University. Stillwater, Oklahoma.

Brandemuehl, M.J., S. Gabel, and I. Andresen. 1992. HVAC2KIT: A Toolkit for Secondary HVAC System Energy Calculations. Atlanta: American Society of Heating, Refrigerating, and Air-Conditioning Engineers, Inc.

Chiasson, A. (1999). Advances in Modeling of Ground-Source Heat Pump Systems. Master's thesis. Oklahoma State University. Stillwater, Oklahoma.

Churchill, S.W. (1977). Friction-Factor Equation Spans All Fluid-Flow Regimes. Chemical Engineering. 7 November: 91-92.

Crane Co., (1957). Flow of Fluids: Technical Paper 410. 4th Printing, Chicago.

Eldridge, D., D.E. Fisher, I.S. Iu, and C. Chantrasrisalai. (2003). Experimental Validation of Design Cooling Load Procedures: Facility Design. *ASHRAE Transactions*. 109(2)151-159.

Gehlin, S., and G. Hellstrom. (2003). Comparison of four models for Thermal Response Test Evaluation. *ASHRAE Transactions*. 109(1)

Gehlin, S., and B. Nordell. (2003). Determining undisturbed ground temperatures for thermal response test. *ASHRAE Transactions*. 109(1): 151-156

Gehlin, S. and J.D. Spitler. (2003). *Thermal Response Test for BTES Applications - State of the Art 2001*. 9th International Conference on Thermal Energy Storage Warsaw, Poland, September 1-4, 2003, pp. 381-387.

Kavanaugh, S. P. and K. Raffferty. (1997). Ground Source Heat pumps: Design of Geothermal Systems for Commercial and Institutional Buildings. Atlanta: American Society of Heating, Refrigerating and Air-Conditioning Engineers.

Kavanaugh, S. P. (1998). A Design Method for Hybrid Ground-Source Heat Pumps. *ASHRAE Transactions.* 104(2): 691-698.

Kline, S.J., and F.A. McClintock. (1953). *Describing Uncertainties in Single-Sample Experiments.* Mechanical Engineering 57(1): 62-6.

Martin, C.A., and S.P. Kavanaugh. (2002). Ground Thermal Conductivity Testing-Controlled Site Analysis. *ASHRAE Transactions*. 108(1): 945-951

McQuiston, F.C., J.D. Parker, and J.D. Spitler. (2000). *Heating, Ventilating, and Air Conditioning: Analysis and Design*, 5th ed. John Wiley & Sons, Inc.

Phetteplace, G., W. Sullivan. (1998). Performance of a Hybrid Ground-Coupled Heat Pump Systems. *ASHRAE Transactions.* 104(1b): 763-770.

Shonder, J.A., and J.V. Beck. (1999). Determining effective soil formation properties from field data using a parameter estimation technique. *ASHRAE Transactions*. 105(1): 458-466.

Shonder, J.A., and J.V. Beck. (2000). Field Test of a New Method for Determining Soil Formation Thermal Conductivity and Borehole Resistance. *ASHRAE Transactions*. 106(1): 843-850.

Shonder, J.A., and J.V. Beck. (2000). A new method to determine the thermal conductivity of soil formations from In Situ Field Tests. ORNL/TM-2000/97. Oak Ridge National Laboratory, Tennessee.

Yavuzturk, C., and J.D. Spitler. (2000). Comparative Study to Investigate Operating and Control Strategies for Hybrid Ground Source Heat Pump Systems Using a Short-Time-Step Simulation Model. *ASHRAE Transactions*. 106(2): 192-209.

Witte, H.J.L., G.L. van Gelder, and J.D. Spitler. (2002). In Situ Measurements of Ground Thermal Conductivity: The Dutch Perspective. *ASHRAE Transactions*. 108(1): 263-272

APPENDICES

Appendix A: Data Logger Channels

Table A1 – Data Logger Channels

Data Logger 1		Data Logger 2		Data Logger 3	
No	Name	No	Name	No	Name
A1	A1	B1	B1	C1	BH1
A2	A2	B2	B2	C2	BH2
A3	A3	B3	B3	C3	BH3
A4	A4	B4	B4	C4	BH4
A5	A5	B5	B5	C5	BH5
A6	A6	B6	B6	C6	BH6
A7	A7	B7	B7	C7	BH7
A8	A8	B8	B8	C8	BH8
A9	A9	B9	B9	C9	BH9
A10	A10	B10	B10	C10	BH10
A11	A11	B11	B11	C11	WT Pump 2
A12	A12	B12	B12	C12	WT Pump 3
A13	A13	B13	B13	C13	WT Pump 4
A14	Flow 1	B14	B14	C14	WT Pump 5
A15	Flow 2	B15	B15	C15	WT Pump 6
A16	Flow 3	B16	B16	C16	WT Pump 7
A17	Flow 4	B17	B17	C17	WT HP1
A18	Flow 5	B18	B18	C18	WT HP2
A19	Flow 6	B19	B19	C19	WT CT
A20	Flow 7	B20	Outside Temp.	C20	RH

Appendix B: Piping Schematic and Bill of Materials

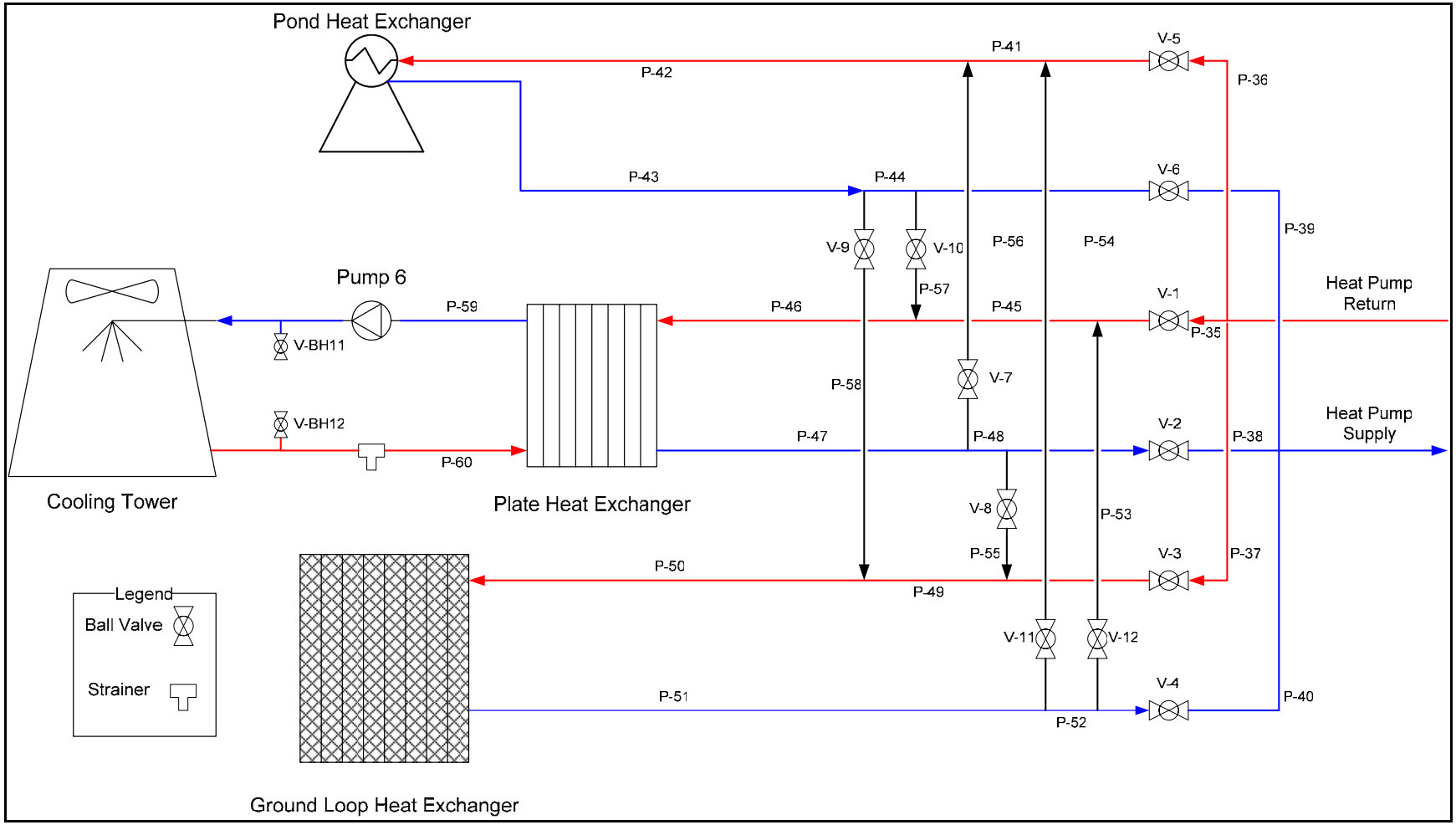

Figure B1 – Source Piping and Valve Schematic

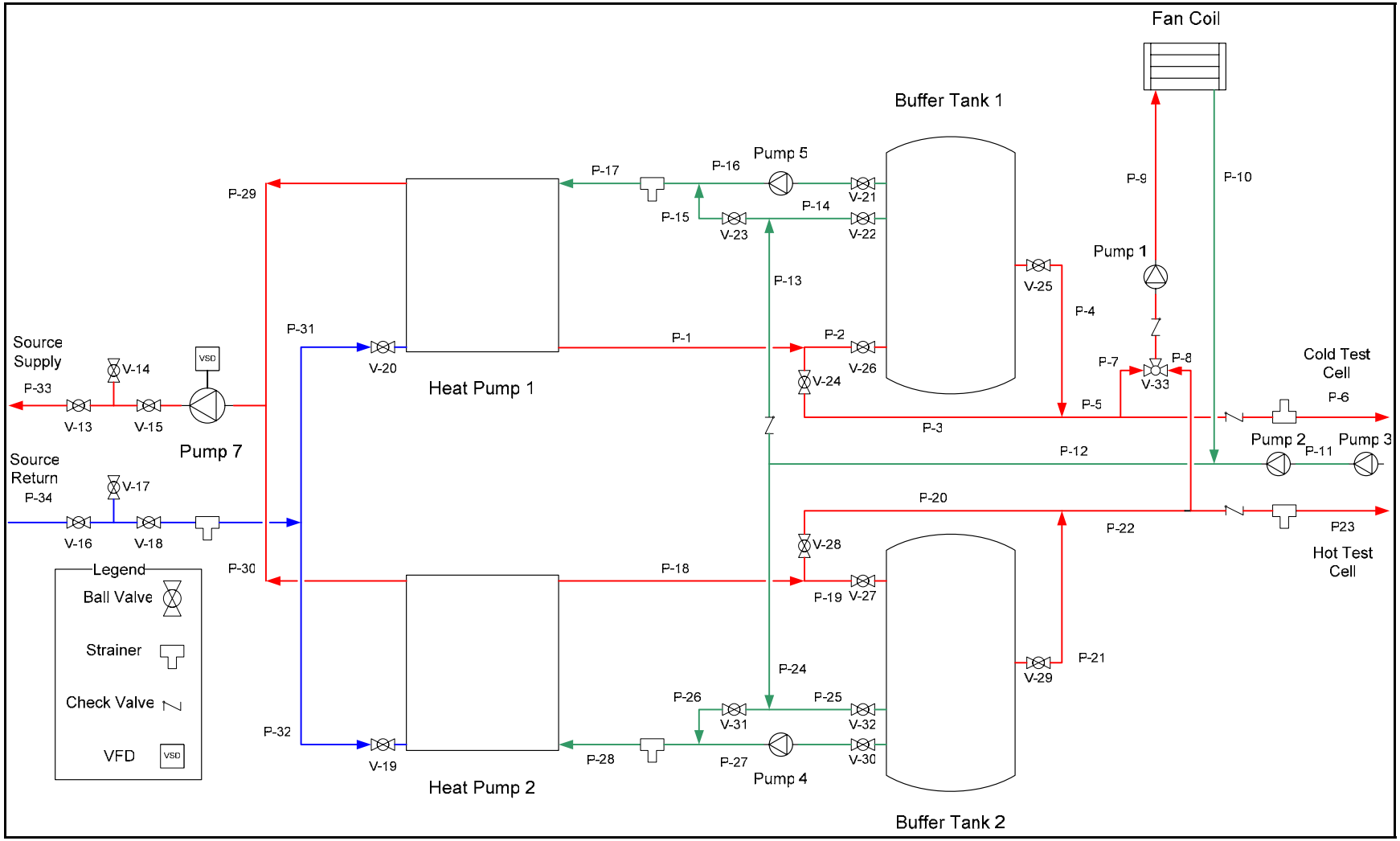

Figure B2 – Primary Equipment and Load Side Piping and Valve Schematic

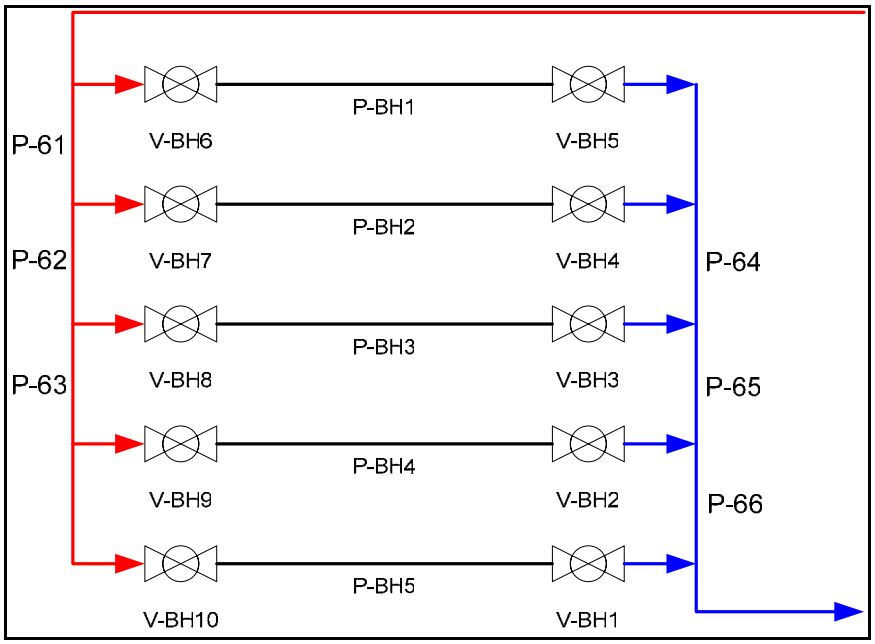

Figure B3 – Ground Loop Piping and Valve Schematic

Note: Pipe sizes are nominal (in) and are copper Type L unless a (-P) follows which designates HDPE.

Pipe length is in (ft).

Expander and reducer sizes are nominal pipe sizes (in).

Table B1 – Pipe Bill of Materials

Section Name	Pipe Size	Length	Strainer	Ball Valve	Union	Check	Expander Size	No.	Reducer Size	No.	Elbow	Flowmeter	T-Branch	T-Through
1	1	2.167	0	0	1	0	.75-1	2	1-.75	1	3	0	1	0
	0.75	1.75	0	0	2	0	0	0	0	0	0	1	0	0
2	1	3.667	0	1	1	0	0	0	0	0	2	0	1	1

3	1	0.333	0	1	0	0	0	0	0	0	0	0	2	0
4	1	0.833	0	1	1	0	0	0	0	0	1	0	0	0
5	1	4.583	0	0	0	0	0	0	0	0	0	0	0	1
6	1	1.833	1	0	0	1	1-1.5	1	0	0	1	0	0	1
	1.5-P													
7	1	2	0	0	0	0	0	0	0	0	2	0	1	0
8	1	2.25	0	0	0	0	0	0	0	0	3	0	1	0
9	1	3	0	0	1	1	0	0	1-.75	1	2	0	0	1
	0.5	1.167	0	0	2	0	.5-1	1	1-.5	1	0	1	0	0
10	1	5.833	0	0	1	0	.75-1	1	0	0	2	0	0	1
11	1.5	0.75	0	0	0	0	0	0	1.5-1	1	1	0	0	0
	1	0.333	0	0	0	0	0	0	0	0	0	0	1	1
	2-P						0	0	2-1.5	1				
12	1	5	0	0	1	0	0	0	0	0	1	0	1	1
13	1	7.25	0	0	2	1	0	0	0	0	2	0	0	0
14	1	0.333	0	1	0	0	0	0	0	0	0	0	1	0
15	1	1	0	1	1	0	0	0	0	0	1	0	2	0
16	1	0.5	0	1	0	0	1-1.5	1	1.5-1	1	0	0	0	1
17	1	5.917	1	0	1	0	0	0	1-.75	1	6	0	1	0
18	1	7.333	0	0	2	0	.75-1	2	1-.75	1	4	0	1	1
	0.75	1.75	0	0	2	0	0	0	0	0	0	1	0	0
19	1	6	0	1	0	0	0	0	0	0	0	0	1	0
20	1	2.417	0	1	1	0	0	0	0	0	2	0	1	1
21	1	0.833	0	1	1	0	0	0	0	0	1	0	0	0
22	1	0.333	0	0	0	0	0	0	0	0	0	0	0	2
23	1	1.917	1	0	0	0	1	1-1.5	1	0	0	0	0	1
	1.5-P													
25	1	0.333	0	1	0	0	0	0	0	0	0	0	1	0
26	1	0.5	0	1	0	0	0	0	0	0	0	0	1	0
27	1	1.167	0	1	0	0	1-1.5	1	1.5-1	1	2	0	0	0
28	1	14.75	1	0	2	0	0	0	1-.75	1	4	0	2	0

29	1.5	2.417	0	0	1-.75"	0	.75-1.5	1	0	0	1	0	1	1
30	1.5	0.5	0	0	1-.75"	0	.75-1.5	1	0	0	0	0	2	0
31	1.5	2.417	0	1-.75"	1-.75"	0	0	0	1.5-.75	1	0	0	1	1
32	1.5	0.5	0	1-.75"	1-.75"	0	0	0	1.5-.75	1	0	0	2	0
33	1.5	10.33	0	2	0	0	0	0	0	0	4	0	0	1
34	1.5	11.67	1	2	1	0	0	0	0	0	4	0	0	1
35	1.5	5.667	0	1	0	0	0	0	0	0	1	0	0	2
36	1.5	1.583	0	1	0	0	0	0	0	0	0	0	1	0
37	1.5	2.667	0	1	0	0	0	0	0	0	0	0	1	1
38	1.5	1.333	0	1	0	0	0	0	0	0	2	0	1	2
39	1.5	4	0	1	0	0	0	0	0	0	2	0	1	0
40	1.5	2.667	0	1	0	0	0	0	0	0	2	0	1	1
41	1.5	0.667	0	0	0	0	0	0	0	0	0	0	1	0
42	1.5	11	0	0	0	0	0	0	0	0	3	0	0	2
	2-P	496	0	0	0	0	0	0	2-1.5	1	1	0	0	0
43	1.5	7.75	0	0	0	0	.75-1.5	1	1.5-.75	1	3	0	0	1
	0.75	1.75	0	0	2	0	0	0	0	0	0	1	0	0
	2-P	496.5	0	0	0	0	1.5-2	1	0	0	1	0	0	0
44	1.5	0.667	0	0	0	0	0	0	0	0	0	0	0	1
45	1.5	1.333	0	0	0	0	0	0	0	0	0	0	0	1
46	1.5	15.75	0	0	0	0	0	0	0	0	5	0	0	1
	1	0.333	0	0	1	0	0	0	1.5-1	0	0	0	1	0
47	1.5	17.17	0	0	0	0	.75-1.5	1	1.5-.75	1	5	0	0	2
	1	0.167	0	0	1	0	1-1.5	1	0	0	0	0	0	0
	0.75	1.75	0	0	2	0	0	0	0	0	0	1	0	0
48	1.5	0.667	0	0	0	0	0	0	0	0	0	0	0	1
49	1.5	2.667	0	0	0	0	0	0	0	0	0	0	0	1
50	1.5	11.25	0	0	0	0	0	0	0	0	3	0	0	1
	1.5-P	123	0	0	0	0	0	0	0	0	3	0	0	0
51	1.5	11.17	0	0	0	0	.75-1.5	1	1.5-.75	1	3	0	0	1
	1.5-P	120.5	0	0	0	0	0	0	0	0	3	0	0	0

	0.75	1.75	0	0	2	0	0	0	0	0	0	1	0	0
52	1.5	0.667	0	0	0	0	0	0	0	0	0	0	0	1
53	1.5	2.167	0	1	0	0	0	0	0	0	3	0	2	0
54	1.5	2.5	0	1	0	0	0	0	0	0	3	0	2	0
55	1.5	2.5	0	1	0	0	0	0	0	0	3	0	2	0
56	1.5	4.167	0	1	0	0	0	0	0	0	3	0	2	0
57	1.5	2.167	0	1	0	0	0	0	0	0	3	0	2	0
58	1.5	3.333	0	1	0	0	0	0	0	0	3	0	2	0
59	1.5	1	0	0	0	0	1-1.5	1	0	0	1	0	0	0
	1.5-P	144	0	0	0	0	0	0	0	0	5	0	1	1
	1	2.833	0	0	1	0	0	0	0	0	1	0	1	0
60	1.5	0.167	1	0	0	0	0	0	1.5-.75	1	1	0	0	0
	1.5-P	144.5	0	0	1	0	0	0	0	0	5	0	1	1
	1	0.583	0	0	1	0	.75-1	1	0	0	0	0	1	0
	0.75	1.75	0	0	2	0	0	0	0	0	0	1	0	0
61	1.5-P	0.333	0	0	0	0	0	0	0	0	0	0	0	1
62	1.5-P	0.167	0	0	0	0	0	0	1.5-.75	1	0	0	0	1
	.75-P	0.167	0	0	0	0	0	0	0	0	0	0	0	0
63	.75-P	0.333	0	0	0	0	0	0	0	0	0	0	0	1
64	.75-P	0.333	0	0	0	0	0	0	0	0	0	0	0	1
65	1.5-P	0.167	0	0	0	0	1.5-.75	1	0	0	0	0	0	1
	.75-P	0.167	0	0	0	0	0	0	0	0	0	0	0	0
66	1.5-P	0.333	0	0	0	0	0	0	0	0	0	0	0	1
BH1	1.5-P	0.333	0	0	0	0	0	0	1.5-.75	1	0	0	1	0
	.75-P	550	0	2	0	0	0	0	0	0	1	0	0	2
BH2	1.5-P	0.333	0	0	0	0	0	0	1.5-.75	1	0	0	1	0
	.75-P	482	0	2	0	0	0	0	0	0	0	0	1	2
BH3	.75-P	508	0	2	0	0	0	0	0	0	0	0	2	2
BH4	1.5-P	0.333	0	0	0	0	.75-1.5	1	0	0	0	0	1	0
	.75-P	524	0	2	0	0	0	0	0	0	0	0	1	2
BH5	1.5-P	0.333	0	0	0	0	.75-1.5	1	0	0	0	0	1	0

	.75-P	658	0	2	0	0	0	0	0	0	1	0	0	2

Appendix C: Standard Operating Procedures

Note: Any number with a V-# references a valve found in Figures B1-3.

Purging the Source Side

Connecting the purge cart.

1) Obtain the large purge cart.
2) Attach the supply and return hoses to the barbed connections on the V-14 and V-17.
3) Connect a water hose to the purge cart from the outside faucet.
4) Turn on the water and fill the purge cart.
5) Connect the power cord to the 120 Vac outlet located on the west wall below the circuit breaker box. This outlet and circuit breaker are rated to be able to handle the amperage that the purge cart can use when in operation.
6) Adjust the 3-way valves on the purge cart to supply and return water from the system.

Purging the heat pumps.

7) Shut valves V-13 and V-16. Open valves V-15, V-18, V-19 and V-20.
8) Turn on the purge cart making sure to maintain at least ½ of a tank full of water so that no air will be pumped into the system. Purge the system for the time period according to IGSHPA (1991).
9) After the time period has passed, turn V-17 off and then V-14 off. Turn the purge cart off. This sequence will maintain pressure in the system so that any leak can be detected and to keep air out of the system.

Purging the source components.

10) Shut valves V-15 and V-18. Open valves V-13 and V-16.

11) Open V1-12 based upon which source component needs to be purged.

12) Turn on the purge cart making sure to maintain at least ½ of a tank full of water so that no air will be pumped into the system. Purge the system for the time period according to IGSHPA (1991).

13) Adjust V-22 so that the flow rate through each vortex flowmeter stays below 16 gpm. Any flow operation above this value for an extended period could damage the flowmeter.

14) After the time period has passed, turn V-14 off and then V-17 off. Turn the purge cart off. This sequence will maintain pressure in the system so that any leak can be detected and to keep air out of the system.

Purging the Load Side

Purging the Buffer Tanks.

1) Attach a water hose to the valve located on the bottom of the buffer tanks.
2) Open the valve located on the top of each tank.
3) Turn on the water from the hydrant. Leave the top valve on each tank until water starts to emerge. At this point, close the top valve.
4) Close the bottom valve and then shut off the water hydrant.

Purging the load components.

5) Obtain the large purge cart.
6) Attach the supply and return hoses to the barbed connections located under the airflow measurement box.

7) Connect a water hose to the purge cart from the outside faucet.
8) Turn on the water and fill the purge cart.
9) Connect the power cord to the 120 Vac outlet located on the north face of the military supply box east of the south test cell. This outlet and circuit breaker are rated to be able to handle the amperage that the purge cart can use when in operation.
10) Adjust the 3-way valves on the purge cart to supply and return water from the system.
11) Turn on the purge cart. Open the valves under the airflow measurement box.
12) Adjust the appropriate values in both the tower and plant side to purge each specific pipe leg. Note that the actuated 2 and 3-way valves will need to be changed to purge different part of the test cell supply piping.
13) Close the supply and return valves and then turn off the purge cart.

Experimental Test Procedures

Plant Building Startup

1) Turn on the circuit breakers for the equipment needed for the plant operation
2) Turn on the computer and NetDAQ loggers.
3) Plug in the power supplies in the control circuit board box.
4) Move the switch on the timer board into the "Test" position. The bottom LED will light and the timer board will then be set to high.

Buffer Tank Operation

5) If using Buffer Tank 1, open V-21, V-22, V-25 and V-26. Close V-23 and V-24.
6) If using Buffer Tank 2, open V-27, V-29, V-30 and V-32. Close V-25 and V-31.

Plant Source Setup

7) Open V-19 and V-20 to operate both heat pump 1 and 2.

8) Open V-13, V-15, V-16, V-18.

9) Open V-1: V-12 on the valve chest to select the source components and configuration needed for testing.

GLHE Setup

10) Remove the manhole lid and adjust V-BH1: V-BH10 to select the boreholes needed for testing.

Cooling Tower Setup

11) Turn on the power disconnect located at the base of the cooling tower.

12) Clean the basin of the cooling tower to remove any dirt of foreign materials.

13) Attach a hose to the water hydrant and small pipe stub-out located next to the GLHE manhole.

14) Turn on the hydrant and fill the cooling tower water basin.

15) Adjust the basin float and overflow drain to the desired position.

Data Acquisition Setup

16) In Windows, click on Start-Programs-Fluke NetDAQ Logger-NetDAQ Logger.

17) In the NetDAQ logger program, open the file “final setup” to bring in the correct setup for the data loggers.

18) Click on the button “Start All Instruments”. The data loggers will then start collecting data.

19) On the Desktop, open the latest “input-output.xls” file. This will load the data acquisition and controls program.

20) In the “input-output.xls” file, click on the “options” worksheet. Select the equipment that is going to be in operation.

21) Click on the “status” worksheet. Adjust the minimum flow set points, delay times, and tank temperatures to the desired values.

22) Click on the “recorded data” worksheet. Adjust the timer period between recorded data readings and the time period between control outputs.

System Startup

23) Click on the “Start” button located on the “recorded data” worksheet. Click “Yes” if a new data set is being started.

24) Click on the “options” worksheet. Click the button “Turn on the Equipment”. After a short time, the equipment will start.

25) The flow rate of each source component can be seen on the “Realtime-Sources” worksheet. Adjust the VFD to obtain the desired flow rate through the source components. Press the button labeled “Hand” on the VFD control panel. Use the arrow buttons to adjust the frequency until the pump is providing the desired flow rate. Press the “Auto” button to the place the VFD back into auto mode so that it can be controlled by the computer.

26) Move the switch on the timer board to “Run”. After a few seconds, the bottom LED should blink indicating that the data acquisition program is working.

27) Monitor the equipment for a few minutes to make sure that the system appears to be operating correctly.

Maintenance

Strainers

1) To ensure that the system operates to peak performance, each strainer needs to be cleaned after 1000 hours of operation or if the system flow rate is below the normal operation point.
2) Find the closest isolations valves immediately up and downstream of the strainer. Close each valve so that the system will need very little purging after cleaning.
3) Unscrew the strainer housing and remove the cartridge.
4) Clean the cartridge and reinstall.
5) Open the isolation valves and then purge the system where the strainer was removed.

Cooling Tower

1) When the cooling tower is not in operation, always drain the basin so that moss and algae will not grow.
2) The supply and return lines need to be drained to prevent water from freezing and breaking the piping.
3) Open V-BH11 and V-BH12 to drain the supply and return lines.
4) Use compressed air or a vacuum to remove the water from the makeup water line.

Appendix D: Equipment Specifications

Fan Coil – (McQuay, http://www.mcquay.com/mcquaybiz/literature/lit_at_fc/Catalogs/Cat700-1Rev10-04.pdf, 12-08-04)

Performance Data – THC Horizontal Concealed (4-Pipe System)

ARI Approved Standard Coil Water Cooling Capacity Ratings ~

UNIT SIZE	FTHC HORIZONTAL CONCEALED UNIT			
	COOLING CAPACITY ~		WATER FLOW GPM	WATER P.D. FT. W.C.
	TOTAL BTUH	SENSIBLE BTUH		
H02	8500	6100	1.94	5.10
H03	11,100	8400	2.51	3.26
H04	14,500	10,800	3.26	5.80
H06	21,200	16,100	4.70	12.82
H08	22,700	18,000	5.14	3.68
H10	25,300	20,000	5.70	4.76
H12	34,200	27,000	7.75	8.29

Standard Coil Water 1-Row Heating Capacity Ratings ~

UNIT SIZE	FTHC HORIZONTAL CONCEALED UNIT		
	1-ROW HEATING CAPACITY ~	WATER FLOW GPM	WATER P.D. FT. W.C.
	SENSIBLE BTUH		
H02	11,500	0.64	1.47
H03	16,300	0.91	2.89
H04	20,400	1.12	5.32
H06	29,600	1.65	10.72
H08	36,100	2.00	3.24
H10	40,300	2.24	4.07
H12	49,800	2.76	6.45

Water heating coils at 70°F DB entering air, 180°F entering water, 40°F water temperature drop and high fan speed with standard 115/60/1 motor.
For heating coil capacity ratings at conditions other than those listed refer to the RepTools Computer Selection Program or consult your McQuay representative.

General Unit Data

		Unit Size						
		H02	H03	H04	H06	H08	H10	H12
Fan								
Type		Centrifugal Fan (forward-curved galvanized steel fan wheel)						
Number of Fans		1	1	2	2	3	3	4
Fan Housing		Galvanized Steel						
Coil								
Number of Rows		3/1 Split						
Type		Water - (3-Row Chilled Water) (1-Row Hot Water)						
Testing Pressure		425 psi for 1 minute; leak test: 225 psi for 5 minutes						
Motor(s)								
Type		PSC						
Number of Motors		1	1	1	1	2	2	2
Power Supply		115/60/1, 208-230/50/60/1, 277/60/1						
Watts - High Speed								
50Hz		62	91	109	171	242	249	321
60Hz		75	109	131	205	291	299	385
Coil Connection		3/4" FPT						
Drain Pipe		3/4" MPT						
Unit with Return Air Plenum and Filter								
Length	in.	21.90	21.90	21.90	21.90	21.90	21.90	21.90
Width	in.	32.05	38.74	43.86	51.73	61.57	65.51	75.75
Height	in.	9.88	9.88	9.88	9.88	9.88	9.88	9.88
Ship Weight	lb.	63.00	73.00	88.00	102.00	134.00	143.00	153.00

Conditions:
~ Cooling Capacity: Entering air temp.80°F (DB), 67°F (WB); Entering water temp.45°F, Leaving water temp. 55°F. ~ Heating Capacity: Entering air temp.70°F (DB); Entering water temp.180°F.
Air Flow: Under dry coil conditions, fan speed high.
Weight: Includes return air plenum and packing.

Dimensional Data – THC Horizontal Concealed, with Extended Drain Pan and Plenum Filter Box

Unit Size		A B		C D		E F	Number of Fans	Filters	
								Size	Qty
H02	32.05"	17.64"	19.17"	19.96"	18.46"	21.13"	1	18 1/8" x 8" x 1"	1
H03	38.74"	24.33"	25.87"	26.65"	25.15"	27.82"	1	24 7/8" x 8" x 1"	1
H04	43.86"	29.45"	30.98"	31.77"	30.20"	32.94"	2	29 7/8" x 8" x 1"	1
H06	51.73"	37.32"	38.86"	39.65"	38.07"	40.82"	2	18 7/8" x 8" x 1"	2
H08	61.57"	47.17"	48.70"	49.49"	47.91"	50.66"	3	23 3/4" x 8" x 1"	2
H10	65.51"	51.10"	52.64"	53.43"	51.85"	54.60"	3	25 3/4" x 8" x 1"	2
H12	75.75"	61.34"	62.87"	63.66"	62.09"	64.83"	4	30 7/8" x 8" x 1"	2

All dimensions ± 0.10"

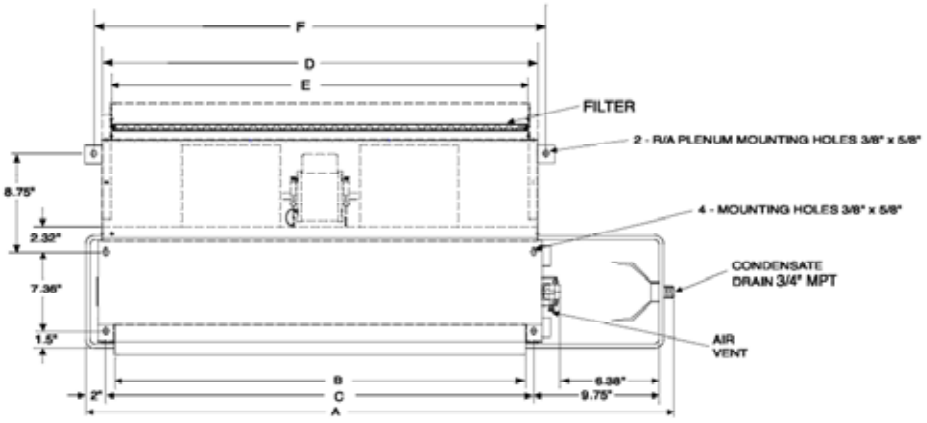

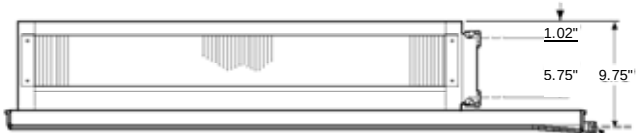

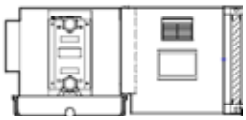

Plenum Back with Filter

1.40"

CONDENSATE DRAIN 3/4" MPT

FILTER RAIL

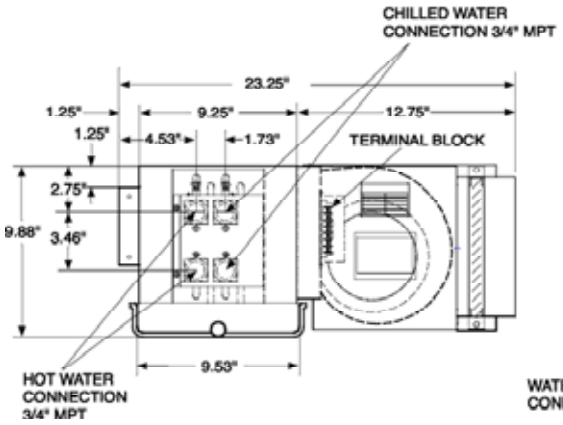

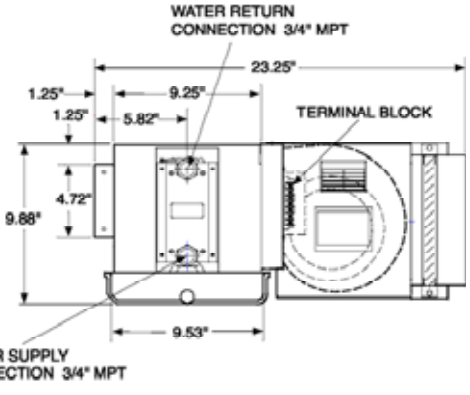

8.125"

Air Volume Capacity Data

Air volume versus external static pressure

Unit Size		Fan Motor Speed: High — External Static Pressure (INCHES OF WATER)							Fan Motor Speed: Medium — External Static Pressure (INCHES OF WATER)							Fan Motor Speed: Low — External Static Pressure (INCHES OF WATER)						
		.00	.05	.10	.15	.20	.25	.30	.00	.05	.10	.15	.20	.25	.30	.00	.05	.10	.15	.20	.25	.30
H02	Air Flow cfm	311	288	270	255	236	224	207	231	211	195	178	164	152	134	181	157	139	125	111	94	87
	RPM	1043	1138	1172	1194	1240	1262	1291	869	879	966	1012	1051	1108	1119	704	773	826	887	965	1032	1091
H03	Air Flow cfm	423	398	383	366	343	326	308	298	277	262	244	229	213	197	235	218	200	184	165	148	133
	RPM	1143	1172	1202	1226	1255	1282	1313	838	890	945	992	1043	1097	1144	714	756	833	886	953	1023	1081
H04	Air Flow cfm	507	472	444	416	386	359	326	340	298	267	239	209	181	153	274	234	197	170	143	111	83
	RPM	1122	1165	1201	1221	1258	1285	1314	788	851	903	964	1043	1093	1156	678	737	811	891	957	1028	1091
H06	Air Flow cfm	798	770	742	714	688	654	627	578	549	534	508	483	456	432	518	497	471	444	425	406	376
	RPM	1295	1311	1333	1361	1382	1399	1416	990	1017	1060	1102	1151	1182	1230	894	937	994	1049	1086	1141	1181
H08	Air Flow cfm	949	918	874	833	788	747	716	740	703	671	632	594	550	517	662	632	601	554	521	490	449
	RPM	1172	1192	1221	1259	1286	1320	1341	931	1003	1027	1072	1124	1167	1219	892	935	956	1014	1070	1121	1174
H10	Air Flow cfm	1032	981	932	881	836	712	716	775	723	688	631	582	533	493	697	643	602	538	496	463	410
	RPM	1251	1279	1303	1331	1344	1386	1412	984	1037	1068	1115	1169	1245	1255	902	969	1001	1062	1123	1161	1204
H12	Air Flow cfm	1428	1380	1334	1287	1229	1173	1114	1067	1022	976	927	875	833	781	960	912	877	826	788	806	705
	RPM	1344	1367	1389	1408	2845	2886	1462	1039	1062	1106	1149	1192	1235	1277	958	1003	1043	1095	1141	1178	1224

Note: Based on 115V operation, and dry coils.

Evaporative Cooling Tower (Amcot, http://www.amcot.com/temp/Fiberglass.pdf, 12-08-04)

Dimensions and Pipe Connections

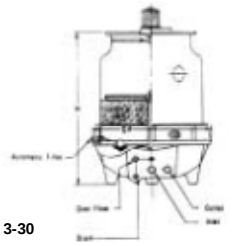

ST 3-30

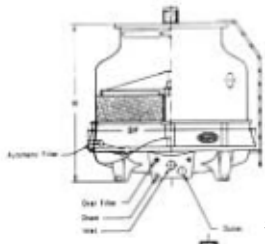

ST 40-175

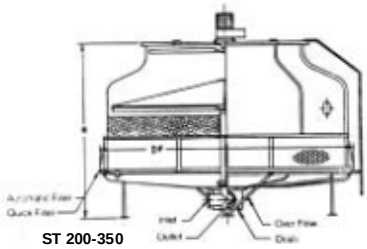

ST 200-350

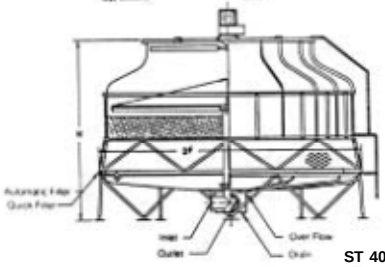

ST 400-1500

PIPING:
ST-3-60
THREAD TYPE
ST-70-1500
IN & OUT: FLANGE TYPE
OTHERS: THREAD TYPE

AMCOT COOLING TOWER												
ST MODEL	DIMENSIONS (INCH)		PIPE CONNECTIONS (INCH)						FAN MOTOR (HP)	FAN DIAMETER (INCH)	AIR VOLUME (CFM)	NOMINAL WATER FLOW (GPM)
	HEIGHT	DIA.	IN	OUT	O	Dr	FLO	Q				
3	50	27	1½	1½	1	¾	½		⅙	19½	870	6
5	52	34	1½	1½	1	¾	½		⅙	19½	2,100	10
8	56	34	1½	1½	1	¾	½		⅙	19½	2,620	16
10	54	42	1½	1½	1	¾	½		¼	26½	3,500	20
15	59	46	2	2	1	1	½		¼	26½	4,700	30
20	63	54	2	2	1	1	½		½	30	6,300	40
25	71	54	2½	2½	1	1	½		¾	30	7,000	50
30	68	62	2½	2½	1	1	½		1	30	8,100	61
40	75	72	2½	2½	1	1	¾		1½	38	9,800	83
50	75	79	3	3	1	1	¾		1½	38	11,500	105
60	75	79	3	3	1	1	¾		1½	46	14,700	125
70	80	86	4	4	1	1	¾		1½	46	17,500	145
80	80	86	4	4	1	1	¾		2	46	18,900	168
100	85	105	4	4	1	1	1		3	58	24,500	208
125	87	120	5	5	2	1	1		3	58	29,060	262
150	90	130	5	5	2	2	1		5	69	33,260	318
175	98	130	5	5	2	2	1		5	69	40,250	369
200	118	149	6	6	2	2	1½	1¼	5	69	43,760	426
225	126	149	6	6	2	2	1½	1¼	7½	93	61,270	460
250	126	149	8	8	2	2	1½	1¼	7½	93	61,270	520
300	132	175	8	8	2	2	1½	1¼	10	93	77,020	620
350	134	189	8	8	2	2	1½	1¼	10	93	77,020	744
400	153	204	8	8	4	2	2	2	15	117	91,030	845
500	155	220	10	10	4	2	2	2	15	117	91,030	1113
600	171	260	10	10	4	2	2	2	20	133	125,000	1278
700	181	260	10	10	4	2	2	2	20	133	125,000	1546
800	194	299	12	12	4	3	2	2	30	141	175,000	1703
1000	203	299	12	12	4	3	2	2	30	141	175,000	2253
1250	231	332	12	12	4	3	2½	2½	40	168	218,900	2824
1500	240	332	14	14	4	3	2½	2½	50	168	264,800	3380

NOMINAL WATER FLOW IS DEFINED AS RATE OF WATER COOLED FROM 95° F TO 85° F WITH 78° F WET BULB TEMPERATURE

MUELLER ACCU-THERM
PLATE HEAT EXCHANGER SPECIFICATION SHEET

Design Data

	Hot-Side	Cold-Side
Heat Transfer Media:	Water	Water
Volume Flow Rate:	10.00	10.00
gpm		
Mass Flow Rate:	4975.4	4990.7
LB/HR		
Inlet Temperature:	100.0	75.0
°F		
Outlet Temperature:	92.8	82.2
°F		
Density:	8.30	8.32
LB/GAL		
Specific Heat:	0.998	0.998
BTU/LB F		
Viscosity:	0.71	0.87
CPS		

Thermal Conductivity:

0.360
0.351

BTU/FT H F

Pressure Drop:

2.3
4.0

PSI

Operating Pressure:

50.
50.

PSI GAGE

Heat Transfer Rate:

35746.

BTU/H

Log Mean Temp Diff:

17.8

°F

Heat Transfer Area (All Frames):

3.0

FT2

Mechanical Description

Frame

Type

C -20 Carbon Steel

Design Code

ASME Section VIII, DIV. 1

Design Pressure

100 PSI GAGE

Design Temp. Max/Min

150 °F /32 °F

Test Pressure

130 PSI GAGE

Frames In Parallel/Series/Total	1/ 1/ 1
A-Dim. Min./Max.	0.85/ 0.87 Inch
Overall Length	11.62 Inch
Overall Width	7.31 Inch
Overall Height	26.00 Inch
Guide Bar Length	11.00 Inch
Compression Bolt Length	5.00 Inch
Weight Operating/Empty	88./ 86. LB

Plates

Type	4 G
Plate Material	0.50 MM 316 S/S
Plates/Frame	8
Passes-H/C	1/ 1
Channels-H/C	4/ 3
Gasket Material	NBR

Connections

Location

Hot In

1.00 Inch 316L S/S TOE Pipe

1F

Out

1.00 Inch 316L S/S TOE Pipe

4F

Cold In

1.00 Inch 316L S/S TOE Pipe

3F

Out

1.00 Inch 316L S/S TOE Pipe

2F

Copper Pipe Specification

Size		Type K		Type L/ACR	
NOM	O.D.	HARD	COILS	HARD	COILS
STANDARD LENGTHS		20' Lengths	60' thru 1-1/2 100' thru 1-1/4 40' and 60'-2" only	20' Lengths	60' thru 1-1/2 100' thru 1-1/4 40' - 2" only
NOM	O.D.	WALL	WGT/FT	WALL	WGT/FT
1/4"	3/8"	.035	.145	.030	.126
3/8"	1/2"	.049	.269	.035	.198
1/2"	5/8"	.049	.344	.040	.285
5/8"	3/4"	.049	.418	.042	.362
3/4"	7/8"	.065	.641	.045	.455
1"	1-1/8"	.065	.839	.050	.655
1-1/4"	1-3/8"	.065	1.04	.055	.884
1-1/2"	1-5/8"	.072	1.36	.060	1.14
2"	2-1/8"	.083	2.06	.070	1.75
2-1/2"	2-5/8"	.095	2.93	.080	2.48
3"	3-1/8"	.109	4.00	.090	3.33
3-1/2"	3-5/8"	.120	5.12	.100	4.29
4"	4-1/8"	.134	6.51	.110	5.38
5"	5-1/8"	.160	9.67	.125	7.61
6"	6-1/8"	.192	13.90	.140	10.20
8"	8-1/8"	.271	25.90	.200	19.30

Heat Pump (Florida Heat Pump, http://www.fhp-mfg.com/ftp/pub/WP%204-04.pdf, 12-08-04)

WP036-072 Series

Reverse Cycle Chillers

MODEL	Dimensions											
	A Height	B Width	C Depth	D	E	F	G	H	J	K	L	Water Conn.
WP036	24.25	32.50	24.00	2.50	2.00	14.88	2.25	2.50	8.25	14.88	2.25	0.75 FPT
WP060	24.25	32.50	24.00	3.00	2.50	17.00	2.50	4.00	3.38	18.00	3.38	1.00 FPT
WP072	24.25	32.50	24.00	3.38	2.50	22.75	4.38	3.38	4.38	22.75	2.50	1.00 FPT

NOTES: All dimensions within +/- 0.125".
Specifications subject to change without notice.

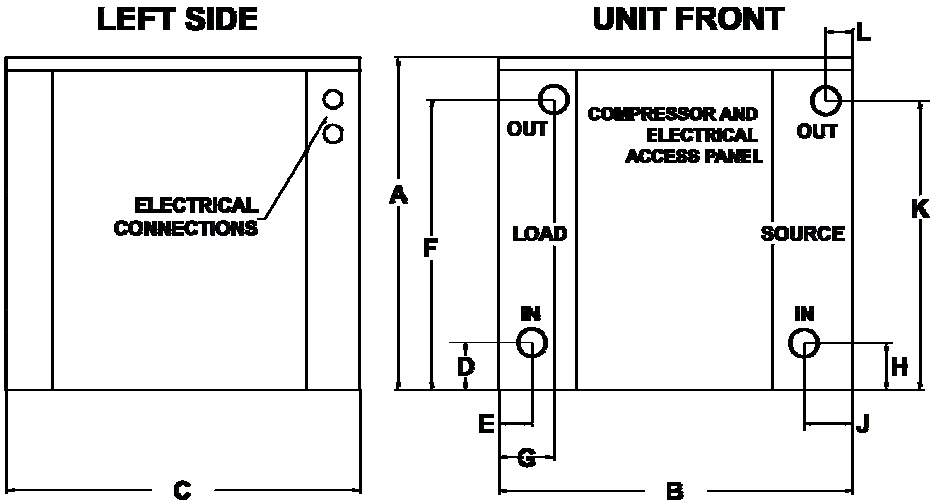

WP Series Reverse Cycle Chiller Nomenclature

WP ___ - ___ - ___

Series:
WP-Water-to-Water

Nominal Capacity:

Voltage:
1-208/230-1-60
Connections:
3-208/230-3-60
4-460-3-60
5-575-3-60

Cabinet Type:
CS-Condensing Section

Supply Air Location:
X-None

Return Air Location:
X-None

Water
F-Front

Condenser Material
C-Copper
N-Cupro-Nickel

FLUID FLOW & PRESSURE DROP

Chilled Fluid Side (@ 55^{O}F)		Cond. Fluid Side (@ 85^{O}F)	
Flow (GPM)	P (FOH)	Flow (GPM)	P (FOH)
4	2.8	4	2.7
5	5.9	5	5.6
7	9.9	7	9.3
9	14.8	9	14
11	20.6	11	19.4

HEATING PERFORMANCE

Based on 10^{0}F load temp. rise & 7 GPM source fluid flow.

Leaving Load Fluid (F)	Entering Source Fluid (F)	Heating Capacity (BtuH)	Power Input Watts	COP	Heat of Absorb. (BtuH)
100^{O}	35^{O}	29,085	2,219	3.8	21,513
	40^{O}	31,872	2,321	4	23,953
	50^{O}	37,802	2,502	4.4	29,266
	60^{O}	44,205	2,651	4.9	35,158
	70^{O}	51,090	2,767	5.4	41,649
110^{O}	35^{O}	27,432	2,296	3.5	19,599
	40^{O}	30,205	2,417	3.7	21,958
	50^{O}	36,035	2,640	4	27,027
	60^{O}	42,308	2,831	4.4	32,649
	70^{O}	49,024	2,988	4.8	38,829
120^{O}	35^{O}	25,686	2,350	3.2	17,667
	40^{O}	28,418	2,494	3.3	19,910
	50^{O}	34,177	2,759	3.6	24,765
	60^{O}	40,311	2,993	3.9	30,098
	70^{O}	46,859	3,193	4.3	35,963
125^{O}	35^{O}	24,772	2,370	3.1	16,685
	40^{O}	27,508	2,524	3.2	18,897
	50^{O}	33,210	2,811	3.5	23,618
	60^{O}	39,282	3,068	3.8	28,813
	70^{O}	45,747	3,291	4.1	34,519
130^{O}	35^{O}	23,839	2,385	2.9	15,703
	40^{O}	26,565	2,549	3.1	17,866
	50^{O}	32,227	2,860	3.3	22,470
	60^{O}	38,236	3,139	3.6	27,526
	70^{O}	44,606	3,385	3.9	33,056

CHILLER PERFORMANCE

Based on 7 GPM chilled fluid & 10^0F condenser fluid temp. rise.

Leaving Chilled Fluid (F)	Entering Cond. Fluid (F)	Total Capacity (Tons)	Total Capacity (BtuH)	Power Input (Watts)	EER	Heat Rejection (BtuH)
40°	75°	2.66	31,965	2,251	14.2	39,645
	80°	2.56	30,717	2,330	13.2	38,667
	85°	2.45	29,456	2,403	12.3	37,654
	90°	2.35	28,184	2,469	11.4	36,609
	95°	2.24	26,906	2,529	10.6	35,536
42°	75°	2.78	33,410	2,277	14.7	41,177
	80°	2.68	32,120	2,360	13.6	40,174
	85°	2.57	30,817	2,438	12.6	39,135
	90°	2.46	29,505	2,509	11.8	38,066
	95°	2.35	28,187	2,574	11	36,969
44°	75°	2.91	34,899	2,300	15.2	42,749
	80°	2.8	33,565	2,389	14.1	41,717
	85°	2.68	32,219	2,471	13	40,651
	90°	2.57	30,864	2,548	12.1	39,556
	95°	2.46	29,504	2,617	11.3	38,434
45°	75°	2.97	35,669	2,311	15.4	43,555
	80°	2.86	34,312	2,402	14.3	42,509
	85°	2.75	32,943	2,487	13.3	41,429
	90°	2.63	31,566	2,566	12.3	40,320
	95°	2.51	30,167	2,639	11.4	39,171
46°	75°	3.04	36,450	2,322	15.7	44,371
	80°	2.92	35,054	2,416	14.5	43,298
	85°	2.81	33,662	2,503	13.5	42,203
	90°	2.69	32,262	2,584	12.5	41,080
	95°	2.57	30,858	2,659	11.6	39,931
48°	75°	3.17	38,032	2,342	16.2	46,023
	80°	3.05	36,603	2,440	15	44,930
	85°	2.93	35,148	2,533	13.9	43,792
	90°	2.81	33,701	2,619	12.9	42,638
	95°	2.69	32,250	2,699	12	41,460
50°	75°	3.31	39,663	2,361	16.8	47,717
	80°	3.18	38,183	2,464	15.5	46,589
	85°	3.06	36,693	2,561	14.3	45,431
	90°	2.93	35,181	2,653	13.3	44,232
	95°	2.81	33,682	2,738	12.3	43,022

Circulation Pump (Grundfos, http://www.us.grundfos.com/web/download.nsf/Pages/DB9E15987978351F88256C4E006EA652/$File/L-UP-PG-001.pdf, 12-08-04 *Effective in USA only and information provided is subject to change without notice.*)

U PS 15-42F/FR — **Closed Systems, 60 Hz**

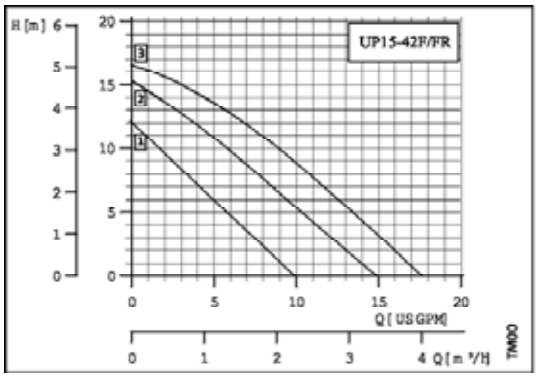

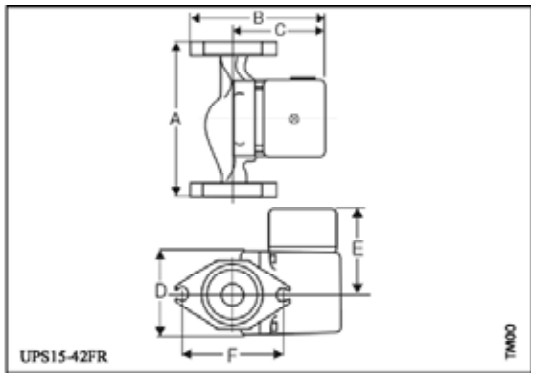

Flow range:	0 - 17.5 U.S. GPM
Head range:	0 - 17 FEET
Motors:	2 Pole, Single Phase
Maximum fluid temperature:	230°F (110°C)
Min. fluid temperature:	36°F (2°C)
Maximum working pressure:	145 PSI

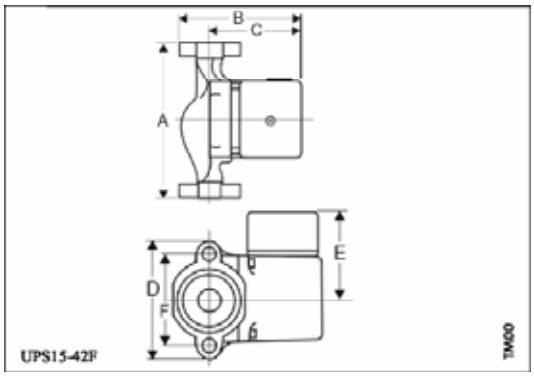

MODEL	Spd.	VOLTS	AMPS	WATTS	HP	CAPACITOR
	3		0.74	85	1/25	10mF/180V
UPS15-42F/FR	2	115	0.57	65	---	---
	1		0.4	45	---	---
	3		0.43	95	1/25	2mF/400V
UPS15-42F/FR	2	230	0.19	40	---	---
	1		0.14	30	---	---

CLOSED SYSTEM MODELS	A	B	C	D	E	F	Connection Type and Size	Shipping Wt. (Lbs.)
UPS15-42F	6 1/2	5 1/4	4	4 3/16	3 1/4	3 5/32	Flange – (2) 1/2" Dia. Bolt Holes	7 1/4
UPS15-42FR	6 1/2	5 15/16	4	3 3/4	3 1/4	3 5/32	Flange – (2) 1/2" Dia. Bolt Holes	7 1/4

U P 26-64F

Closed Systems, 60 Hz

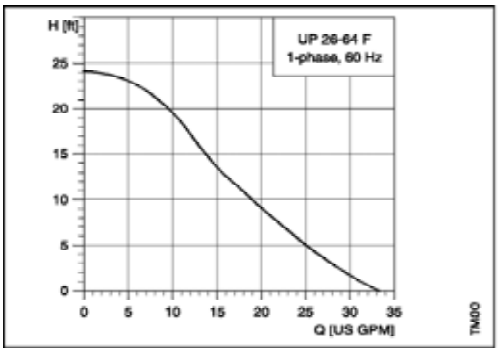

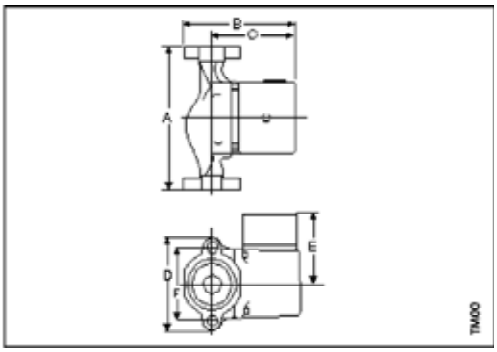

Flow range:	0 - 34 U.S. GPM
Head range:	0 - 24 FEET
Motors:	2 Pole, Single Phase
Maximum fluid temperature:	230°F (110°C)
Min. fluid temperature:	36°F (2°C)
Maximum working pressure:	145 PSI

MODEL	VOLTS	AMPS	WATTS	HP	CAPACITOR
UP26-64F	115	1.7	185	1/12	8mF/180V
	230	0.8	175	1/12	2.5mF/380V

CLOSED SYSTEM MODELS	A	B	C	D	E	F	Connection Type and Size	Shipping Wt. (Lbs.)
UP26-64F	6 1/2	6 3/8	5 1/16	4 1/8	3 1/2	3 5/32	Flange – (2) 1/2" Dia. Bolt Holes	11 1/4

UP 43-75F

Closed Systems, 60 Hz

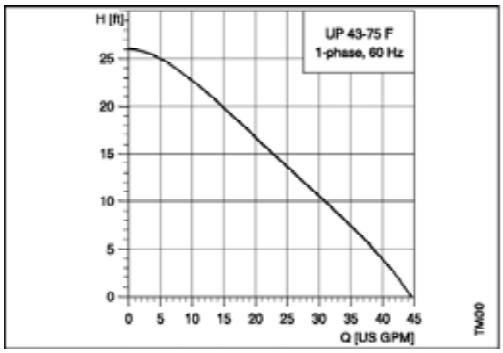

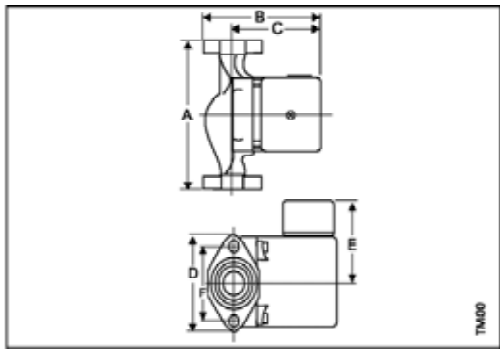

Flow range:	0 - 45 U.S. GPM
Head range:	0 - 26 FEET
Motors:	2 Pole, Single Phase
Maximum fluid temperature:	230°F (110°C)
Min. fluid temperature:	36°F (2°C)
Maximum working pressure:	145 PSI

MODEL	VOLTS	AMPS	WATTS	HP	CAPACITOR
UP43-75F	115	2.15	185	1/6	10mF/180V
	230	1.07	175	1/6	2.5mF/380V

CLOSED SYSTEM MODELS	A	B	C	D	E	F	Connection Type and Size	Shipping Wt. (Lbs.)
UP43-75F	8 1/2	6 2/3	5 3/16	4 3/4	3 1/2	3 7/16	Flange – (2) 1/2" Dia. Bolt Holes	13 1/2

Circulation Pump (ITT Bell and Gossett, http://fhaspapp.ittind.com/literature/files/155.pdf, 12-08-04)

CAST IRON			BRONZE			STANDARD 60 CYCLE SINGLE PHASE MOTOR CHARACTERISTICS			
MODEL NUMBER	PART NUMBER	QTY.	MODEL NUMBER	PART NUMBER	QTY.	HP	VOLTAGE	F.L. AMPS	RPM
PL-30	1 BL012		PL-30B	1 BL013		1/12	115	1.4	2650
PL-30	1 BL014		PL-30B	1 BL015		1/12	230	0.8	2650
PL-36	1 BL001		PL-36B	1 BL003		1/6	115	2.1	3300
PL-36	1 BL006		PL-36B	1 BL008		1/6	230	1.1	3300
PL-45	1 BL002		PL-45B	1 BL004		1/6	115	2.1	3300
PL-45	1 BL007		PL-45B	1 BL009		1/6	230	1.1	3300
PL-50	1 BL016		PL-50B	1 BL017		1/6	115	1.8	3300
PL-50	1 BL018		PL-50B	1 BL019		1/6	230	1.0	3300
PL-55	1 BL032		PL-55B	1 BL068		2/5	115	4.7	3250
PL-55	1 BL033		PL-55B	1 BL069		2/5	230	2.4	3250
PL-75	1 BL034		PL-75B	1 BL035		1/6	115	2.1	3400
PL-75	1 BL036		PL-75B	1 BL037		1/6	230	1.1	3400
PL-130/2"	1 BL063		PL-130B/2"	1 BL065		2/5	115	4.8	3200
PL-130/2"	1 BL064		PL-130B/2"	1 BL066		2/5	230	2.4	3200
PL-130/3"	1 BL070		PL-130B/3"	1 BL072		2/5	115	4.8	3200
PL-130/3"	1 BL071		PL-130B/3"	1 BL073		2/5	230	2.4	3200

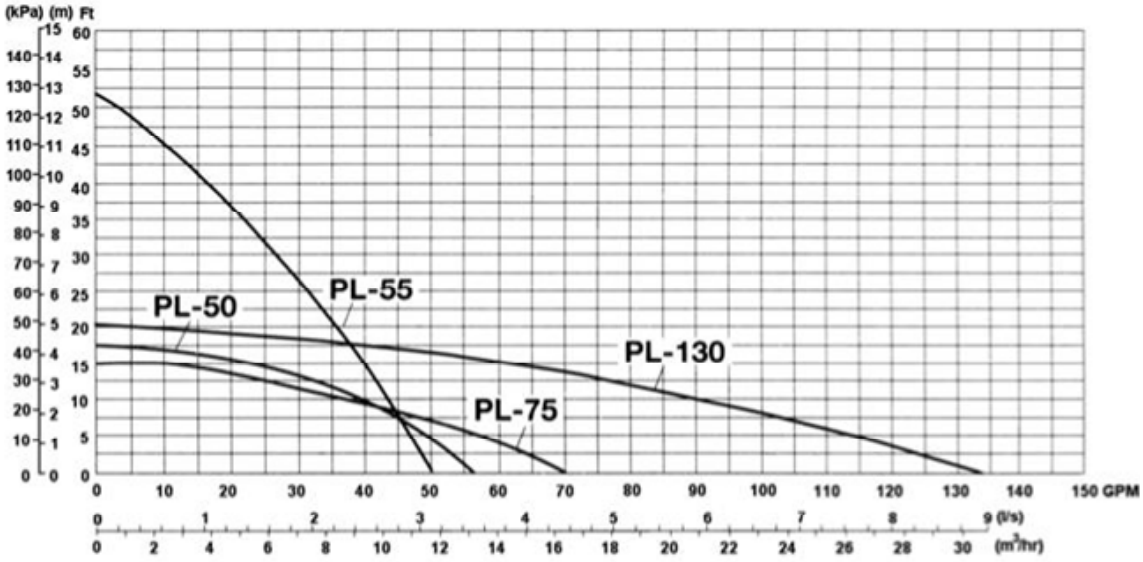

Circulation Pump (ITT Bell and Gossett, http://fhaspapp.ittind.com/literature/files/484.pdf, 12-08-04)

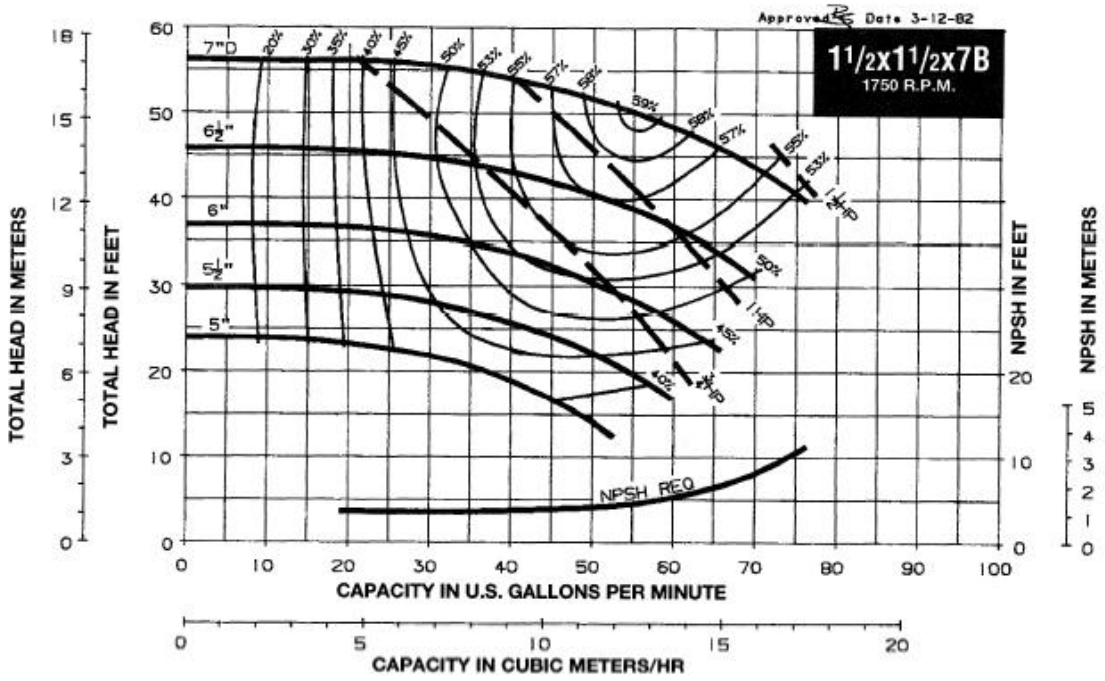

Variable Frequency Drive (Siemens, http://www.us.sbt.siemens.com/HVP/Components/Documentation/1253202.pdf, 12-08-04)

Specification	Description
Operating temperature ranges	IP20 and NEMA Type 1: 14°F to 104°F (–10°C to 40°C) IP54 and NEMA Type 12: 14°F to 104°F (–10°C to 40°C)
Storage temperature	–40°F to 158°F (–40°C to 70°C)
Humidity	95% relative humidity — non-condensing.
Altitude	Up to 3280 ft (1000 m) above sea level without performance decrease.
Overload capacity	10% periodic overload capacity for 60 seconds within 5 minutes relative to the nominal output current.
Protection functions	Protection against: Undervoltage, overvoltage, ground fault, short-circuit, stall, rotor jam, motor overtemperature, SED2 overtemperature.
Electromagnetic compatibility	Integrated EMC filter as per EN 55011 class B as footprint filter for frame sizes A to C, IP20. The filter is integrated in the SED2 for frame sizes D to F, IP20 and for all IP54 devices. Satisfies the requirements of EMC product standard EN 61800-3.
Input frequency	47 to 63 Hz
Setpoint resolution	0.01 Hz digital, 0.01 Hz serial, 10 bit analog
Switching frequency	4 to 16 kHz (2 kHz steps).
Fixed frequencies	15 programmable
Masking frequencies	4 programmable
Analog inputs	Number: 2 Can be changed over to 0/2 to 10V (programmable scaling) or 0/4 to 20 mA (programmable scaling). Terminals used: 3, 4, 10, 11 Resolution: 10 bits Read cycle: 10 ms. Analog inputs AIN1 and AIN2 are configurable for direct connection of an Ni 1000 temperature sensor.

Specification	Description
Digital inputs	6 (potential-free) inputs (extendable to 8) Freely programmable and possible changeover (sink, source) Terminals used: 5, 6, 7, 8, 16, 17 Min. input current: 6 mA (actual: 8 mA) at 15V Logical 0 = <3V, logical 1 = >13V Max. input voltage: 33V
Analog outputs	Number: 2 Can be changed over for 0 to 10V or 0/4 to 20 mA, (programmable scaling/parameter). Factory setting: 0 to 10V. Terminals used: 12, 13, 26, 27 Impedance on configuration 0 to 10V: 1 K Read cycle: 10 ms
Relay outputs	2 programmable relays, 6 contacts. Relay 1 Terminals: 18, 19, 20 Relay 2 Terminals: 23, 24, 25 Max. contact rating: DC 30V/5 A, (resistive) AC 250V/2 A (resistive)
Auxiliary supply 24V	Galvanically separated, unregulated auxiliary supply (18 to 32V), 100 mA Terminal 9.
Serial interface	RS-485 (RS-232 optional with converter) Protocols: USS, P1, and N2 Transmission rate: Up to 38.4K Baud (default 9.6K Baud)
Power factor	0.7 total PF 0.98 displacement
VFD degree of efficiency	96 to 97%
Switch-on current:	Less than nominal input current
Braking	DC braking, dynamic braking
CE conformity	Corresponds to the requirements of the low-voltage guideline 73/23/EEC, supplemented by guideline 98/68/EEC and EMC. If installed according to the recommendations issued in this manual, the SED2 satisfies all EMC guideline requirements as defined in the *EMC Product Standard for Power Drive Systems EN 61800-3*.

Armaflex Insulation (Armacell, http://www.armaflex.com/www/armacell/ACwwwAttach.nsf/ansFiles/017S-001-NA(NA).pdf/$File/017S-001-NA(NA).pdf, 10-08-04)

Physical Data

Physical Properties		Test Method
Thermal conductivity, Btu • in./h • ft² • °F (W/m • K) 75°F mean temp (24°C) 90°F mean temp (32°C)	 0.27 (0.039) 0.276 (0.040)	 ASTM C 177 or C 518
Water vapor permeability, perm-in. [Kg/(s•m•Pa)]	0.08 (1.16 x 10^{-13})	ASTM E 96 Procedure A
Water absorption, % by volume	0.2	ASTM C 209
Flame spread and smoke developed index through 1" (25mm)	25/50	ASTM E 84
Ozone resistance	GOOD	—
Upper use limit, °F (See note 1)	220 (105°C)	—
Lower use limit, °F (See note 2)	-70 (-57°C)*	—
Sizes Wall thickness, (nominal) Inside diameter, tubular form Length of sections, feet, tubular form	 3/8", 1/2", 3/4", 1" (10, 13, 19, 25mm) 3/8" ID to 6" IPS (10mm ID to 168mm) 6 (1.8m)	 — — —
Density, typical range (See note 3)	3.0 - 6.0 lbs./ft.³	ASTM D 1662 or D 1667

Notes

① On the heating cycle, AP Armaflex Pipe Insulation will withstand temperatures as high as 220°F (105°C). 520 or 520 BLV Adhesive may be used with pipe insulation applications up to 220°F (105°C).

② At -20°F (-29°C), flexible AP Armaflex insulation becomes hard and, as temperatures drop below -20°F (-29°C), will be increasingly brittle; however, this hardening characteristic does not affect thermal efficiency or water vapor permeability.

* For applications of -40°F to -70°F (-40°C to -57°C), contact Armacell.

③ Reference only.

Performance approved through continuing supervision by Factory Mutual Approvals.

Armaflex Pipe Insulation Thickness Recommendations

For Controlling Outer Insulation Surface Condensation
(Based upon available manufactured thicknesses)

Pipe Size	Line Temperatures			
	50°F (10°C)	35°F (2°C)	0°F (–18°C)	–20°F (–29°C)
BASED ON **NORMAL** DESIGN CONDITIONS*				
3/8" ID through 1-1/8" ID (10mm–28mm)	Nom 3/8" (10mm)	Nom 1/2" (13mm)	Nom 3/4" (19mm)	Nom 1" (25mm)
Over 1-1/8" ID through 2-1/8" ID (28mm–54mm)	Nom 3/8" (10mm)	Nom 1/2" (13mm)	Nom 1" (25mm)	Nom 1" (25mm)
Over 2-1/8" ID through 2-5/8" ID (54mm–65mm)	Nom 3/8" (10mm)	Nom 1/2" (13mm)	Nom 1" (25mm)	Nom 1-1/4" (32mm)
Over 2-5/8" ID through 6" IPS (65mm–168mm)	Nom 1/2" (13mm)	Nom 3/4" (19mm)	Nom 1" (25mm)	Nom 1-1/4" (32mm)
BASED ON **MILD** DESIGN CONDITIONS**				
3/8" ID through 2-5/8" ID (10mm–65mm)	Nom 3/8" (10mm)	Nom 3/8" (10mm)	Nom 1/2" (13mm)	Nom 3/4" (19mm)
Over 2-5/8" ID through 6" IPS (65mm–168mm)	Nom 1/2" (13mm)	Nom 1/2" (13mm)	Nom 1/2" (13mm)	Nom 3/4" (19mm)
BASED ON **SEVERE** DESIGN CONDITIONS***				
3/8" ID through 1-5/8" ID (10mm–40mm)	Nom 3/4" (19mm)	Nom 1" (25mm)	Nom 1-1/2" (38mm)	Nom 1-1/2" (38mm)
Over 1-5/8" ID through 3-5/8" ID (40mm–90mm)	Nom 3/4" (19mm)	Nom 1" (25mm)	Nom 1-1/2" (38mm)	Nom 1-3/4" (44mm)
Over 3-5/8" ID through 6" IPS (90mm–168mm)	Nom 3/4" (19mm)	Nom 1" (25mm)	Nom 1-1/2" (38mm)	Nom 2" (50mm)

NOTE: Thicknesses greater than 1" (25mm) are multiple-layer applications, see technical bulletin #30.

*BASED ON **NORMAL** DESIGN CONDITIONS AP Armaflex in the thicknesses noted and within the specified temperature ranges will control outer insulation surface condensation indoors under **normal** design conditions, a maximum severity of **85°F (29°C) and 70% RH.** Armacell research and field experience indicate that indoor conditions anywhere in the United States seldom exceed this degree of severity.

BASED ON **MILD DESIGN CONDITIONS AP Armaflex in the thicknesses noted and within the specified temperature ranges will control outer insulation surface condensation indoors under **mild** design conditions, a maximum severity of **80°F (27°C) and 50% RH.** Typical of these conditions are most air-conditioned spaces and arid climates.

***BASED ON **SEVERE** DESIGN CONDITIONS AP Armaflex in the thicknesses noted and within the specified temperature ranges will control outer insulation surface condensation indoors under **severe** design conditions, a maximum severity of **90°F (32°C) and 80% RH.** Typical of these conditions are indoor areas in which excessive moisture is introduced or in poorly ventilated confined areas where the temperature may be depressed below ambient.

Fluke NetDAQ (Fluke, http://assets.fluke.com/manuals/netdaq__umeng0200.pdf, 12-08-04)

2640A/2645A General Specifications

Specification	Characteristic
Channel Capacity	20
I/O Lines Total	12
Size	9.3 cm high, 21.6 cm wide, 36.2 cm deep (3.67 in high, 8.5 in wide, 14.28 in deep)
Weight	Net, 4 kg (8.8 lb.) Shipping, 6.0 kg (13.2 lb.)
Power	107 to 264V ac (no switching required), 50 and 60 Hz, 15VA maximum 9V dc to 16V dc, 6W maximum If both sources are applied simultaneously, ac voltage is used if it exceeds approximately 8 times the dc voltage. Automatic switchover occurs between ac and dc without interruption.
Safety Standards	Both instruments comply with: IEC 1010-1 UL 1244 CSA Bulletin 556B. ANSI/ISA-S82.01-1994 CSA C22.2 No. 1010.1-92
EMC Standards	When shielded cables are used, both instruments comply with: Vfg. 243/1991 FCC-15B, at the Class B level EN 50081-1 EN 50082-1
Serial Interface (RS-232C)	Connector: 9 pin male (DI-9P) Signals: TX, RX, DTR, RTS, GND Modem Control: full duplex Baud rates: 4800, 9600, 19200, 38400 Data format: 8 data bits, no parity bit, one stop bit Flow control: XON/XOFF Echo: Off
Common Mode Voltage	2640A 150V (300V on channels 1 and 11) 2645A 50V dc or 30V ac rms.

2640A/2645A General Specifications (cont)

Specification	Characteristic
Maximum Measurement Speed (Scanning Rates)	2640A Slow - 6 readings per second Medium - 45 readings per second (60 Hz) Fast - 143 readings per second (20 configured channels) 2645A Slow - 54 readings per second (60 Hz) Medium - 200 readings per second Fast - 1000 readings per second (20 configured channels) Fast single Channel - 400 readings per second
Accuracy of Medium Scanning Rate	= (Fast Accuracy + Slow Accuracy)/2
Additional error if “Automatic drift correction” is turned off.	If the instrument was fully warmed-up at the time drift correction was disabled, i.e. turned-on at least 1 hour earlier; 1/10 of the 90 day specification per C change in ambient temperature from the temperature when drift correction was disabled. If the instrument was NOT fully warmed-up at the time drift correction was disabled; Add an error equal to the 90 day specification for instrument warm-up + 1/10 of the 90 day specification per C change in ambient temperature from the temperature when drift correction was disabled.

2640A DC Voltage Measurement General Specifications

Specification	Characteristic
Input Impedance	100 M in parallel with 150 pF maximum for ranges 3V 10 M in parallel with 100 pF maximum for ranges >3V
Normal Mode Rejection	50dB minimum at 50 Hz/60 Hz 0.1 %, Slow Rate
Common Mode Rejection	120dB minimum at dc, 50 Hz/60 Hz 0.1 %, 1 imbalance, Slow Rate
	80dB minimum at dc, 50 Hz/60 Hz 0.1 %, 1 imbalance, Medium and Fast Rates
Channel-to-Channel Crosstalk	120dB minimum Slow Rate (e.g., 30V dc on channel 1 may cause a 30µV error on channel 2) 100dB minimum Medium and Fast Rates (e.g., 1V dc on channel 1 may cause a 10 µV error on channel 2)
Temperature Coefficient	Add 1/10th the 90-day specification per C above 28C or below 18C. (Generally, only the %input portion is affected.)
Accuracy at -20C	Multiply the -10C to + 60C accuracy specification by 2. After 1 hour warm-up. For accuracy between -10C and -20C, interpolate linearly.
Maximum Input Voltage	150V (300V for channels 1 and 11) to any input terminal.

2640A DC Voltage Range and Resolution Specifications

	Resolution	
Range	**Slow**	**Fast**
90 mV	.3 µV	1 µV
300 mV	1 µV	3 µV
3V	10 µV	30 µV
30V	100 µV	300 µV
150V/300V	1 mV	3 mV
Note 300V range applies to channels 1 and 11 only.		

2640A DC Voltage Accuracy Specifications

Range	Accuracy, 3 (% input + V)					
	18C to 28C				-10C to 60C	
	90 Day		1 Year		1 Year	
	Slow	Fast	Slow	Fast	Slow	Fast
90 mV	.01%+7 µV	.01%+17 µV	.013%+8 µV	.013%+18 µV	.042%+18.2µV	.042%+44.2µV
300 mV	.01%+15 µV	.01%+30 µV	.013%+17 µV	.013%+35 µV	.042%+39 µV	.042%+78 µV
3V	.01%+.1 mV	.01%+.2 mV	.013%+.15 mV	.013%+.2 mV	.042%+.26 mV	.042%+.52mV
30V	.01%+1.5 mV	.02%+3 mV	.013%+1.7 mV	.026%+3.5 mV	.042%+3.9 mV	.084%+7.8mV
150/300V	.01%+15 mV	.04%+30 mV	.013%+17 mV	.052%+35 mV	.042%+39 mV	.168%+78 mV
Note 300V range applies to channels 1 and 11 only.						

2640A Thermocouple General Specifications

Specification	Characteristic
Input Impedance	100 M minimum in parallel with 300 pF
Open Thermocouple Detect	Operates by injecting a small ac signal into the input after each measurement. A thermocouple resistance greater than 1 k to 10k is detected as an open input.
Temperature Coefficient	To calculate thermocouple accuracy for temperatures between 28°C and 60°C, or -10°C and 18°C, use a linear interpolation between the two applicable points. e.g., if the applicable spec at 28°C is .6 and the spec at 60°C is 1.1, then the spec at 40°C = (1.1-.6)*(40-28)/(60-28)+.6= .5* (12/32) + .6 = .7875.
Accuracy at -20C	Multiply the -10C to + 60C accuracy specification by 2. After 1 hour warm-up. For accuracy between -10C and -20C, interpolate linearly.

2640A Thermocouple Specifications

Thermocouple		Resolution	Accuracy °C				
			18°C to 28°C			-10°C to 60°C	
			90 Day	1 Year		1 Year	
Type	Temperature °C	Slow	Slow	Slow	Fast	Slow	Fast
J	-100 to 80	.03	0.45	0.50	0.80	0.60	0.80
	80 to 230	.02	0.35	0.50	0.70	0.60	0.80
	230 to 760	.02	0.40	0.50	0.70	0.80	0.90
K	-100 to -25	.04	0.55	0.60	0.90	0.70	1.00
	-25 to 120	.03	0.40	0.50	0.80	0.60	0.90
	120 to 800	.03	0.50	0.65	0.90	1.00	1.20
	800 to 1372	.03	0.70	1.00	1.30	1.60	1.90
N	-100 to -25	.05	0.65	0.75	1.20	0.80	1.30
	-25 to 120	.05	0.55	0.60	1.00	0.70	1.10
	120 to 1000	.04	0.45	0.60	0.90	1.00	1.20
	1000 to 1300	.03	0.55	0.75	1.00	1.20	1.50
E	-100 to -25	.03	0.45	0.50	0.80	0.60	0.80
	-25 to 20	.02	0.35	0.40	0.60	0.50	0.70
	20 to 600	.02	0.30	0.40	0.60	0.50	0.80
	600 to 1000	.02	0.40	0.50	0.70	0.90	1.00
T	-100 to 0	.04	0.60	0.65	1.00	0.70	1.10
	0 to 150	.03	0.40	0.50	0.80	0.60	0.90
	150 to 400	.02	0.30	0.40	0.60	0.60	0.80
R	250 to 600	0.1	0.90	1.00	2.10	1.20	2.20
	600 to 1500	0.1	0.80	0.90	1.80	1.30	2.00
	1500 to 1767	0.1	0.85	0.85	1.90	1.70	2.50
S	250 to 1000	0.1	0.95	1.10	2.30	1.30	2.40
	1000 to 1400	0.1	0.80	1.00	1.90	1.40	2.30
	1400 to 1767	0.1	1.00	1.30	2.20	1.80	2.80
B	600 to 900	0.2	1.20	1.40	3.10	1.50	3.20
	900 to 1200	0.2	0.90	1.00	2.20	1.20	2.40
	1200 to 1820	0.1	0.75	1.00	1.90	1.30	2.20
C	0 to 150	0.2	0.80	0.90	1.60	1.00	1.70
	150 to 650	0.1	0.65	0.75	1.40	1.00	1.50
	650 to 1000	.05	0.65	0.85	1.40	1.20	1.80
	1000 to 1800	.05	1.00	1.30	2.10	2.10	2.80
	1800 to 2316	.05	1.60	2.10	3.20	3.40	4.60

HOBO Data Logger (Onset, http://www.onsetcomp.com/Products/ Product_Pages/pdfs/external_sensors.pdf, 12-08-04)

TMC6-HC Stainless Steel Temp Probe

Stainless Steel temperature probe (TMC6-HC)

10.2 cm (4") food-grade stainless-steel probe with pointed tip; 0.3 cm (0.12") diameter, 1.8 m (6') cable
Range: -40° to 100°C (-40° to 212°F) in air or water
Accuracy: w/H6; ±0.5° at 20°C (±0.9° at 68°F)
Accuracy: w/U12; ±0.25° at 20°C (±0.45° at 68°F)
Resolution: w/H8; 0.41° at 20°C (0.7° at 68°F)
Resolution: w/U12; 0.03° at 20°C (0.05° at 68°F)
Response time in air moving 1 m/sec (2.2 mph)
3 min. typical to 90%;
in stirred water 15 sec. typical to 90%

Vortex Flowmeter (Asahi, http://www.asahi-america.com/pdf/flowMeters/universalVortex/operationsManual/Vortex_Manual.pdf, 12-08-04)

V1 SERIES

VORTEX FLOW TRANSMITTERS

V1 MECHANICAL INSTALLATION

This meter will provide years of accurate service if good flow meter installation practices are followed. The flow tube should be installed where pipe vibration is minimal. Observe the upstream piping requirements listed under "Piping Requirements". **Upstream valves should not be used to control flow rate. They should always be kept fully open.** Good quality ball valves with integral unions may be connected directly to the flow tube if the valves are fully open during operation. This allows easy isolation and removal of the flow tube, should maintenance be required. Cavitation and flow rate pulsation will adversely affect flow meter performance.

Diaphragm or piston pumps may not be used. Do not use Teflon tape or any kind of pipe dope when piping. If flanges are used, do not allow gaskets to protrude into the flow stream.

The simple appearance of the flow meter may tempt an installer to handle it as an ordinary nipple. **Remember, it is a precision electronic instrument.** Treat it with care.

Do not use excessive force. Mating fittings (FNPT) and flanges should be screwed into flow meter tightly by hand. Then tighten an additional 1/2 to 3/4 turn with a wrench.

Always use two wrenches when turning the flow tube into a fitting, one across the flats on the flow tube end, close to the fitting, and one on the fitting.

Do not use tools inside the flow tube, as this may damage the vortex sensor, and invalidate the warranty.

The flow tube may be mounted in any orientation. Three holes, tapped .250–20 UNC-2B, .375-inch deep, on .75-inch centers are provided on the 3/4-inch and smaller flow meters. These holes may be used (at the user's discretion) to provide

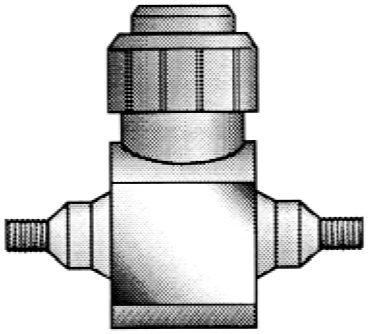

Turndown Ratio:	12:1 (except 1/4"; 8:1 and 1/2" L.C.; 10:1)
Accuracy:	±1 % of designed full scale
Repeatability:	±0.25% actual flow
Output Signal:	Linear 4–20 mA
Power Supply:	13 to 30 Vdc
CSA Certified:	CSA-LR110814
Weatherproof:	Type 4X
Maximum Overrange:	125% for 1/2 hour (standard) No overrange for Hi-temp units
Response time:	1.5 sec, first order: a 7.5 sec delay until true flowrate is indicated

SPECIFICATIONS

Max Fluid Temp	Max Operating Pressure, PSIG (KPa)			
° F (° C)	PVC	PP	CPVC	PVDF
203 (95)	N.R.	N.R.	CF	CF
150 (66)	N.R.	90 (621)	63 (434)	130 (896)
100 (38)	93 (641)	130 (896)	120 (827)	150 (1034)
70 (21)	150 (1034)	150 (1034)	150 (1034)	150 (1034)

ELECTRONICS MODULE CONTAINMENT

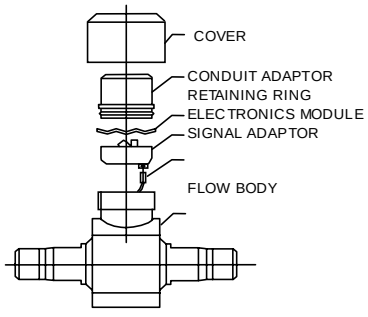

ELECTRONICS MODULE TOP VIEW

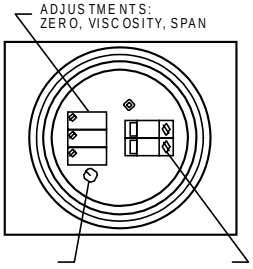

V1 SERIES

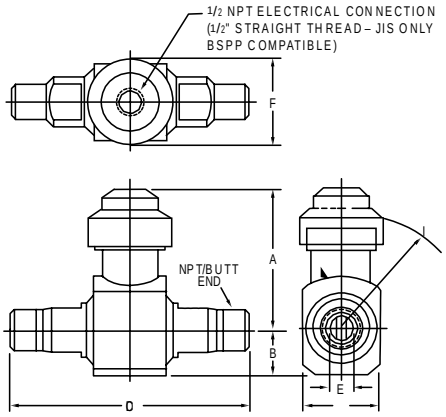

Replacement electronics: To order modules by number, match meter line size as follows:

Line Size (inches)	Part Number
1/4, 1/2 LC	8642010
1/2	8642015
3/4 and 1	8642020
1/2 and 2	8642030

DIMENSIONS

Size	PVC													
	A		B		C		D		E		F		I	
(inches)	(in)	(mm)	(in)	(mm)	(in)	(mm)	(in)	(mm)	(in)	(mm)	(in)	(mm)	(in)	(mm)
1/4	3.81	97	1.75	45	5.25	133	2.50	64	.30	8	2.88	73	3.00	76
1/2	3.81	97	1.75	45	7.13	181	2.50	64	.55	14	2.88	73	3.00	76
3/4	3.81	97	1.75	45	7.63	194	2.50	64	.74	19	2.88	73	3.00	76
1	3.92	100	1.75	45	8.03	204	2.50	64	.96	24	2.88	73	3.00	76
1 1/2	3.90	99	2.00	51	8.37	213	2.50	64	1.50	38	2.88	73	3.38	86
2	4.31	109	2.00	51	8.37	213	2.50	64	1.94	49	2.88	73	3.38	86

DIMENSIONS

Size	PVDF (BUTT FUSION ONLY)													
	A		B		C		D		E		F		I	
(inches)	(in)	(mm)	(in)	(mm)	(in)	(mm)	(in)	(mm)	(in)	(mm)	(in)	(mm)	(in)	(mm)
1/4	5.90	150	.63	16	4.87	124	1.31	33	.302	8	2.88	73	3.00	76
1/2	5.75	146	.78	20	4.87	124	1.31	33	.550	14	2.88	73	3.00	76
3/4	5.75	146	.94	24	4.87	124	1.44	37	.740	19	2.88	73	3.00	76
1	5.88	149	1.19	30	5.09	129	2.00	51	.960	24	2.88	73	3.00	76
1 1/2	6.21	158	1.50	38	6.24	158	2.50	64	1.500	38	2.88	73	3.38	86
2	6.60	168	1.88	48	6.77	172	3.00	76	1.940	49	2.88	73	3.38	86

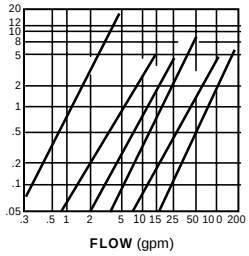

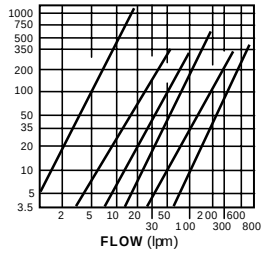

Paddle Wheel Flowmeter (Gems Sensors, http://www.gemssensors.com/PDF/Catalog/RFA.pdf, 12-08-04)

Flow Rate Monitoring – RFA Types

CE cULus File No. E45168

0 to 10 VDC Analog Output

GEMS Sensors popularized the RotorFlow's paddlewheel design by combining high visibility rotors with solid-state electronics that are packaged into compact, panel mounting housings. They provide accurate flow rate output with integral visual confirmation...all with an unprecedented price/performance ratio. RFA Types feature a 0 to 10 VDC analog output which is proportional to flow rate.

Typical Applications

- Water Purification/Dispensing Systems • Chemical Metering Equipment
- Lasers and Welders • Water Injection Systems
- Semiconductor Processing Equipment • Chillers and Heat Exchangers

Specifications

Wetted Materials	
Body	Brass, 316 Stainless Steel or Polypropylene (Hydrolytically Stable, Glass Reinforced)
Rotor Pin	Ceramic
Rotor	PPS Composite, Black[1]
Lens	Polysulfone
O-Ring	Viton® (Alloy Bodies); Buna N (Polypropylene Body)
Low Flow Adaptor	Glass Reinforced Polypropylene
Operating Pressure, Maximum	
Brass or Stainless Steel Body	200 PSIG @ 70°F, 100 PSIG @ 212°F[2]
Polypropylene Body	100 PSIG @ 70°F, 40 PSI Max. @ 180°F
Operating Temperature,	
Brass or Stainless Steel Body	-20°F to 212°F (-29°C to 100°C)
Polypropylene Body	-20°F to 180°F (-29°C to 82°C)
Electronics	150°F (65°C) Ambient
Viscosity, Maximum	200 SSU
Input Power	24 VDC, ±10%
Output Signal	0-10 VDC Analog Signal @ 1 mA, Max.
Current Consumption	25 mA, Max.
Current Source Output, Max.	70 mA
Frequency Output Range	15 Hz (Low Flow) to 225 Hz (High Flow)
Accuracy	See Table Below
Electrical Termination	22 AWG PVC-Jacketed, 24~ Cable. Color Coded: Red = +VDC; Black = Ground; White = Signal Output

Notes:
1. Standard on Stainless Steel bodies.
2. For higher pressure/temperature ratings stainless steel face plates are available. Consult factory.

Dimensions

Polypropylene Bodies

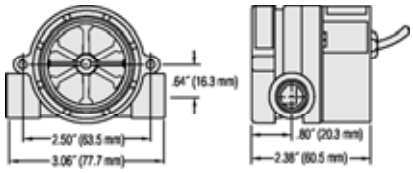

Brass and Stainless Steel Bodies - .25~ and .50~ Ports

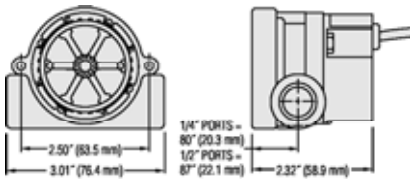

Brass Bodies – .75" and 1.00" NPT Ports

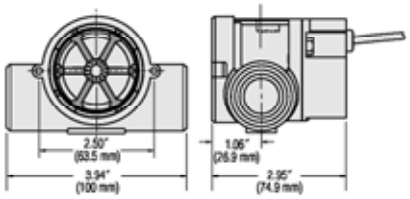

High Resolution Black Rotor

PPS composite. Each of the six rotor arms is magnetized. A PTFE loaded bushing ensures long life.

How To Order

For standard configurations, specify Part Number based on desired body material and port size.

Body Material	Port Size NPT	Flow Ranges – GPM			
		Low Range (Accuracy)	Part Number	Standard Range (Accuracy)	Part Number
Polypropylene	.25~	0.1 to 1.0 (±7.0%)	170290	0.5 to 5.0 (±7.0%)	170280
	.50~	1.5 to 12.0 (±7.0%)	170291	4.0 to 20.0 (±15.0%)	170281
Brass	.25~	0.1 to 1.0 (±7.0%)	170292	0.5 to 5.0 (±7.0%)	170282
	.50~	1.5 to 12.0 (±7.0%)	170293	4.0 to 20.0 (±15.0%)	170283
	.75~	—	—	5.0 to 30.0 (±10.0%)	180407
	1.00~	—	—	8.0 to 60.0 (±15.0%)	182098
Stainless Steel	9/16~-18	0.1 to 1.0 (±7.0%)	170295	0.5 to 5.0 (±7.0%)	170285
	.50~	1.5 to 12.0 (±7.0%)	170296	4.0 to 20.0 (±15.0%)	170286
	.75~	—	—	5.0 to 30.0 (±10.0%)	182097
	1.00~	—	—	8.0 to 60.0 (±15.0%)	182099

Watt Transducer (Ohio Semitronics, http://www.ohiosemi.com/pdf/gw5.pdf, 12-08-04)

PRECISION AC WATT TRANSDUCER MODEL GW5

ACCURATE TO 0.2% OF READING

DESCRIPTION

The model GW5 provides power measurement to within ±0.2% of reading accuracy in single or polyphase systems. The electrically isolated dc output is proportional to the instantaneous power averaged over several cycles.

Currents up to 20 amperes and voltages up to 600Vac can be directly connected to the GW5, thus eliminating the additional cost and additive errors of current and voltage transformers for these ranges. The GW5 can be used with OSI metering class current transformers for measurements up to 10 kiloamperes.

Specific outputs can be selected to interface with any data acquisition system from a simple recorder to computer, SCADA, or PLC based system.

The GW5 is widely used in a variety of applications, including hydro electric generator output measurement, end-of-line appliance testing for energy consumption, building automation, energy management, and cogeneration systems.

FEATURES:

- Accurate regardless of variations in voltage, current, power factor, or load.
- Available with 1, 1 1/2, 2, 2 1/2 or 3 element configurations. Provides bi-directional operation.
- Accuracy maintained over wide temperature range, calibration traceable to **NIST**.

APPLICATIONS:

- Equipment monitoring for process control.
- Integration into energy management systems, or a variety of sub-metering applications.
- Measurement using direct-connection, current transformers, and/or potential transformers.

SINGLE-PHASE MODELS - INTERNAL SENSOR (ONE ELEMENT)

INPUTS		F.S. (WATTS)	STANDARD OUTPUTS, MODEL GW5-							
VOLTS	AMPS		±1mA*	±1mA	±10Vdc*	±10Vdc	4-20mA	4-20mA*	±5Vdc*	±5Vdc
0 - 150	0 - 5	500	001A	001B	001C	001D	001E	001EG	001CX5	001X5
	0 - 10	1000	010A	010B	010C	010D	010E	010EG	010CX5	010X5
	0 - 20	2000	019A	019B	019C	019D	019E	019EG	019CX5	019X5
0 - 300	0 - 5	1000	002A	002B	002C	002D	002E	002EG	002CX5	002X5
	0 - 10	2000	011A	011B	011C	011D	011E	011EG	011CX5	011X5
	0 - 20	4000	020A	020B	020C	020D	020E	020EG	020CX5	020X5
0 - 600	0 - 5	2000	003A	003B	003C	003D	003E	003EG	003CX5	003X5
	0 - 10	4000	012A	012B	012C	012D	012E	012EG	012CX5	012X5
	0 - 20	8000	021A	021B	021C	021D	021E	021EG	021CX5	021X5

THREE-PHASE, THREE-WIRE MODELS - INTERNAL SENSOR (TWO ELEMENT)

INPUTS		F.S. (WATTS)	STANDARD OUTPUTS, MODEL GW5-							
VOLTS	AMPS		±1mA*	±1mA	±10Vdc*	±10Vdc	4-20mA	4-20mA*	±5Vdc*	±5Vdc
0 - 150	0 - 5	1000	004A	004B	004C	004D	004E	004EG	004CX5	004X5
	0 - 5	1000	4.5A	4.5B	4.5C	4.5D	4.5E	4.5EG	4.5CX5	4.5X5
	0 - 10	2000	013A	013B	013C	013D	013E	013EG	013CX5	013X5
0 - 300	0 - 20	4000	022A	022B	022C	022D	022E	022EG	022CX5	022X5
	0 - 5	2000	005A	005B	005C	005D	005E	005EG	005CX5	005X5
	0 - 10	4000	014A	014B	014C	014D	014E	014EG	014CX5	014X5
0 - 600	0 - 20	8000	023A	023B	023C	023D	023E	023EG	023CX5	023X5
	0 - 5	4000	006A	006B	006C	006D	006E	006EG	006CX5	006X5
	0 - 10	8000	015A	015B	015C	015D	015E	015EG	015CX5	015X5
	0 - 20	16000	024A	024B	024C	024D	024E	024EG	024CX5	024X5

ACCURATE TO 0.2% OF READING

THREE-PHASE, FOUR-WIRE MODELS - INTERNAL SENSOR (THREE ELEMENT)

INPUTS		F.S. (WATTS)	STANDARD OUTPUTS MODEL GW5-							
VOLTS	AMPS		±1mA*	±1mA	±10Vdc*	±10Vdc	4-20mA	4-20mA*	±5Vdc*	±5Vdc
0 - 150	0 - 5	1500	007A	007B	007C	007D	007E	007EG	007CX5	007X5
	0 - 5	1500	7.5A	7.5B	7.5C	7.5D	7.5E	7.5EG	7.5CX5	7.5X5
	0 - 10	3000	016A	016B	016C	016D	016E	016EG	016CX5	016X5
	0 - 20	6000	025A	025B	025C	025D	025E	025EG	025CX5	025X5
0 - 300	0 - 5	3000	008A	008B	008C	008D	008E	008EG	008CX5	008X5
	0 - 10	6000	017A	017B	017C	017D	017E	017EG	017CX5	017X5
	0 - 20	12000	026A	026B	026C	026D	026E	026EG	026CX5	026X5

NOTE: PART NUMBER 7.5 DENOTES 2 1/2 ELEMENT UNIT.

Highlighted models, (5A), can be used with customer's existing current transformers, or OSI Low Cost Current Transformers shown on page 89.

Voltage specifications are **line-to-neutral voltage**.

***Denotes self-powered unit, limiting input voltage ranges to:**

85 - 135 for 150V models
200 - 280 for 300V models
380 - 550 for 600V models

All others require 85 - 135 Vac instrument power, (60 Hz.).
All option "**- 22**" for 220Vac instrument power

ORDERING INFORMATION

Example: Self-powered, three-phase, four-wire, 120V, 5A input with 0 - 5Vdc output, proportional to 0 - 1500 Watts.
GW5-007CX5

50 HERTZ MODELS
Self-powered units - Add suffix "**- 50**" to part number.
Units requiring external instrument power:
120V, 50Hz. - Add suffix "**- 51**" to part number.
220V, 50Hz. - Add suffix "**- 52**" to part number.

MODEL GW5 SPECIFICATIONS

INPUT

VOLTAGE: See tables
CURRENT: See tables
FREQUENCY RANGE: 58 - 62 Hz.
Optional 50 Hz.: 48 - 52 Hz.
POWER FACTOR: Any
BURDEN:
Voltage: Less than 0.1VA per phase
Current: Less than 0.28VA per phase
Output amplifier: 2 Watts
OVERLOAD:
Voltage (cont.): 150V range: 175V
300V range: 350V
600V range: 600V
Current (cont.): 5A range: 2 times full-scale
10A range: 2 times full-scale
20A range: Full-scale
(transient): All ranges
50A (10 sec./hr.)
250A (1 sec./hr.)
DIELECTRIC TEST (Input/Output/Case): 1800 Vac (RMS)
SURGE: Withstands IEEE SWC test

OUTPUT

ACCURACY: ±0.2% RDG.; ±0.04% F.S.
(Includes combined effects of voltage, current, load and power factor.)
OUTPUT RIPPLE: Less than 0.5% F.S.
OUTPUT LOADING (ohms):
0 - 1mA: 0 - 10K
0 - 10Vdc: 2K min.
4 - 20mA: 0 - 500
0 - 5Vdc: 2K min.
RESPONSE TIME (99%): Less than 200 milliseconds
FIELD ADJUSTABLE CAL.: ±2% min.
COMPLIANCE VOLTAGE: 12Vdc min.
OPEN CIRCUIT VOLTAGE:
0 - 1mA, 0 - 10Vdc, 0 - 5Vdc outputs: ±15Vdc
4 - 20mA output: 15Vdc
TEMPERATURE EFFECT (-20° to +65°C):
±0.005% per degree C
OPERATING HUMIDITY: 0 - 95% non-condensing
INSTRUMENT POWER (std.): 85 - 135Vac, 60 Hz, 7VA.

I/O Board (Measurement Computing, http://www.measurementcomputing.com/pdfs/pci-dio24_24h.pdf, 12-08-04)

Digital Type	82C55
Configuration	2 banks of 8, 2 banks of 4, programmable by bank as input or output
Number of channels	24 I/O
Output High	3.7 volts min @ -2.5 mA
Output Low	0.4 volts max @ 2.5 mA
Input High	2.2 volts min, 5.3 volts absolute max
Input Low	0.8 volts max, -0.3 volts absolute min
Power-up / reset state	Input mode (high impedance)
Interrupts	INTA# - mapped to IRQn via PCI BIOS at boot-time
Interrupt enable	External (IR ENABLE, active low, disabled by default through internal resistor to TTL high) and programmable through PCI9052. 0 = disabled 1 = enabled (default)
Interrupt sources	External source (IR INPUT), polarity programmable through PCI9052. 1 = active high 0 = active low (default)

Vita

Shawn Alex Hern

Candidate for the Degree of

Master of Science

Thesis: DESIGN OF AN EXPERIMENTAL FACILITY FOR HYBRID GROUND SOURCE HEAT PUMP SYSTEMS

Major Field: Mechanical Engineering

Biographical:

Personal Data: Born in Enid, Oklahoma on March 14, 1980, the son of Rodney and Patricia Hern.

Education: Graduated from Wakita High School, Wakita, Oklahoma in May 1998. Received a Bachelor of Science degree in Mechanical Engineering from Oklahoma State University, Stillwater, Oklahoma in December 2002. Completed the requirements for the Master of Science degree with a major in Mechanical Engineering at Oklahoma State University in December 2004.

Experience: Raised on a farm near Wakita, Oklahoma, employed as a farm laborer. Employed by Oklahoma State University, Department of Mechanical and Aerospace Engineering, as a graduate research assistant from January 2003 to July 2004. Employed by ClimateMaster, Oklahoma City Oklahoma, Oklahoma, July 2004 to present.

Professional Memberships: Pi Tau Sigma, American Society of Mechanical Engineers, American Society of Heating, Refrigeration and Air-Conditioning Engineers, Society of Automotive Engineers.

Name: Shawn Alex Hern Date of Degree: December, 2004

Institution: Oklahoma State University Location: Stillwater, Oklahoma

Title of Study: DESIGN OF AN EXPERIMENTAL FACILITY FOR HYBRID GOUND SOURCE HEAT PUMP SYSTEMS

Pages in Study: 156 Candidate for the Degree of Master of Science

Major Field: Mechanical Engineering

Scope and Method of Study: This study reports on the development and commissioning of an experimental facility to test and validate hybrid ground-source heat pump models in hourly building energy simulation programs such as EnergyPlus and HVACSim+. Validation of simulation models over long time periods will allow researchers to ensure that simulation results accurately model true system performance. After validation, design engineers can use these programs to improve future system designs to reduce first and operating costs.

Findings and Conclusions: A well instrumented experimental facility for hybrid ground source heat pump system research was designed, built and tested. Experiments performed in the completed facility determined that heat balance and heat transfer rates were within an acceptable range as calculated by the uncertainty analysis. The performance of the system met the requirements specified for the system design. Transient effects were found to account for a significant portion of the cycle time on all components. A circulation pump model was also developed and validated to give future researchers a tool to estimate the main circulation pump power input which can be used as an input into a simulation. Future research is required to determine the simulation error that results from transient effects in the system.

ADVISOR'S APPROVAL: _____